



Contents lists available at ScienceDirect

Physics Letters B

www.elsevier.com/locate/physletb



Correlated long-range mixed-harmonic fluctuations measured in pp , $p+Pb$ and low-multiplicity $Pb+Pb$ collisions with the ATLAS detector

The ATLAS Collaboration *

ARTICLE INFO

Article history:

Received 6 July 2018

Received in revised form 7 October 2018

Accepted 13 November 2018

Available online xxxx

Editor: D.F. Geesaman

ABSTRACT

Correlations of two flow harmonics v_n and v_m via three- and four-particle cumulants are measured in 13 TeV pp , 5.02 TeV $p+Pb$, and 2.76 TeV peripheral $Pb+Pb$ collisions with the ATLAS detector at the LHC. The goal is to understand the multi-particle nature of the long-range collective phenomenon in these collision systems. The large non-flow background from dijet production present in the standard cumulant method is suppressed using a method of subevent cumulants involving two, three and four subevents separated in pseudorapidity. The results show a negative correlation between v_2 and v_3 and a positive correlation between v_2 and v_4 for all collision systems and over the full multiplicity range. However, the magnitudes of the correlations are found to depend on the event multiplicity, the choice of transverse momentum range and collision system. The relative correlation strength, obtained by normalisation of the cumulants with the $\langle v_n^2 \rangle$ from a two-particle correlation analysis, is similar in the three collision systems and depends weakly on the event multiplicity and transverse momentum. These results based on the subevent methods provide strong evidence of a similar long-range multi-particle collectivity in pp , $p+Pb$ and peripheral $Pb+Pb$ collisions.

© 2019 The Author. Published by Elsevier B.V. This is an open access article under the CC BY license (<http://creativecommons.org/licenses/by/4.0/>). Funded by SCOAP³.

1. Introduction

One of the goals in the studies of azimuthal correlations in high-energy nuclear collisions at the Relativistic Heavy Ion Collider (RHIC) and the Large Hadron Collider (LHC) is to understand the multi-parton dynamics of QCD in the strongly coupled non-perturbative regime [1]. Measurements of azimuthal correlations in small collision systems, such as pp , $p+A$ or $d+A$ collisions, have revealed the ridge phenomenon [2–6]: enhanced production of particle pairs at small azimuthal angle separation, $\Delta\phi$, extended over a wide range of pseudorapidity separation, $\Delta\eta$. The azimuthal structure has been related to harmonic modulation of particle densities, characterised by a Fourier expansion, $dN/d\phi \propto 1 + 2 \sum_{n=1}^{\infty} v_n \cos n(\phi - \Phi_n)$, where v_n and Φ_n represent the magnitude and the event-plane angle of the n th-order flow harmonic. They are also conveniently represented by the flow vector: $\mathbf{V}_n = v_n e^{in\Phi_n}$. The v_n are known to depend on the collision system, but have weak dependence on collision energies [6,7]. The ridge reflects multi-parton dynamics early in the collision and has generated significant interest in the high-energy physics community. A key question is whether the long-range multi-particle collectivity reflects initial momentum correlation from gluon sat-

uration effects [8], or a final-state hydrodynamic response to the initial transverse collision geometry [9].

Further insight into the ridge phenomenon is obtained via a multi-particle correlation technique, known as cumulants, involving three or more particles [10–12]. The multi-particle cumulants probe the event-by-event fluctuation of a single flow harmonic v_n , as well as the correlated fluctuations between two flow harmonics, v_n and v_m . These event-by-event fluctuations are often represented by probability density distributions $p(v_n)$ and $p(v_n, v_m)$, respectively. For instance, the four-particle cumulants $c_n\{4\} = \langle v_n^4 \rangle - 2 \langle v_n^2 \rangle^2$ constrain the width of $p(v_n)$ [10], while the four-particle symmetric cumulants $sc_{n,m}\{4\} = \langle v_n^2 v_m^2 \rangle - \langle v_n^2 \rangle \langle v_m^2 \rangle$ quantify the lowest-order correlation between v_n and v_m [12]. The three-particle asymmetric cumulants such as $ac_n\{3\} = \langle \mathbf{V}_n^2 \mathbf{V}_{2n}^* \rangle = \langle v_n^2 v_{2n} \cos 2n(\Phi_n - \Phi_{2n}) \rangle$ [5,13] are sensitive to correlations involving both the flow magnitude v_n and flow phase Φ_n .

One of the challenges in the study of azimuthal correlations in small collision systems is how to distinguish the long-range ridge from “non-flow” correlations involving only a few particles, such as resonance decays, jets, or dijets. For two-particle correlations, the non-flow contribution is commonly suppressed by requiring a large $\Delta\eta$ gap between the two particles in each pair and a peripheral subtraction procedure [3–5,7,14,15]. For multi-particle cumulants, the non-flow contributions can be suppressed by requiring correlation between particles from different subevents separated in η ,

* E-mail address: atlas_publications@cern.ch.

<https://doi.org/10.1016/j.physletb.2018.11.065>

0370-2693/© 2019 The Author. Published by Elsevier B.V. This is an open access article under the CC BY license (<http://creativecommons.org/licenses/by/4.0/>). Funded by SCOAP³.

while preserving the genuine long-range multi-particle correlations associated with the ridge. Here each subevent is a collection of particles in a given η range. This so-called “subevent method” has been demonstrated to measure reliably $c_n\{4\}$ and $sc_{n,m}\{4\}$ [13, 16]. In contrast, $c_n\{4\}$ and $sc_{n,m}\{4\}$ based on the standard cumulant method are contaminated by non-flow correlations over the full multiplicity range in pp collisions and the low multiplicity region in $p+A$ collisions [16]. In small collision systems, measurements have been performed for $c_n\{4\}$ with both the standard [15, 17] and subevent methods [18], and for $sc_{n,m}\{4\}$ with the standard method [19]. The subevent method has not yet been used to measure $sc_{n,m}\{4\}$, and no measurements of $ac_n\{3\}$ have ever been attempted in small collision systems.

This Letter presents measurements of $sc_{2,3}\{4\}$, $sc_{2,4}\{4\}$ and $ac_2\{3\}$ in pp collisions at $\sqrt{s} = 13$ TeV, $p+Pb$ collisions at $\sqrt{s_{NN}} = 5.02$ TeV and low-multiplicity Pb+Pb collisions at $\sqrt{s_{NN}} = 2.76$ TeV. They are obtained using two-, three- and four-subevent cumulant methods and are compared with results from the standard cumulant method. The cumulants are normalised by the $\langle v_n^2 \rangle$ obtained from a two-particle correlation analysis [7] to quantify their relative correlation strength. The measurements suggest that the results obtained with the standard method are strongly contaminated by correlations from non-flow sources. The results obtained with the three-subevent method or the four-subevent method provide new evidence of long-range three- or four-particle azimuthal correlations.

The Letter is organised as follows. Details of the ATLAS detector, the trigger system, datasets, as well as event and track selections are provided in Sections 2 to 4. Section 5 describes the standard and subevent cumulant methods used in this analysis. The analysis procedure and systematic uncertainties are described in Sections 6 and 7, respectively. The measured cumulants are presented in Section 8. A summary is given in Section 9.

2. Detector and trigger

The ATLAS detector [20] provides nearly full solid-angle coverage around the collision point with tracking detectors, calorimeters, and muon chambers, and is well suited for measurement of multi-particle correlations over a large pseudorapidity range.¹ The measurements were performed using primarily the inner detector (ID), minimum-bias trigger scintillators (MBTS) and the zero-degree calorimeters (ZDC). The ID detects charged particles within $|\eta| < 2.5$ using a combination of a silicon pixel detector, a silicon microstrip detector (SCT), and a straw-tube transition radiation tracker, all immersed in a 2 T axial magnetic field [21]. An additional pixel layer, the “insertable B-layer” (IBL) [22] is installed between the Run-1 (2010–2013) and Run-2 (2015–2018) periods. The MBTS detects charged particles within $2.1 \lesssim |\eta| \lesssim 3.9$ using two hodoscopes of counters positioned at $z = \pm 3.6$ m. The ZDC, used only in $p+Pb$ and Pb+Pb collisions, are positioned at ± 140 m from the collision point, and detect neutral particles, primarily neutrons and photons, with $|\eta| > 8.3$.

The ATLAS trigger system [23,24] consists of a first-level (L1) trigger implemented using a combination of dedicated electronics and programmable logic, and a high-level trigger (HLT) implemented in processors. The HLT reconstructs charged-particle tracks

Table 1

The list of datasets used in this analysis.

	Pb+Pb	$p+Pb$	pp
Integrated luminosity (year)	$7 \mu\text{b}^{-1}$ (2010)	28 nb^{-1} (2013) 0.3 nb^{-1} (2016)	0.07 pb^{-1} (2015) 0.84 pb^{-1} (2016)

using methods similar to those applied in the offline analysis. The HLT enables the high-multiplicity track triggers (HMT) to select events according to the number of tracks having $p_T > 0.4$ GeV matched to the primary vertex, $N_{\text{ch}}^{\text{HLT}}$. The different HMT triggers apply additional requirements on either the total transverse energy (E_T) in the calorimeters or the number of hits in the MBTS found by the L1 trigger, as well as on $N_{\text{ch}}^{\text{HLT}}$ by the HLT trigger. The pp and $p+Pb$ data were collected using combinations of the minimum-bias and HMT triggers. The minimum-bias trigger required either a hit in at least one MBTS counter, or a hit in at least one MBTS counter on each side, or at least one reconstructed track at the HLT seeded by a random trigger at L1. More detailed information about the triggers used for the pp and $p+Pb$ data and their performance can be found in Refs. [7,25] and Refs. [5,26], respectively.

3. Datasets and Monte Carlo simulations

This analysis is based on ATLAS datasets corresponding to integrated luminosities of 0.9 pb^{-1} of pp data recorded at $\sqrt{s} = 13$ TeV, 28 nb^{-1} of $p+Pb$ data recorded at $\sqrt{s_{NN}} = 5.02$ TeV, and $7 \mu\text{b}^{-1}$ of Pb+Pb data at $\sqrt{s_{NN}} = 2.76$ TeV. The 2.76 TeV Pb+Pb data were collected in 2010. The $p+Pb$ data were mainly collected in 2013, but also include 0.3 nb^{-1} of data collected in 2016, which increase the number of events at moderate multiplicity (see Section 4). During both $p+Pb$ runs, the LHC was configured to provide a 4 TeV proton beam and a 1.57 TeV per-nucleon Pb beam, which produced collisions at $\sqrt{s_{NN}} = 5.02$ TeV, with a rapidity shift of 0.465 of the nucleon-nucleon centre-of-mass frame towards the proton beam direction relative to the ATLAS rest frame. The direction of the Pb beam is always defined to have negative pseudorapidity. The 13 TeV pp data were collected during several special runs of the LHC with low pile-up in 2015 and 2016. A summary of the datasets used in this analysis is shown in Table 1.

The track reconstruction efficiency was determined using simulated Monte Carlo (MC) event samples (Section 4). The pp events were simulated with the PYTHIA8 MC event generator [27] using the A2 set of tuned parameters with MSTW2008LO parton distribution functions [28]. The HIJING event generator [29] was used to produce Pb+Pb and $p+Pb$ collisions with the same energy and the same boost of the centre-of-mass system as in the data. The detector response was simulated using GEANT4 [30,31] with detector conditions matching those during the data-taking. The simulated events and data events are reconstructed with the same algorithms. The MC sample for Pb+Pb events in the multiplicity region of interest is very small, and so the track reconstruction efficiency for Pb+Pb was taken from the larger $p+Pb$ sample reconstructed with the same reconstruction algorithm. The efficiency in $p+Pb$ events was found to be consistent with the efficiency from the Pb+Pb MC simulation [17].

4. Event and track selection

The offline event selection for the pp and $p+Pb$ data requires at least one reconstructed vertex with its longitudinal position satisfying $|z_{\text{vtx}}| < 100$ mm relative to the nominal interaction point. The vertex is required to have at least two associated tracks with $p_T > 0.4$ GeV. The mean number of collisions per bunch crossing, μ , was 0.002–0.8 for the 13 TeV pp data, 0.03 for the 2013

¹ ATLAS typically uses a right-handed coordinate system with its origin at the nominal interaction point (IP) in the centre of the detector and the z -axis along the beam pipe. The x -axis points from the IP to the centre of the LHC ring, and the y -axis points upward. Cylindrical coordinates (r, ϕ) are used in the transverse plane, ϕ being the azimuthal angle around the beam pipe. By default, the pseudorapidity is defined in terms of the polar angle θ as $\eta = -\ln \tan(\theta/2)$. However, for asymmetric $p+Pb$ or $Pb+p$ collisions, the $-z$ direction is always defined as the direction of the Pb beam.

p +Pb data, and 0.001–0.006 for the 2016 p +Pb data. In order to suppress additional interactions in the same bunch crossing (referred to as pile-up) in pp collisions, events containing additional vertices with at least four associated tracks are rejected. In p +Pb collisions, events with more than one good vertex, defined as any vertex for which the scalar sum of the p_T of the associated tracks is greater than 5 GeV, are rejected. The remaining pile-up events are further suppressed by using the signal in the ZDC in the direction of the Pb beam. This signal is calibrated to the number of detected neutrons, N_n , by using the location of the peak corresponding to a single neutron. The distribution of N_n in events with pile-up is broader than that for the events without pile-up. Hence a simple requirement on the ZDC signal distribution is used to further suppress events with pile-up, while retaining more than 98% of events without pile-up. The impact of residual pile-up, at the level of $\lesssim 10^{-3}$, is studied by comparing the results obtained from data with different μ values.

The offline event selection for the Pb+Pb data requires $|z_{\text{vtx}}| < 100$ mm. The selection also requires a time difference $|\Delta t| < 3$ ns between signals in the MBTS trigger counters on either side of the interaction point to suppress non-collision backgrounds. A coincidence between the ZDC signals at forward and backward pseudorapidity is required to reject a variety of background processes, while maintaining high efficiency for inelastic processes. The fraction of events with more than one interaction after applying these selection criteria is less than 10^{-4} .

Charged-particle tracks and collision vertices are reconstructed using algorithms optimised for improved performance for Run-2. In order to compare directly with the pp and p +Pb systems using event selections based on the multiplicity of the collisions, a subset of data from low-multiplicity Pb+Pb collisions, collected during the 2010 LHC heavy-ion run with a minimum-bias trigger, was analysed using the same track reconstruction algorithm as that used for p +Pb collisions. For the Pb+Pb and 2013 p +Pb analyses, tracks are required to have a p_T -dependent minimum number of hits in the SCT. The transverse (d_0) and longitudinal ($z_0 \sin \theta$) impact parameters of the track relative to the vertex are required to be less than 1.5 mm. Additional requirements $|d_0|/\sigma_{d_0} < 3$ and $|z_0 \sin \theta|/\sigma_{z_0} < 3$ are imposed, where σ_{d_0} and σ_{z_0} are the uncertainties of the transverse and longitudinal impact parameter values, respectively. A more detailed description of the track selection for the 2010 Pb+Pb data and 2013 p +Pb data can be found in Refs. [5,17].

For all the data taken since the start of Run-2, the track selection criteria make use of the IBL, as described in Refs. [14,25]. For the pp and 2016 p +Pb analyses, the tracks are required to satisfy $|d_0^{\text{BL}}| < 1.5$ mm and $|z_0 \sin \theta| < 1.5$ mm, where d_0^{BL} is the transverse impact parameter of the track relative to the beam line (BL).

The cumulants are calculated using tracks passing the above selection requirements, and having $|\eta| < 2.5$ and $0.3 < p_T < 3$ GeV or $0.5 < p_T < 5$ GeV. These two p_T ranges are chosen because they were often used in the previous ridge measurements at the LHC [6,7,14,15,17]. However, to count the number of reconstructed charged particles for event-class definition (denoted by $N_{\text{ch}}^{\text{rec}}$), tracks with $p_T > 0.4$ GeV and $|\eta| < 2.5$ are used for compatibility with the requirements in the HLT selections described above. Due to different trigger requirements, most of the p +Pb events with $N_{\text{ch}}^{\text{rec}} > 150$ are provided by the 2013 dataset, while the 2016 dataset provides most of the events at lower $N_{\text{ch}}^{\text{rec}}$.

The efficiency of the combined track reconstruction and track selection requirements is estimated using MC samples reconstructed with the same algorithms and selection requirements as in data. Efficiencies, $\epsilon(\eta, p_T)$, are evaluated as a function of track η , p_T and the number of reconstructed charged-particle tracks, but averaged over the full range in azimuth. The efficiencies are simi-

lar for events with the same multiplicity. For all collision systems, the efficiency increases by about 4% as track p_T increases from 0.3 GeV to 0.6 GeV. Above 0.6 GeV, the efficiency is independent of p_T and reaches 86% (72%) for Run-1 pp and p +Pb, and 83% (70%) for Pb+Pb and Run-2 p +Pb collisions, at $\eta \approx 0$ ($|\eta| > 2$). The efficiency is independent of the event multiplicity for $N_{\text{ch}}^{\text{rec}} > 40$. For lower-multiplicity events the efficiency is smaller by up to 3% due to broader d_0 and $z_0 \sin \theta$ distributions [17].

The fraction of falsely reconstructed charged-particle tracks is also estimated and found to be negligibly small in all datasets. This fraction decreases with increasing track p_T , and even at the lowest transverse momenta of 0.3 GeV it is below 1% of the total number of tracks. Therefore, there is no correction for the presence of such tracks in the analysis.

In the simulated events, the reconstruction efficiency reduces the measured charged-particle multiplicity relative to the generated multiplicity for primary charged particles. A correction factor b is used to correct $N_{\text{ch}}^{\text{rec}}$ to obtain the efficiency-corrected average number of charged particles per event, $\langle N_{\text{ch}} \rangle = b \langle N_{\text{ch}}^{\text{rec}} \rangle$. The value of the correction factor is obtained from the MC samples described above, and is found to be nearly independent of $N_{\text{ch}}^{\text{rec}}$ in the range used in this analysis, $N_{\text{ch}}^{\text{rec}} < 400$. Its value and the associated uncertainties are $b = 1.29 \pm 0.05$ for the Pb+Pb and 2013 p +Pb collisions and $b = 1.18 \pm 0.05$ for Run-2 p +Pb and pp collisions [32]. Both $sc_{n,m}\{4\}$ and $ac_2\{3\}$ are then studied as a function of $\langle N_{\text{ch}} \rangle$.

5. Cumulant method

The multi-particle cumulant method [10] has the advantage of directly reducing non-flow correlations from jets and dijets. The mathematical framework for the standard cumulant is based on the Q-cumulants discussed in Refs. [11,12,33]. It was extended recently to the case of subevent cumulants in Refs. [13,16]. These methods are briefly summarised below.

5.1. Cumulants in the standard method

The standard cumulant method calculates k -particle azimuthal correlations, $\langle \{k\} \rangle$, in one event using a complex number notation [11,12]:

$$\begin{aligned} \langle \{2\}_n \rangle &= \left\langle e^{in(\phi_1 - \phi_2)} \right\rangle, \quad \langle \{3\}_n \rangle = \left\langle e^{in(\phi_1 + \phi_2 - 2\phi_3)} \right\rangle, \\ \langle \{4\}_{n,m} \rangle &= \left\langle e^{in(\phi_1 - \phi_2) + im(\phi_3 - \phi_4)} \right\rangle, \end{aligned} \quad (1)$$

where “ $\langle \rangle$ ” denotes a single-event average over all pairs, triplets or quadruplets, respectively. The averages from Eq. (1) can be expressed in terms of per-particle normalised flow vectors $\mathbf{q}_{n;l}$ with $l = 1, 2, \dots$ in each event [11]:

$$\mathbf{q}_{n;l} \equiv \sum_j w_j^l e^{in\phi_j} / \sum_j w_j^l, \quad (2)$$

where the sum runs over all tracks in the event and w_j is a weight assigned to the j th track. This weight is constructed to correct for both detector non-uniformity and tracking inefficiency as explained in Section 6.

The multi-particle asymmetric and symmetric cumulants are obtained from $\langle \{k\} \rangle$ as:

$$ac_n\{3\} = \langle \{3\}_n \rangle, \quad sc_{n,m}\{4\} = \langle \{4\}_{n,m} \rangle - \langle \{2\}_n \rangle \langle \{2\}_m \rangle, \quad (3)$$

where “ $\langle \langle \rangle \rangle$ ” represents a weighted average of $\langle \{k\} \rangle$ over an event ensemble with similar $N_{\text{ch}}^{\text{rec}}$. One averages first over all distinct

pairs, triplets or quadruplets in one event to obtain $\langle\{2\}_n\rangle$, $\langle\{2\}_m\rangle$, $\langle\{3\}_n\rangle$ and $\langle\{4\}_{n,m}\rangle$. Then the obtained values are averaged over an event ensemble with similar $N_{\text{ch}}^{\text{rec}}$ to obtain $\text{sc}_{n,m}\{4\}$ and $\text{ac}_n\{3\}$. In the absence of non-flow correlations, $\text{sc}_{n,m}\{4\}$ and $\text{ac}_n\{3\}$ measure the correlation between v_n and v_m or between v_n and v_{2n} :

$$\begin{aligned}\text{ac}_n\{3\} &= \langle \mathbf{v}_n^2 \mathbf{v}_{2n}^* \rangle = \langle v_n^2 v_{2n} \cos 2n(\Phi_n - \Phi_{2n}) \rangle, \\ \text{sc}_{n,m}\{4\} &= \langle v_n^2 v_m^2 \rangle - \langle v_n^2 \rangle \langle v_m^2 \rangle,\end{aligned}\quad (4)$$

where the averages are taken over the events. This analysis measures three types of cumulants defined in Eq. (3): $\text{sc}_{2,3}\{4\}$, $\text{sc}_{2,4}\{4\}$ and $\text{ac}_2\{3\}$.

5.2. Cumulants in the subevent method

In the standard cumulant method described above, all k -particle multiplets involved in $\langle\{k\}_n\rangle$ and $\langle\{k\}_{n,m}\rangle$ are selected using tracks in the entire ID acceptance of $|\eta| < \eta_{\text{max}} = 2.5$. To suppress further the non-flow correlations that typically involve a few particles within a localised region in η , the tracks are divided into several subevents, each covering a unique η interval. The multi-particle correlations are then constructed by only correlating tracks between different subevents.

In the two-subevent cumulant method, the tracks are divided into two subevents, labelled by a and b , according to $-\eta_{\text{max}} < \eta_a < 0$ and $0 \leq \eta_b < \eta_{\text{max}}$. The per-event k -particle azimuthal correlations are evaluated as:

$$\begin{aligned}\langle\{2\}_n\rangle_{a|b} &= \langle e^{in(\phi_1^a - \phi_2^b)} \rangle, \quad \langle\{3\}_n\rangle_{2a|b} = \langle e^{in(\phi_1^a + \phi_2^a - 2\phi_3^b)} \rangle, \\ \langle\{4\}_{n,m}\rangle_{2a|2b} &= \langle e^{in(\phi_1^a - \phi_2^b) + im(\phi_3^a - \phi_4^b)} \rangle,\end{aligned}\quad (6)$$

where the superscript or subscript a (b) indicates tracks chosen from the subevent a (b). Here the three- and four-particle cumulants are defined as:

$$\begin{aligned}\text{ac}_n^{2a|b}\{3\} &= \langle\langle\{3\}_n\rangle\rangle_{2a|b}, \\ \text{sc}_{n,m}^{2a|2b}\{4\} &= \langle\langle\{4\}_{n,m}\rangle\rangle_{2a|2b} - \langle\langle\{2\}_n\rangle\rangle_{a|b} \langle\langle\{2\}_m\rangle\rangle_{a|b}.\end{aligned}$$

The two-subevent method suppresses correlations within a single jet (intra-jet correlations), since particles from one jet usually fall in one subevent.

In the three-subevent cumulant method, tracks in each event are divided into three subevents a , b and c , each covering one third of the η range, $-\eta_{\text{max}} < \eta_a < -\eta_{\text{max}}/3$, $|\eta_b| \leq \eta_{\text{max}}/3$ and $\eta_{\text{max}}/3 < \eta_c < \eta_{\text{max}}$. The multi-particle azimuthal correlations and cumulants are then evaluated as:

$$\begin{aligned}\langle\{3\}_n\rangle_{a,b|c} &= \langle e^{in(\phi_1^a + \phi_2^b - 2\phi_3^c)} \rangle, \\ \langle\{4\}_{n,m}\rangle_{a,b|2c} &= \langle e^{in(\phi_1^a - \phi_2^b) + im(\phi_3^b - \phi_4^c)} \rangle,\end{aligned}\quad (7)$$

and

$$\begin{aligned}\text{ac}_n^{a,b|c}\{3\} &= \langle\langle\{3\}_n\rangle\rangle_{a,b|c}, \\ \text{sc}_{n,m}^{a,b|2c}\{4\} &= \langle\langle\{4\}_{n,m}\rangle\rangle_{a,b|2c} - \langle\langle\{2\}_n\rangle\rangle_{a|c} \langle\langle\{2\}_m\rangle\rangle_{b|c}.\end{aligned}\quad (8)$$

Since a dijet event usually produces particles in at most two subevents, the three-subevent method efficiently suppresses the non-flow contribution from inter-jet correlations associated with dijets. To maximise the statistical precision, the η range for subevent a is swapped with that for subevent b or c , and the results are averaged to obtain the final values.

The four-subevent cumulant method is only relevant for the symmetric cumulants $\text{sc}_{n,m}\{4\}$. Tracks in each event are divided into four subevents a , b , c , and d , each covering one quarter of the η range: $-\eta_{\text{max}} < \eta_a < -\eta_{\text{max}}/2$, $-\eta_{\text{max}}/2 \leq \eta_b < 0$, $0 \leq \eta_c < \eta_{\text{max}}/2$, and $\eta_{\text{max}}/2 \leq \eta_d < \eta_{\text{max}}$. The multi-particle azimuthal correlations and cumulants are then evaluated as:

$$\langle\{4\}_{n,m}\rangle_{a,b|c,d} = \langle e^{in(\phi_1^a - \phi_2^c) + im(\phi_3^b - \phi_4^d)} \rangle, \quad (9)$$

$$\text{sc}_{n,m}^{a,b|c,d}\{4\} = \langle\langle\{4\}_{n,m}\rangle\rangle_{a,b|c,d} - \langle\langle\{2\}_n\rangle\rangle_{a|c} \langle\langle\{2\}_m\rangle\rangle_{b|d}. \quad (10)$$

The four-subevent method based on Eqs. (9) and (10) should further suppress the residual non-flow contributions, for instance when each of the two jets from the dijet falls across the boundary between two neighbouring subevents. To maximise the statistical precision, the η ranges for the four subevents are swapped with each other, and the results are averaged to obtain the final values.

5.3. Normalised cumulants

Although the cumulants reflect the nature of the correlation between v_n and v_m , their magnitudes also depend on the square of single flow harmonics v_n^2 and v_m^2 , see Eq. (4). The dependence on the single flow harmonics can be scaled out via the normalised cumulants [34,35]:

$$\text{nsc}_{2,3}\{4\} = \frac{\text{sc}_{2,3}\{4\}}{v_2\{2\}^2 v_3\{2\}^2} = \frac{\langle v_2^2 v_3^2 \rangle}{\langle v_2^2 \rangle \langle v_3^2 \rangle} - 1, \quad (11)$$

$$\text{nsc}_{2,4}\{4\} = \frac{\text{sc}_{2,4}\{4\}}{v_2\{2\}^2 v_4\{2\}^2} = \frac{\langle v_2^2 v_4^2 \rangle}{\langle v_2^2 \rangle \langle v_4^2 \rangle} - 1, \quad (12)$$

$$\begin{aligned}\text{nac}_2\{3\} &= \frac{\text{ac}_2\{3\}}{\sqrt{(2v_2\{2\}^4 + c_2\{4\})c_4\{2\}}}} \\ &= \frac{\langle v_2^2 v_4 \cos 4(\Phi_2 - \Phi_4) \rangle}{\sqrt{\langle v_2^4 \rangle \langle v_4^2 \rangle}},\end{aligned}\quad (13)$$

where the $v_n\{2\}^2 = \langle v_n^2 \rangle$ are flow harmonics obtained using a two-particle correlation method based on a peripheral subtraction technique [7,14], and $c_2\{4\} = \langle v_4^4 \rangle - 2\langle v_2^2 \rangle^2$ are four-particle cumulant results from Refs. [17,18]. This definition for $\text{nac}_2\{3\}$ is motivated by Ref. [36].

6. Analysis procedure

The measurement of the $\text{sc}_{n,m}\{4\}$ and $\text{ac}_2\{3\}$ follows the same analysis procedure as for the four-particle cumulants $c_n\{4\}$ in Ref. [18]. The multi-particle cumulants are calculated in three steps using charged particles with $|\eta| < 2.5$. In the first step, $\langle\{2\}_n\rangle$, $\langle\{3\}_n\rangle$ and $\langle\{4\}_{n,m}\rangle$ from Eqs. (1), (6), (7) and (9) are calculated for each event from particles in one of two different p_T ranges, $0.3 < p_T < 3$ GeV and $0.5 < p_T < 5$ GeV. The numbers of reconstructed charged particles in these p_T ranges are denoted by $N_{\text{ch}}^{\text{sel1}}$ and $N_{\text{ch}}^{\text{sel2}}$, respectively.

In the second step, the correlators $\langle\{k\}\rangle$ for $0.3 < p_T < 3$ GeV ($0.5 < p_T < 5$ GeV) are averaged over events with the same $N_{\text{ch}}^{\text{sel1}}$ ($N_{\text{ch}}^{\text{sel2}}$) to obtain $\langle\langle\{k\}\rangle\rangle$, and then $\text{sc}_{2,3}\{4\}$, $\text{sc}_{2,4}\{4\}$ and $\text{ac}_2\{3\}$. The $\text{sc}_{2,3}\{4\}$, $\text{sc}_{2,4}\{4\}$ and $\text{ac}_2\{3\}$ values are then averaged in broader multiplicity ranges of the event ensemble, weighted by number of events, to obtain statistically significant results.

In the third step, the $\text{sc}_{2,3}\{4\}$, $\text{sc}_{2,4}\{4\}$ and $\text{ac}_2\{3\}$ values obtained for a given $N_{\text{ch}}^{\text{sel1}}$ or $N_{\text{ch}}^{\text{sel2}}$ are mapped to $\langle N_{\text{ch}}^{\text{rec}} \rangle$, the average number of reconstructed charged particles with $p_T > 0.4$ GeV.

The mapping procedure is necessary so that $sc_{2,3}\{4\}$, $sc_{2,4}\{4\}$ and $ac_2\{3\}$ obtained for the two different p_T ranges can be compared using a common x -axis defined by $\langle N_{ch}^{rec} \rangle$. The $\langle N_{ch}^{rec} \rangle$ value is then converted to $\langle N_{ch} \rangle$, the efficiency-corrected average number of charged particles with $p_T > 0.4$ GeV, as discussed in Section 4.

In order to account for detector inefficiencies and non-uniformity, particle weights used in Eq. (2) are defined as:

$$w(\phi, \eta, p_T) = d(\phi, \eta) / \epsilon(\eta, p_T).$$

The additional weight factor $d(\phi, \eta)$ accounts for non-uniformities in the azimuthal acceptance of the detector as a function of η . All reconstructed charged particles with $p_T > 0.3$ GeV are entered into a two-dimensional histogram $N(\phi, \eta)$, and the weight factor is then obtained as $d(\phi, \eta) \equiv \langle N(\eta) \rangle / N(\phi, \eta)$, where $\langle N(\eta) \rangle$ is the track density averaged over ϕ in the given η bin. This procedure removes most of the ϕ -dependent non-uniformity in the detector acceptance [17].

In order to calculate the normalised cumulants from Eqs. (11)–(13), the flow harmonics $v_n\{2\}$ are obtained from a “template fit” of two-particle $\Delta\phi$ correlation as described in Refs. [7,14]. The $v_n\{2\}$ values are calculated identically to the procedure used in the previous ATLAS publications [7,14], but are further corrected for a bias, which exists only if $v_n\{2\}$ changes with N_{ch}^{rec} . The details of the correction procedure are given in the Appendix A and are discussed briefly below.

The standard procedure of Refs. [7,14] first constructs a $\Delta\phi$ distribution for pairs of tracks with $|\Delta\eta| > 2$: the per-trigger-particle yield $Y(\Delta\phi)$ for a given N_{ch}^{rec} range. The dominating non-flow jet peak at $\Delta\phi \sim \pi$ is estimated using low-multiplicity events with $N_{ch}^{rec} < 20$ and separated via a template fit procedure, and the harmonic modulation of the remaining component is taken as the $v_n\{2\}^2$ [7]:

$$Y(\Delta\phi) = F Y(\Delta\phi)^{peri} + G^{tmp} \left(1 + 2 \sum_{n=2}^{\infty} v_n\{2, tmp\}^2 \cos n\Delta\phi \right),$$

where superscripts “peri” and “tmp” indicate quantities for the $N_{ch}^{rec} < 20$ event class and quantities after the template fit for the event class of interest, respectively. The scale factor F and pedestal G^{tmp} are fixed by the fit, and $v_n\{2, tmp\}$ are calculated from a Fourier transform. This procedure implicitly assumes that $v_n\{2\}$ is independent of N_{ch}^{rec} , and requires a small correction if $v_n\{2\}$ does change with N_{ch}^{rec} (Appendix A). In p +Pb and Pb+Pb collisions, this correction in the $N_{ch}^{rec} > 100$ region amounts to a 2–6% reduction for $v_2\{2, tmp\}$ and a 4–9% reduction for $v_3\{2, tmp\}$ and $v_4\{2, tmp\}$. The correction is smaller for $v_2\{2, tmp\}$ in pp collisions as it is nearly independent of N_{ch}^{rec} [7].

7. Systematic uncertainties

The evaluation of the systematic uncertainties follows closely the procedure established for the four-particle cumulants $c_n\{4\}$ and described in Ref. [18]. The main sources of systematic uncertainties are related to the detector azimuthal non-uniformity, track selection, track reconstruction efficiency, trigger efficiency and pile-up. Due to the relatively poor statistics and larger non-flow effects, the systematic uncertainties are typically larger in pp collisions. The systematic uncertainties are also generally larger, in percentage, for four-particle cumulants $sc_{n,m}\{4\}$ than for the three-particle cumulants $ac_2\{3\}$, since the $|sc_{n,m}\{4\}|$ values are much smaller than those for $ac_2\{3\}$. The systematic uncertainties are generally similar among the two- and three- and four-subevent methods, but are different from those for the standard method, which is strongly

influenced by non-flow correlations. The following discussion focuses on the three-subevent method, which is the default method used to present the final results.

The effect of detector azimuthal non-uniformity is accounted for using the weight factor $d(\phi, \eta)$. The impact of the weighting procedure is studied by fixing the weight to unity and repeating the analysis. The results are mostly consistent with the nominal results. The corresponding uncertainties for $sc_{n,m}\{4\}$ vary in the range of 0–4%, 0–2% and 1–2% in pp , p +Pb and Pb+Pb collisions, respectively. The uncertainties for $ac_2\{3\}$ vary in the range of 0–2% in pp collisions, and 0–1% in p +Pb and Pb+Pb collisions, respectively.

The systematic uncertainty associated with the track selection is estimated by tightening the $|d_0|$ and $|z_0 \sin \theta|$ requirements. They are each varied from the default requirement of less than 1.5 mm to less than 1 mm. In p +Pb and Pb+Pb collisions, the requirement on the significance of impact parameters, $|d_0|/\sigma_{d_0}$ and $|z_0 \sin \theta|/\sigma_{z_0}$ are also varied from less than 3 to less than 2. For each variation, the tracking efficiency is re-evaluated and the analysis is repeated. For $ac_2\{3\}$, which has a large flow signal, the differences from the nominal results are observed to be less than 2% for all collision systems. For $sc_{n,m}\{4\}$, for which the signal is small, the differences from the nominal results are found to be in the range of 2–10% in pp collisions, 2–7% in p +Pb collisions and 2–4% in Pb+Pb collisions. The differences are smaller for results obtained for $0.5 < p_T < 5$ GeV than those obtained for $0.3 < p_T < 3$ GeV.

Previous measurements indicate that the azimuthal correlations (both the flow and non-flow components) have a strong dependence on p_T , but a relatively weak dependence on η [5,7]. Therefore, p_T -dependent systematic effects in the track reconstruction efficiency could affect the cumulant values. The uncertainty in the track reconstruction efficiency is mainly due to differences in the detector conditions and material description between the simulation and the data. The efficiency uncertainty varies between 1% and 4%, depending on track η and p_T [7,17]. Its impact on multi-particle cumulants is evaluated by repeating the analysis with the tracking efficiency varied up and down by its corresponding uncertainty as a function of track p_T . For the standard cumulant method, which is more sensitive to jets and dijets, the evaluated uncertainty amounts to 2–6% in pp collisions and less than 2% in p +Pb collisions for $\langle N_{ch} \rangle > 100$. For the subevent methods, the evaluated uncertainty is typically less than 3% for most of the $\langle N_{ch} \rangle$ ranges.

Most events in pp and p +Pb collisions are collected with the HMT triggers with several online N_{ch}^{rec} thresholds. In order to estimate the possible bias due to trigger inefficiency as a function of $\langle N_{ch} \rangle$, the offline N_{ch}^{rec} requirements are changed such that the HMT trigger efficiency is at least 50% or 80%. The results are obtained independently for each variation. These results are found to be consistent with each other for the subevent methods, and show some differences for the standard cumulant method in the low $\langle N_{ch} \rangle$ region. The nominal analysis is performed using the 50% efficiency selection and the differences between the nominal results and those from the 80% efficiency selection are included in the systematic uncertainty. The changes for pp collisions are in the range of 5–15% for $sc_{2,3}\{4\}$, 2–8% for $sc_{2,4}\{4\}$ and 1–5% for $ac_2\{3\}$. The ranges for p +Pb collisions are much smaller due to the much sharper turn-on of the trigger efficiency and larger signal: they are estimated to be 1–3% for $sc_{2,3}\{4\}$, 2–4% for $sc_{2,4}\{4\}$ and 1–2% for $ac_2\{3\}$.

In this analysis, a pile-up rejection criterion is applied to reject events containing additional vertices in pp and p +Pb collisions. In order to check the impact of residual pile-up, the analysis is repeated without the pile-up rejection criterion. No differences are observed in p +Pb collisions, as is expected since the μ values in p +Pb are modest. For the 13 TeV pp dataset, the differences with

and without pile-up rejection are in the range of 0–7% for $sc_{2,3}\{4\}$, 2–15% for $sc_{2,4}\{4\}$ and 2–3% for $ac_2\{3\}$. As a cross-check, the pp data are divided into two samples with approximately equal number of events based on the μ value: $\mu > 0.4$ and $\mu < 0.4$, and the results are compared. No systematic differences are observed between the two independent datasets.

The systematic uncertainties from different sources are added in quadrature to determine the total systematic uncertainty. In p +Pb and Pb+Pb collisions, the total uncertainties are in the range of 3–8% for $sc_{2,3}\{4\}$, 1–5% for $sc_{2,4}\{4\}$ and 1–4% for $ac_2\{3\}$. In pp collisions, the total uncertainties are larger, mainly due to larger non-flow contribution, larger pile-up and the less sharp turn-on of the HMT triggers. They are in the ranges of 10–20% for $sc_{2,3}\{4\}$, 10–20% for $sc_{2,4}\{4\}$ and 2–5% for $ac_2\{3\}$. The total systematic uncertainties are generally smaller than the statistical uncertainties.

The $v_n\{2\}$ values used to obtain normalised cumulants from Eqs. (11)–(13) are measured following the prescription of the previous ATLAS publications [7,14], resulting in very similar systematic uncertainties. The correction for the bias of the template fit procedure, as described in Section 6, reduces the sensitivity to the choice of the peripheral N_{ch}^{rec} bin. The uncertainties of normalised cumulants are obtained by propagation of the uncertainties from the original cumulants and $v_n\{2\}$, taking into account that the correlated systematic uncertainties partially cancel out.

8. Results

The results are presented in two parts. Section 8.1 presents a detailed comparison between the standard method and subevent methods to demonstrate the ability of the subevent methods to suppress non-flow correlations. Section 8.2 compares the cumulants among pp , p +Pb and Pb+Pb collisions to provide insight into the common nature of collectivity in these systems.

8.1. Comparison between standard and subevent methods

The top row of Fig. 1 compares the $sc_{2,3}\{4\}$ values obtained from the standard, two-, three- and four-subevent methods from pp collisions in $0.3 < p_T < 3$ GeV (left panel) and $0.5 < p_T < 5$ GeV (right panel). The values from the standard method are positive over the full $\langle N_{ch} \rangle$ range, and are larger at lower $\langle N_{ch} \rangle$ or in the higher p_T range. This behaviour suggests that the $sc_{2,3}\{4\}$ values from the standard method in pp collisions, including those from Ref. [19], are strongly influenced by non-flow effects in all $\langle N_{ch} \rangle$ and p_T ranges [16]. In contrast, the values from the subevent methods are negative over the full $\langle N_{ch} \rangle$ range, and they are slightly more negative at lowest $\langle N_{ch} \rangle$ and also more negative at higher p_T . The results are consistent among the various subevent methods for $0.3 < p_T < 3$ GeV. For the high p_T region of $0.5 < p_T < 5$ GeV, results from the two-subevent method are systematically lower than those from the three- and four-subevent methods, suggesting that the two-subevent method may be affected by negative non-flow contributions. Such negative non-flow correlation has been observed in a PYTHIA8 calculation [16].

The middle row of Fig. 1 shows $sc_{2,3}\{4\}$ from p +Pb collisions. At $\langle N_{ch} \rangle > 140$, the values are negative and consistent among all four methods, reflecting genuine long-range collective correlations. At $\langle N_{ch} \rangle < 140$, the values are different between the standard method and the subevent methods. The $sc_{2,3}\{4\}$ from the standard method changes sign around $\langle N_{ch} \rangle \sim 80$ and remains positive at lower $\langle N_{ch} \rangle$, reflecting the contribution from non-flow correlations. In contrast, the $sc_{2,3}\{4\}$ from various subevent methods are negative and consistent with each other at $\langle N_{ch} \rangle < 140$, suggesting that they mainly reflect the genuine long-range correlations.

The bottom row of Fig. 1 shows $sc_{2,3}\{4\}$ from Pb+Pb collisions. The results are consistent among all four methods across most of the $\langle N_{ch} \rangle$ range. In the low $\langle N_{ch} \rangle$ region, where the non-flow contribution is expected to be significant, the uncertainties of the results are too large to distinguish between different methods.

The results for the symmetric cumulant $sc_{2,4}\{4\}$ are presented in Fig. 2. The top row shows the $sc_{2,4}\{4\}$ obtained from the standard, two-subevent, three-subevent and four-subevent methods from pp collisions in $0.3 < p_T < 3$ GeV (left panel) and $0.5 < p_T < 5$ GeV (right panel). The values of $sc_{2,4}\{4\}$ are positive for all four methods. However, the results from the standard method are much larger than those from the subevent methods and also exhibit a much stronger increase towards the lower $\langle N_{ch} \rangle$ region. This behaviour is consistent with the expectation that the standard method is more affected by dijets. Significant differences are also observed between the two-subevent and three- or four-subevent methods at low $\langle N_{ch} \rangle$, but these differences decrease and disappear for $\langle N_{ch} \rangle > 100$. Within the statistical uncertainties of the measurement, no differences are observed between the three- and four-subevent methods. This comparison suggests that the two-subevent method may not be sufficient to reject non-flow correlations from dijets in pp collisions, and methods with three or more subevents are required to suppress the non-flow contribution over the measured $\langle N_{ch} \rangle$ range.

The middle row of Fig. 2 shows $sc_{2,4}\{4\}$ from p +Pb collisions. Significant differences are observed between the standard method and the subevent methods over the full $\langle N_{ch} \rangle$ range. However, no differences are observed among the various subevent methods. These results suggest that the standard method is contaminated by large contributions from non-flow correlations at low $\langle N_{ch} \rangle$, and these contributions may not vanish even at large $\langle N_{ch} \rangle$ values. All subevent methods suggest an increase of $sc_{2,4}\{4\}$ toward lower $\langle N_{ch} \rangle$ for $\langle N_{ch} \rangle < 40$, which may reflect some residual non-flow correlations in this region.

The bottom row of Fig. 2 shows $sc_{2,4}\{4\}$ from Pb+Pb collisions. The $sc_{2,4}\{4\}$ values increase gradually with $\langle N_{ch} \rangle$ for all four methods. This increase reflects the known fact that the v_2 increases with $\langle N_{ch} \rangle$ in Pb+Pb collisions [37]. The values from the standard method are systematically larger than those from the subevent methods, and this difference varies slowly with $\langle N_{ch} \rangle$, similar to the behaviour observed in p +Pb collisions in the high $\langle N_{ch} \rangle$ region.

The results for the asymmetric cumulant $ac_2\{3\}$ are presented in Fig. 3. The top row shows the results obtained from the standard, two-subevent, and three-subevent methods from pp collisions in $0.3 < p_T < 3$ GeV (left panel) and $0.5 < p_T < 5$ GeV (right panel). The results are positive for all methods. The results from the standard method are much larger than those from the subevent methods, consistent with the expectation that the standard method is more affected by non-flow correlations from dijets. Significant differences are also observed between the two-subevent and three-subevent methods at low $\langle N_{ch} \rangle$, but these differences decrease and disappear at $\langle N_{ch} \rangle > 100$. The $ac_2\{3\}$ values from the three-subevent method show a slight increase for $\langle N_{ch} \rangle < 40$ but are nearly constant for $\langle N_{ch} \rangle > 40$. This behaviour suggests that in the three-subevent method, the non-flow contribution may play some role at $\langle N_{ch} \rangle < 40$, but is negligible for $\langle N_{ch} \rangle > 40$. Therefore, the $ac_2\{3\}$ from the three-subevent method supports the existence of a three-particle long-range collective flow that is nearly independent of $\langle N_{ch} \rangle$ in pp collisions, consistent with the $\langle N_{ch} \rangle$ -independent behaviour of v_2 and v_4 observed previously in the two-particle correlation analysis [7].

The middle and bottom rows of Fig. 3 show $ac_2\{3\}$ from p +Pb and Pb+Pb collisions, respectively. The $ac_2\{3\}$ values from the standard method have a significant non-flow contribution up to

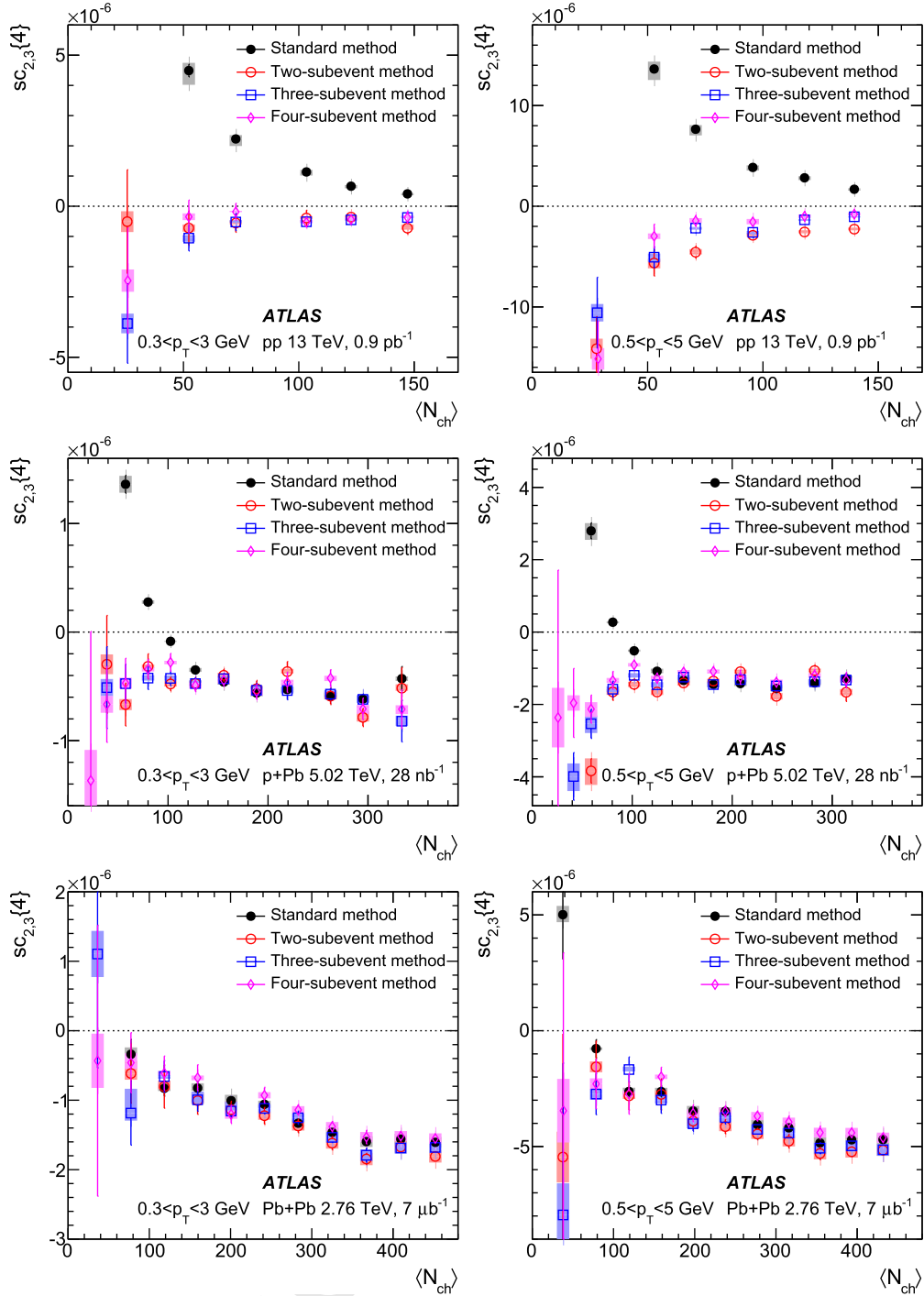


Fig. 1. The symmetric cumulant $sc_{2,3}\{4\}$ as a function of $\langle N_{ch} \rangle$ for $0.3 < p_T < 3$ GeV (left panels) and $0.5 < p_T < 5$ GeV (right panels) obtained for pp collisions (top row), $p+Pb$ collisions (middle row) and low-multiplicity $Pb+Pb$ collisions (bottom row). In each panel, the $sc_{2,3}\{4\}$ is obtained from the standard method (filled symbol), the two-subevent method (open circles), three-subevent method (open squares) and four-subevent method (open diamonds). The error bars and shaded boxes represent the statistical and systematic uncertainties, respectively.

$\langle N_{ch} \rangle \sim 200$ in $p+Pb$ collisions and $\langle N_{ch} \rangle \sim 80$ in $Pb+Pb$ collisions. In the subevent methods, the influence of non-flow contributions is very small for $\langle N_{ch} \rangle > 60$ in both collision systems, and therefore the $\langle N_{ch} \rangle$ dependence of $ac_2\{3\}$ reflects the $\langle N_{ch} \rangle$ dependence of the v_2 and v_4 . The $ac_2\{3\}$ values from the subevent methods increase with $\langle N_{ch} \rangle$, and the increase is stronger in $Pb+Pb$ collisions. This is consistent with previous observations that v_2 and v_4 increase with $\langle N_{ch} \rangle$ more strongly in $Pb+Pb$ than in $p+Pb$ collisions [17].

The values of $sc_{2,4}\{4\}$ and $ac_2\{3\}$, which are both measures of correlations between v_2 and v_4 , show significant differences between the standard method and the subevent methods, as shown in Figs. 2 and 3. The $\langle N_{ch} \rangle$ dependence of these differences decreases gradually with $\langle N_{ch} \rangle$, and is consistent with an influence of non-flow that is expected to scale as $1/\langle N_{ch} \rangle$. However, these differences seem to persist for $\langle N_{ch} \rangle > 200$ in $p+Pb$ collisions and for $\langle N_{ch} \rangle > 150$ in $Pb+Pb$ collisions, which is not compatible with the predicted behaviour of non-flow correlations. The differences at

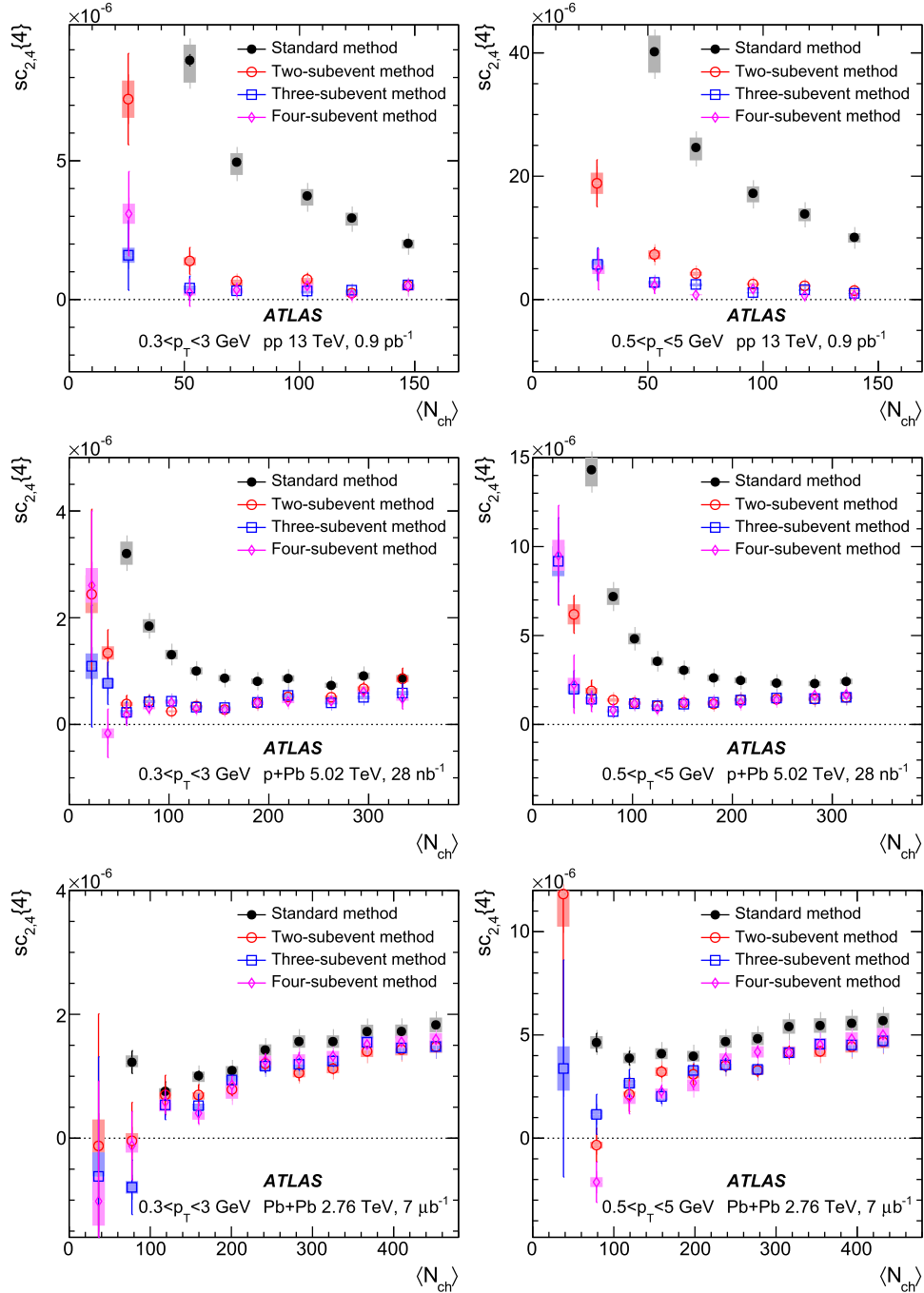


Fig. 2. The symmetric cumulant $sc_{2,4}\{4\}$ as a function of $\langle N_{ch} \rangle$ for $0.3 < p_T < 3$ GeV (left panels) and $0.5 < p_T < 5$ GeV (right panels) obtained for pp collisions (top row), $p+Pb$ collisions (middle row) and low-multiplicity $Pb+Pb$ collisions (bottom row). In each panel, the $sc_{2,4}\{4\}$ is obtained from the standard method (filled symbol), two-subevent method (open circles), three-subevent method (open squares) and four-subevent method (open diamonds). The error bars and shaded boxes represent the statistical and systematic uncertainties, respectively.

large $\langle N_{ch} \rangle$ may arise from longitudinal flow decorrelations [38,39], which have been measured by CMS [40] and ATLAS [41]. Decorrelation effects are found to be large for v_4 and strongly correlated with v_2 , and therefore they are expected to reduce the $sc_{2,4}\{4\}$ and $ac_2\{3\}$ in the subevent method. Therefore, the observed differences between the standard method and subevent method reflect the combined contribution from non-flow correlations, which dominates in the low $\langle N_{ch} \rangle$ region, and decorrelation, which is more important at large $\langle N_{ch} \rangle$ (see further discussion in the Appendix B).

The results presented above suggest that the three-subevent method is sufficient to suppress most of the non-flow effects. It is therefore used as the default method for the discussion below.

8.2. Comparison between collision systems

Fig. 4 shows a direct comparison of cumulants for the three collision systems. The three panels in the top row show the results for $sc_{2,3}\{4\}$, $sc_{2,4}\{4\}$ and $ac_2\{3\}$, respectively, for $0.3 < p_T < 3$ GeV. These results support the existence of a negative correlation between v_2 and v_3 and a positive correlation between v_2 and v_4 .

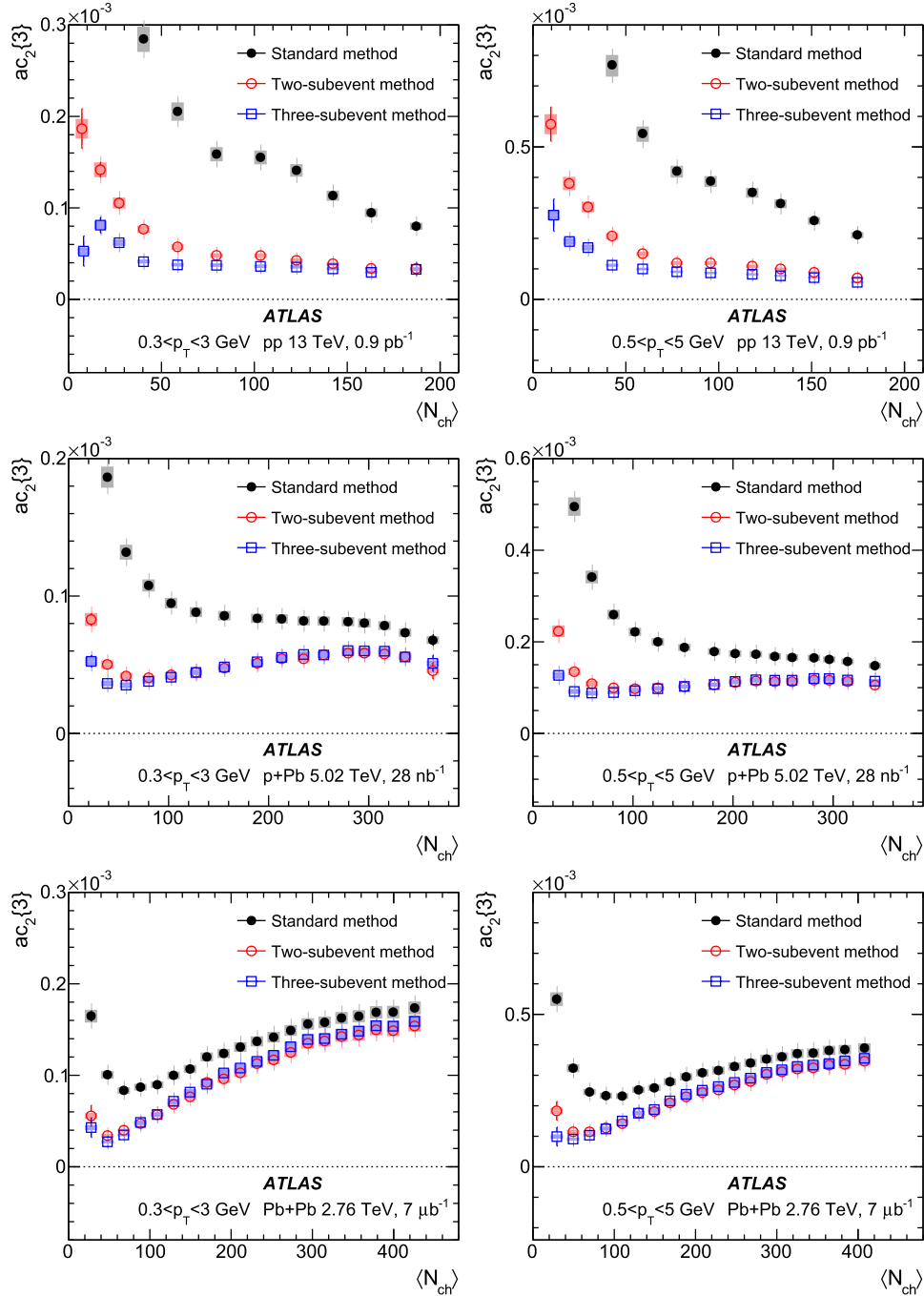


Fig. 3. The asymmetric cumulant $ac_2\{3\}$ as a function of $\langle N_{ch} \rangle$ for $0.3 < p_T < 3$ GeV (left panels) and $0.5 < p_T < 5$ GeV (right panels) obtained for pp collisions (top row), $p+Pb$ collisions (middle row) and low-multiplicity $Pb+Pb$ collisions (bottom row). In each panel, the $ac_2\{3\}$ is obtained from the standard method (filled symbol), two-subevent method (open circles), and three-subevent method (open squares). The error bars and shaded boxes represent the statistical and systematic uncertainties, respectively.

Such correlation patterns have previously been observed in large collision systems [42–44], but are now confirmed also in the small collision systems, once non-flow effects are adequately suppressed. In the multiplicity range covered by the pp collisions, $\langle N_{ch} \rangle < 150$, the results for symmetric cumulants $sc_{2,3}\{4\}$ and $sc_{2,4}\{4\}$ are similar among the three systems. In the range $\langle N_{ch} \rangle > 150$, $|sc_{2,3}\{4\}|$ and $sc_{2,4}\{4\}$ are larger in $Pb+Pb$ than in $p+Pb$ collisions. The results for $ac_2\{3\}$ are similar among the three systems at $\langle N_{ch} \rangle < 100$, but they deviate from each other at higher $\langle N_{ch} \rangle$. The pp data are approximately constant or decrease slightly with $\langle N_{ch} \rangle$, while the $p+Pb$ and $Pb+Pb$ data show significant increases as a function of

$\langle N_{ch} \rangle$. The bottom row shows the results for the higher p_T range of $0.5 < p_T < 5$ GeV, where similar trends are observed.

Fig. 5 shows the results for normalised cumulants, $nsc_{2,3}\{4\}$, $nsc_{2,4}\{4\}$ and $nac_2\{3\}$, compared among the three systems. The normalised cumulants generally show a much weaker $\langle N_{ch} \rangle$ dependence at $\langle N_{ch} \rangle > 100$, where the statistical uncertainties are small. This behaviour implies that the strong $\langle N_{ch} \rangle$ dependence of the $sc_{n,m}\{4\}$ and $ac_2\{3\}$ values reflects the $\langle N_{ch} \rangle$ dependence of the v_n values, and these dependences are removed in the normalised cumulants. The normalised cumulants are also similar among different collision systems at large $\langle N_{ch} \rangle$, although some differences

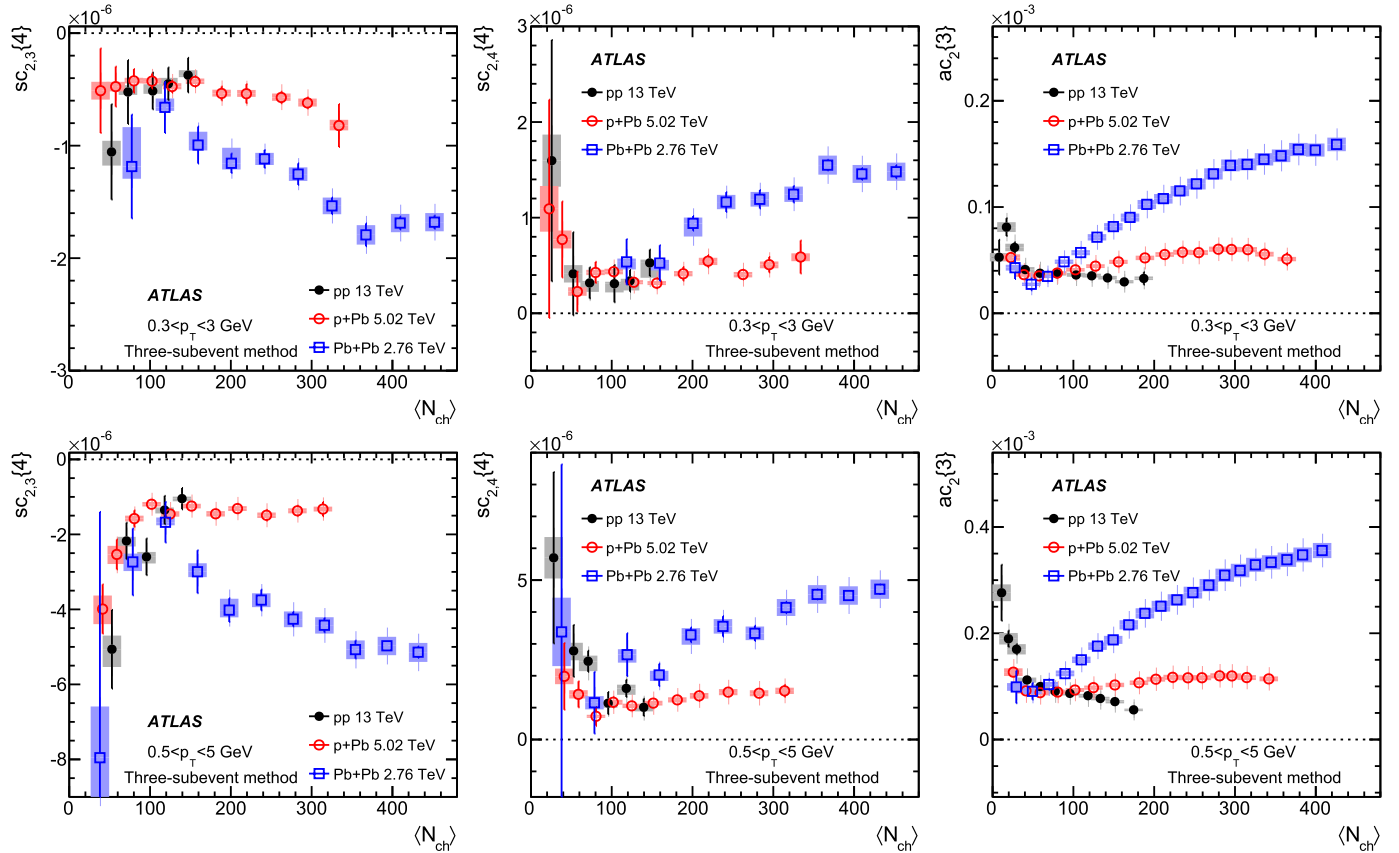


Fig. 4. The $\langle N_{ch} \rangle$ dependence of $sc_{2,3}\{4\}$ (left panels), $sc_{2,4}\{4\}$ (middle panels) and $ac_2\{3\}$ (right panels) in $0.3 < p_T < 3$ GeV (top row) and $0.5 < p_T < 5$ GeV (bottom row) obtained for pp collisions (solid circles), $p+Pb$ collisions (open circles) and low-multiplicity $Pb+Pb$ collisions (open squares). The error bars and shaded boxes represent the statistical and systematic uncertainties, respectively.

at the relative level of 20–30% are observed for smaller $\langle N_{ch} \rangle$. The only exception is $nsc_{2,3}\{4\}$, whose values in the pp collisions are very different from those in $p+Pb$ and $Pb+Pb$ collisions. In contrast, the $sc_{2,3}\{4\}$ values in Fig. 4 are close among different systems. This suggests that the $\langle v_2^2 \rangle$ values from the template fit method [7] may be significantly underestimated. As pointed out in Ref. [7] and emphasised in Appendix A, the template fit method, and other methods based on peripheral subtraction in general [5,15], tend to underestimate the odd flow harmonics, due to the presence of a large away-side peak at $\Delta\phi \sim \pi$ in the two-particle correlation function. The comparison of $sc_{2,3}\{4\}$ and $nsc_{2,3}\{4\}$ among different collision systems provides indirect evidence of this underestimation of $\langle v_2^2 \rangle$.

Fig. 5 shows that the normalised cumulants are consistent between $0.3 < p_T < 3$ GeV and $0.5 < p_T < 5$ GeV. On the other hand, the magnitudes of the cumulants in Fig. 4 differ by a large factor between the two p_T ranges: about a factor of three for $sc_{2,3}\{4\}$ and $sc_{2,4}\{4\}$, and a factor of two for $ac_2\{3\}$. These results suggest that the p_T dependence of $sc_{2,3}\{4\}$, $sc_{2,4}\{4\}$ and $ac_2\{3\}$ largely reflects the p_T dependence of the v_n at the single-particle level.

9. Discussion

Three- and four-particle cumulants involving correlations between two harmonics of different order v_n and v_m are measured in $\sqrt{s} = 13$ TeV pp , $\sqrt{s_{NN}} = 5.02$ TeV $p+Pb$, and low-multiplicity $\sqrt{s_{NN}} = 2.76$ TeV $Pb+Pb$ collisions with the ATLAS detector at the LHC, with total integrated luminosities of 0.9 pb^{-1} , 28 nb^{-1} , and $7 \text{ } \mu\text{b}^{-1}$, respectively. The correlation between v_n and v_m is studied using four-particle symmetric cumulants, $sc_{2,3}\{4\}$ and

$sc_{2,4}\{4\}$, and the three-particle asymmetric cumulant $ac_2\{3\}$. The symmetric cumulants $sc_{n,m}\{4\} = \langle v_n^2 v_m^2 \rangle - \langle v_n^2 \rangle \langle v_m^2 \rangle$ probe the correlation of the flow magnitudes, while the asymmetric cumulant $ac_2\{3\} = \langle v_2^2 v_4 \cos 4(\Phi_2 - \Phi_4) \rangle$ is sensitive to correlations involving both the flow magnitude v_n and flow phase Φ_n . They are calculated using the standard cumulant method, as well as the two-, three- and four-subevent methods to suppress non-flow effects. The final results are presented as a function of the average number of charged particles with $p_T > 0.4$ GeV, $\langle N_{ch} \rangle$.

Significant differences are observed between the standard method and the subevent methods over the full $\langle N_{ch} \rangle$ range in pp collisions, as well as over the low $\langle N_{ch} \rangle$ range in $p+Pb$ and $Pb+Pb$ collisions. The differences are larger for particles at higher p_T or at smaller $\langle N_{ch} \rangle$. When analysed with the standard method in pp collisions, this behaviour is compatible with the dominance of the non-flow correlations rather than the long-range collective flow correlations. Systematic, but much smaller, differences are also observed in the low $\langle N_{ch} \rangle$ region between the two-subevent method and three- or four-subevent methods, which indicate that the two-subevent method may still be affected by correlations arising from jets. On the other hand no differences are observed between the three-subevent and four-subevent methods, within experimental uncertainties, suggesting that methods with three or more subevents are sufficient to reject non-flow correlations from jets. Therefore, the three-subevent method is used to present the main results in this analysis.

The three-subevent method provides a measurement of negative $sc_{2,3}\{4\}$ and positive $sc_{2,4}\{4\}$ and $ac_2\{3\}$ over nearly the full $\langle N_{ch} \rangle$ range and in all three collision systems. These results indicate a negative correlation between v_2 and v_3 and a positive

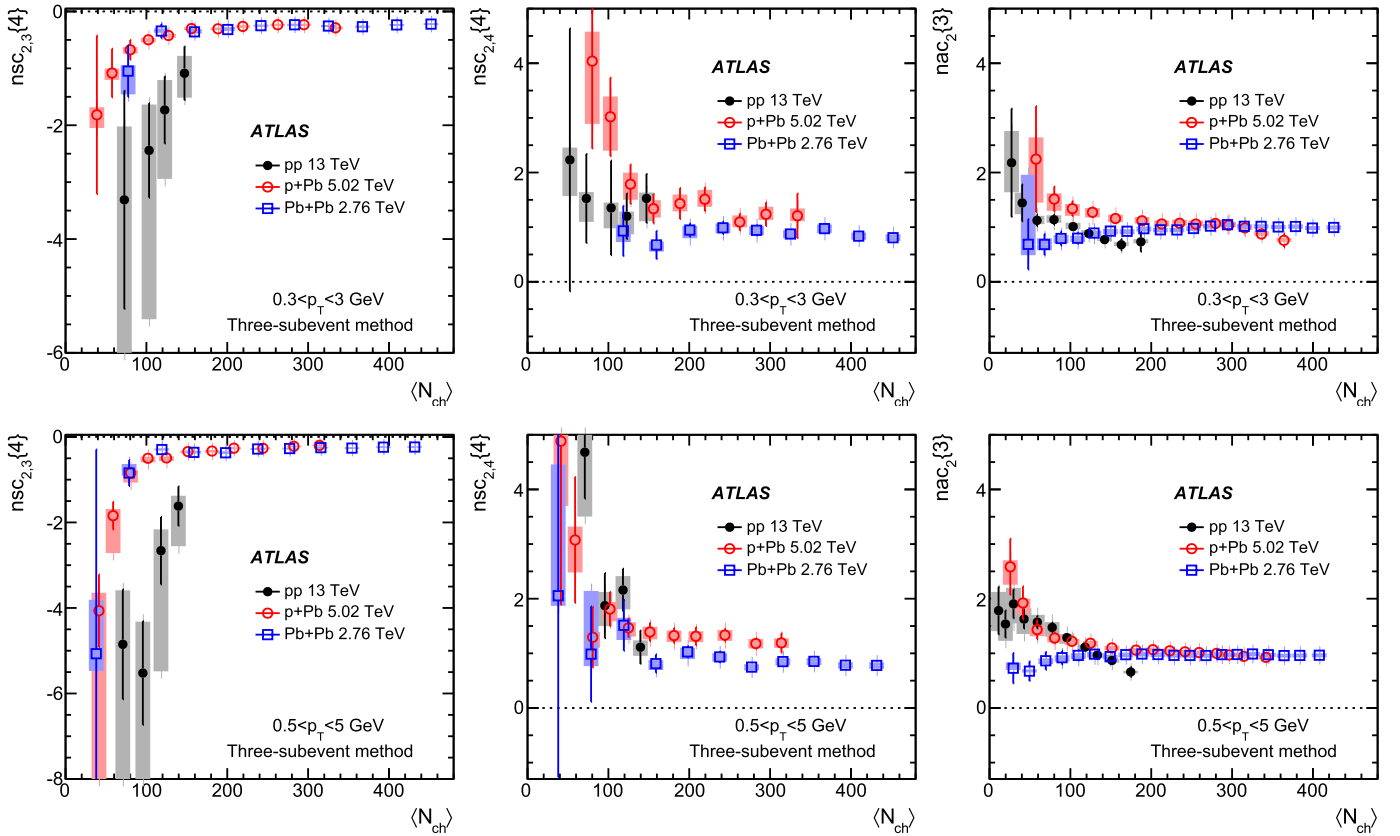


Fig. 5. The $\langle N_{ch} \rangle$ dependence of $nsc_{2,3}\{4\}$ (left panels), $nsc_{2,4}\{4\}$ (middle panels) and $nac_2\{3\}$ (right panels) in $0.3 < p_T < 3$ GeV (top row) and $0.5 < p_T < 5$ GeV (bottom row) obtained for pp collisions (solid circles), $p+Pb$ collisions (open circles) and low-multiplicity $Pb+Pb$ collisions (open squares). The error bars and shaded boxes represent the statistical and systematic uncertainties, respectively.

correlation between v_2 and v_4 . Such correlation patterns have previously been observed in large collision systems [42–44], but are now confirmed in small collision systems, once non-flow effects are adequately suppressed. The values of $sc_{2,3}\{4\}$ and $sc_{2,4}\{4\}$ are consistent in pp and $p+Pb$ collisions over the same $\langle N_{ch} \rangle$ range, but their magnitudes at large $\langle N_{ch} \rangle$ are much smaller than those for $Pb+Pb$ collisions. The values of $ac_2\{3\}$ are similar at very low $\langle N_{ch} \rangle$ among the three systems, but are very different at large $\langle N_{ch} \rangle$. On the other hand, after scaling by the $\langle v_n^2 \rangle$ estimated from a two-particle analysis [7,14], the resulting normalised cumulants $nsc_{2,3}\{4\}$, $nsc_{2,4}\{4\}$ and $nac_2\{3\}$ show a much weaker dependence on $\langle N_{ch} \rangle$, and their values are much closer to each other among the three systems. The magnitudes of the normalised cumulants are also similar to each other for $0.5 < p_T < 5$ GeV as well as $0.3 < p_T < 3$ GeV. This suggests that the $\langle N_{ch} \rangle$, p_T and system dependence of the $sc_{2,3}\{4\}$, $sc_{2,4}\{4\}$ and $ac_2\{3\}$ reflect mostly the $\langle N_{ch} \rangle$, p_T and system dependence of $\langle v_n^2 \rangle$, but the relative strengths of the correlations are similar for the three collision systems.

The new results obtained with the subevent cumulant technique provide further evidence that the ridge is indeed a long-range collective phenomenon involving many particles distributed across a broad rapidity interval. The similarity between different collision systems for $nsc_{2,3}\{4\}$, $nsc_{2,4}\{4\}$ and $nac_2\{3\}$, and the weak dependence of these observables on the p_T range and $\langle N_{ch} \rangle$, largely free from non-flow effects, provide an important input towards understanding the space-time dynamics and the properties of the medium created in small collision systems. These results provide inputs to distinguish between models based on initial-state momentum correlations and models based on final-state hydrodynamics.

Acknowledgements

We thank CERN for the very successful operation of the LHC, as well as the support staff from our institutions without whom ATLAS could not be operated efficiently.

We acknowledge the support of ANPCyT, Argentina; YerPhI, Armenia; ARC, Australia; BMWFW and FWF, Austria; ANAS, Azerbaijan; SSTC, Belarus; CNPq and FAPESP, Brazil; NSERC, NRC and CFI, Canada; CERN; CONICYT, Chile; CAS, MOST and NSFC, China; COLCIENCIAS, Colombia; MSMT CR, MPO CR and VSC CR, Czech Republic; DNRF and DNSRC, Denmark; IN2P3-CNRS, CEA-DRF/IRFU, France; SRNSFG, Georgia; BMBF, HGF, and MPG, Germany; GSRT, Greece; RGC, Hong Kong SAR, China; ISF and Ben-Zvi Center, Israel; INFN, Italy; MEXT and JSPS, Japan; CNRS, Morocco; NWO, Netherlands; RCN, Norway; MNiSW and NCN, Poland; FCT, Portugal; MNE/IFA, Romania; MES of Russia and NRC KI, Russian Federation; JINR; MESTD, Serbia; MSSR, Slovakia; ARRS and MIZŠ, Slovenia; DST/NRF, South Africa; MINECO, Spain; SRC and Wallenberg Foundation, Sweden; SERI, SNSF and Cantons of Bern and Geneva, Switzerland; MOST, Taiwan; TAEK, Turkey; STFC, United Kingdom; DOE and NSF, United States of America. In addition, individual groups and members have received support from BCKDF, the Canada Council, CANARIE, CRC, Compute Canada, FQRNT, and the Ontario Innovation Trust, Canada; EPLANET, ERC, ERDF, FP7, Horizon 2020 and Marie Skłodowska-Curie Actions, European Union; Investissements d'Avenir Labex and Idex, ANR, Région Auvergne and Fondation Partager le Savoir, France; DFG and AvH Foundation, Germany; Herakleitos, Thales and Aristeia programmes co-financed by EU-ESF and the Greek NSRF; BSF, GIF and Minerva, Israel; BRF, Norway; CERCA Programme Generalitat de Catalunya, Generalitat

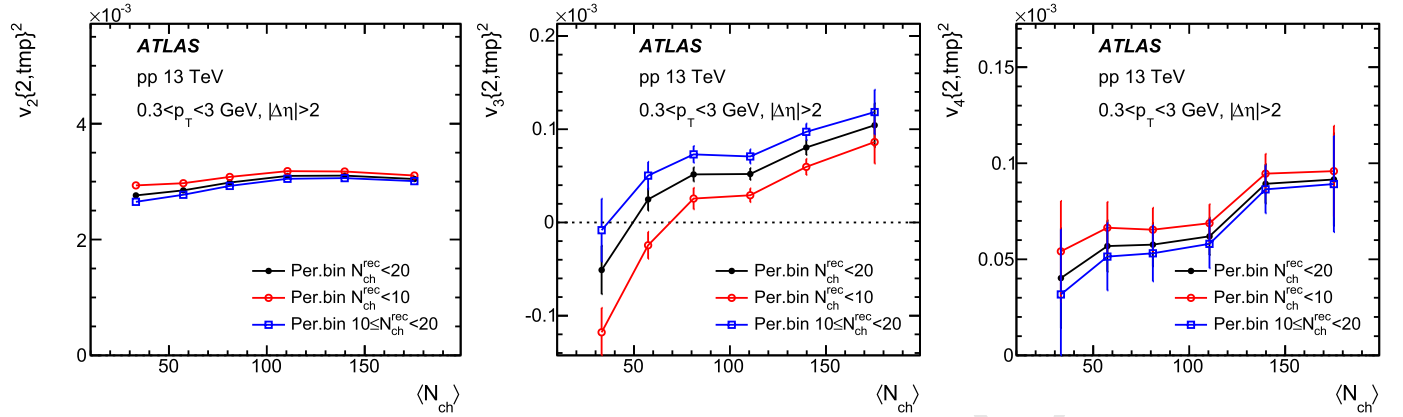


Fig. 6. The values of $v_n\{2, \text{tmp}\}^2$ obtained following the template fit procedure given in Eq. (14) [7] in pp collisions for $n = 2$ (left panel), $n = 3$ (middle panel) and $n = 4$ (right panel). In each panel, the values are calculated for three peripheral $N_{\text{ch}}^{\text{rec}}$ intervals: $N_{\text{ch}}^{\text{rec}} < 20$, $N_{\text{ch}}^{\text{rec}} < 10$ and $10 \leq N_{\text{ch}}^{\text{rec}} < 20$. Only statistical uncertainties are shown.

Valenciana, Spain; the Royal Society and Leverhulme Trust, United Kingdom.

The crucial computing support from all WLCG partners is acknowledged gratefully, in particular from CERN, the ATLAS Tier-1 facilities at TRIUMF (Canada), NDGF (Denmark, Norway, Sweden), CC-IN2P3 (France), KIT/GridKA (Germany), INFN-CNAF (Italy), NL-T1 (Netherlands), PIC (Spain), ASGC (Taiwan), RAL (UK) and BNL (USA), the Tier-2 facilities worldwide and large non-WLCG resource providers. Major contributors of computing resources are listed in Ref. [45].

Appendix A. Improvement to the template fit procedure

In order to separate the long-range ridge from other non-flow sources, especially dijets, the ATLAS Collaboration developed a template fitting procedure described in Refs. [7,14]. The first step is to construct a $\Delta\phi$ distribution of particle pairs with large pseudorapidity separation $|\Delta\eta| > 2$, the so-called “per-trigger” particle yield, $Y(\Delta\phi)$, for a given $N_{\text{ch}}^{\text{rec}}$ range. The $|\Delta\eta| > 2$ requirement suppresses the intra-jet and other short-range correlations, and in small collision systems the resulting $Y(\Delta\phi)$ distributions are known to be dominated by away-side jet correlations [4,5,14]. This away-side non-flow component is peaked at $\Delta\phi \sim \pi$, and leads to a significant bias in the flow coefficients v_n , especially for the odd harmonics.

To subtract the away-side jet correlations, the measured $Y(\Delta\phi)$ distribution in a given $N_{\text{ch}}^{\text{rec}}$ interval is assumed to be a sum of a scaled “peripheral” distribution $Y(\Delta\phi)^{\text{peri}}$, obtained for low-multiplicity events $N_{\text{ch}}^{\text{rec}} < 20$, and a constant pedestal modulated by $\cos(n\Delta\phi)$ for $n \geq 2$ [7,14]:

$$Y(\Delta\phi) = F Y(\Delta\phi)^{\text{peri}} + G^{\text{tmp}} \left(1 + 2 \sum_{n=2}^{\infty} v_n\{2, \text{tmp}\}^2 \cos n\Delta\phi \right). \quad (14)$$

The scale factor F and pedestal G^{tmp} are fixed by the fit, and $v_n\{2, \text{tmp}\}$ are calculated from a Fourier transform. On the other hand, both $Y(\Delta\phi)$ and $Y(\Delta\phi)^{\text{peri}}$ contain a dijet component and flow component:

$$Y(\Delta\phi) = Y(\Delta\phi)_{\text{jet}}^{\text{cent}} + G^{\text{cent}} \left(1 + 2 \sum_{n=2}^{\infty} v_n\{2\}^2 \cos n\Delta\phi \right), \quad (15)$$

$$Y(\Delta\phi)^{\text{peri}} = Y(\Delta\phi)_{\text{jet}}^{\text{peri}} + G^{\text{peri}} \left(1 + 2 \sum_{n=2}^{\infty} v_n\{2, \text{peri}\}^2 \cos n\Delta\phi \right). \quad (16)$$

With the assumption that the shape of the dijet component is independent of $N_{\text{ch}}^{\text{rec}}$, and the magnitudes of the dijet components are related by the scale factor F : $Y(\Delta\phi)_{\text{jet}}^{\text{cent}} = F Y(\Delta\phi)_{\text{jet}}^{\text{peri}}$, Eq. (14) can be written as:

$$Y(\Delta\phi) = Y(\Delta\phi)_{\text{jet}}^{\text{cent}} + (G^{\text{tmp}} + F G^{\text{peri}}) + 2 \sum_{n=2}^{\infty} \left(G^{\text{tmp}} v_n\{2, \text{tmp}\}^2 + F G^{\text{peri}} v_n\{2, \text{peri}\}^2 \right) \times \cos n\Delta\phi.$$

Comparing with Eqs. (15) and (16), one obtains $G^{\text{cent}} = G^{\text{tmp}} + F G^{\text{peri}}$ and the following relation:

$$v_n\{2\}^2 = v_n\{2, \text{tmp}\}^2 - \frac{F G^{\text{peri}}}{G^{\text{cent}}} \left(v_n\{2, \text{tmp}\}^2 - v_n\{2, \text{peri}\}^2 \right),$$

which shows that $v_n\{2, \text{tmp}\}$ from the template fit differs from the true $v_n\{2\}$ by a correction term that vanishes if and only if $v_n\{2\}$ is independent of $N_{\text{ch}}^{\text{rec}}$. Since the true flow harmonics in the peripheral interval $v_n\{2, \text{peri}\}$ are unknown in principle, the correction is applied starting from the third-lowest $N_{\text{ch}}^{\text{rec}}$ interval ($40 \leq N_{\text{ch}}^{\text{rec}} < 60$) in this analysis, by using $v_n\{2, \text{tmp}\}$ of the second $N_{\text{ch}}^{\text{rec}}$ interval ($20 \leq N_{\text{ch}}^{\text{rec}} < 40$) as an estimate of the true flow harmonics. Since the non-flow contribution primarily affects the odd harmonics, the $v_3\{2, \text{tmp}\}^2$ may become negative in the first few $N_{\text{ch}}^{\text{rec}}$ intervals in pp collisions. In such cases, the correction starts from the second $N_{\text{ch}}^{\text{rec}}$ interval with positive $v_3\{2, \text{tmp}\}^2$ ($60 \leq N_{\text{ch}}^{\text{rec}} < 80$) by using $v_3\{2, \text{tmp}\}$ from the previous $N_{\text{ch}}^{\text{rec}}$ interval ($40 \leq N_{\text{ch}}^{\text{rec}} < 60$).

One important feature of the template fit analysis is the assumption that the dijet component $Y(\Delta\phi)_{\text{jet}}$ is independent of $\langle N_{\text{ch}} \rangle$. In Ref. [7], the uncertainty associated with this assumption is studied by changing the default peripheral interval from $N_{\text{ch}}^{\text{rec}} < 20$ to $N_{\text{ch}}^{\text{rec}} < 10$ and $10 \leq N_{\text{ch}}^{\text{rec}} < 20$. It was found that the $v_n\{2, \text{tmp}\}$ values are relatively insensitive to the choice of peripheral interval for $n = 2$ and $n = 4$, but the sensitivity is much larger for $n = 3$. This finding is reproduced in Fig. 6 for pp collisions, which shows that the $v_3\{2, \text{tmp}\}^2$ values obtained via Eq. (14) differ substantially for the different $N_{\text{ch}}^{\text{rec}}$ ranges.

In addition to the template fit with and without the above mentioned correction procedure, the ATLAS and CMS collaborations

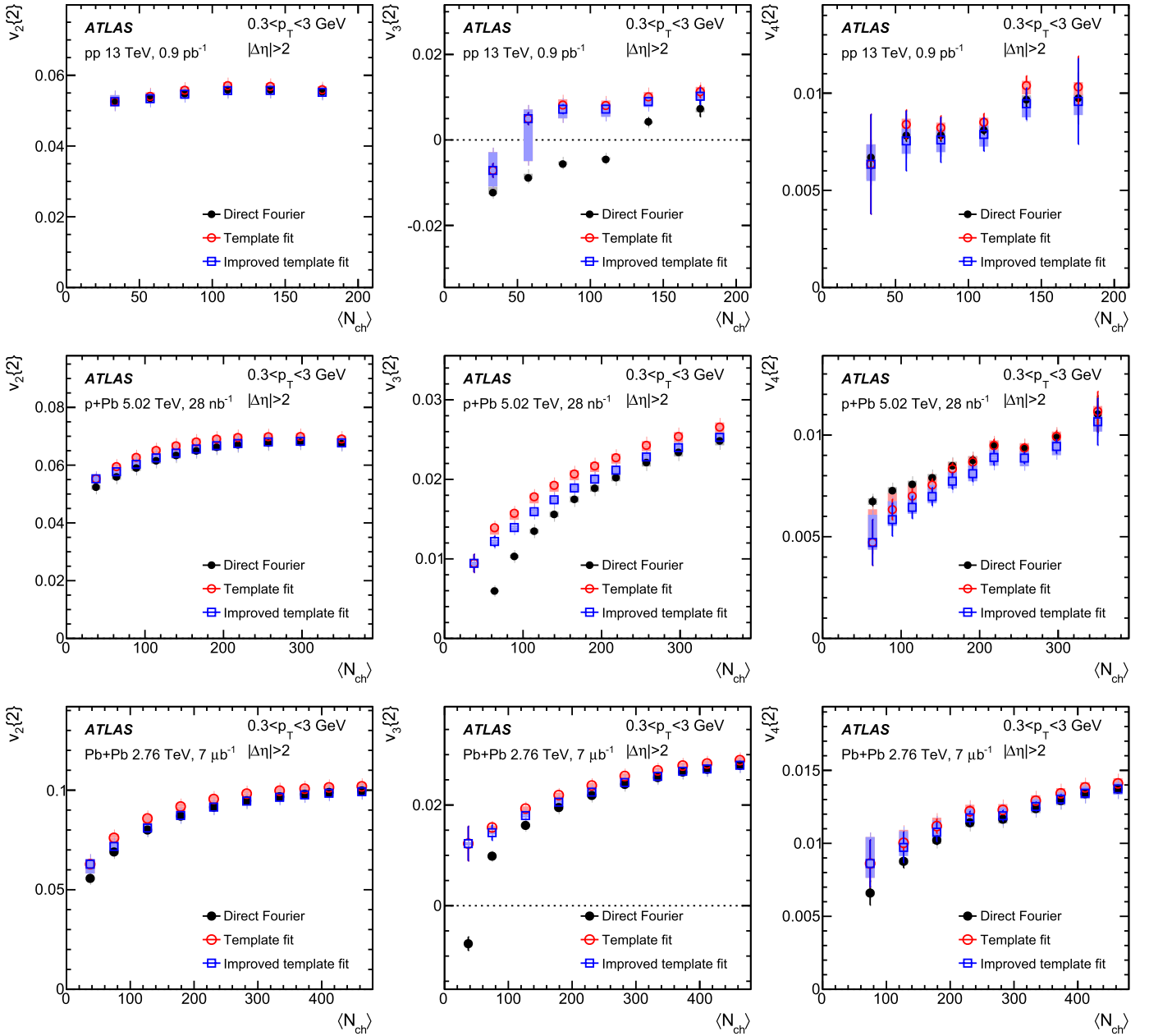


Fig. 7. The v_2 (left column), v_3 (middle column) and v_4 (right column) obtained from two-particle correlations in $0.3 < p_T < 3$ GeV in pp (top row), $p+Pb$ (middle row) and $Pb+Pb$ (bottom row) collisions. In each panel, they are compared between three methods: direct Fourier transformation (solid circles), template fit (open circles) and the improved template fit (open squares). The error bars and shaded boxes represent the statistical and systematic uncertainties, respectively.

also calculated directly the $v_n\{2\}$ values via a Fourier transform of the $Y(\Delta\phi)$ distribution without dijet subtraction [7,19]. The differences between the direct Fourier transform and template fit reflect mainly the away-side jet contribution subtracted by the template fit procedure, and therefore give a sense of the magnitude of unknown systematic uncertainties associated with the template fit procedure. If these differences are too large, the $v_n\{2, \text{tmp}\}$ values may be sensitive to the systematic effects associated with the assumption that the shape of $Y(\Delta\phi)_{\text{jet}}$ is independent of $N_{\text{ch}}^{\text{rec}}$.

Fig. 7 compares the $v_n\{2\}$ in $0.3 < p_T < 3$ GeV obtained from $Y(\Delta\phi)$ using three methods: a direct Fourier transform (solid circles), a template fit (open circles) and a template fit corrected for the bias (open squares), as described above. The systematic uncertainties for the template fit results are nearly the same as those from Ref. [7]. Fig. 7 shows that the changes introduced by

the correction procedure described above are small in all cases and for all harmonics. The values of the even-order harmonics, v_2 and v_4 , are also quite similar to those obtained from the direct Fourier transformation, reflecting the fact that the dijet correlations have very little influence on the even-order harmonics. On the other hand, significant differences are observed between the direct Fourier transform and template fit for v_3 , especially in the pp collisions, due to the influence of $Y(\Delta\phi)_{\text{jet}}$, a trend observed and discussed previously in Refs. [7,15]. The template fit procedure is able to subtract the dijet correlations and change the sign of v_3 , but also introduces a large uncertainty associated with the procedure. As discussed in Section 8.2, the behaviour of the symmetric cumulants $sc_{2,3}\{4\}$ in Fig. 4 and normalised cumulants $nsc_{2,3}\{4\}$ in Fig. 5 in pp collisions, suggest that the v_3 values from the template fit procedure are significantly underestimated due to the presence

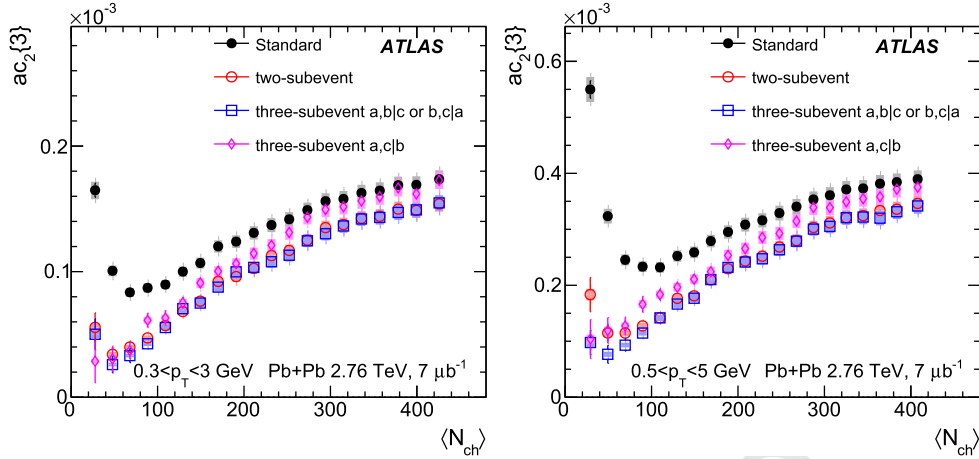


Fig. 8. The $ac_2\{3\}$ in $0.3 < p_T < 3$ GeV (left panel) and $0.5 < p_T < 5$ GeV (right panel) in Pb+Pb collisions. In each panel, they are compared between the standard method (solid circles), two-subevent method (open circles), three-subevent where V_4 is determined in subevent a or c (open boxes), and three-subevent where V_4 is determined in subevent b (diamonds) according to Eq. (8). The error bars and shaded boxes represent the statistical and systematic uncertainties, respectively.

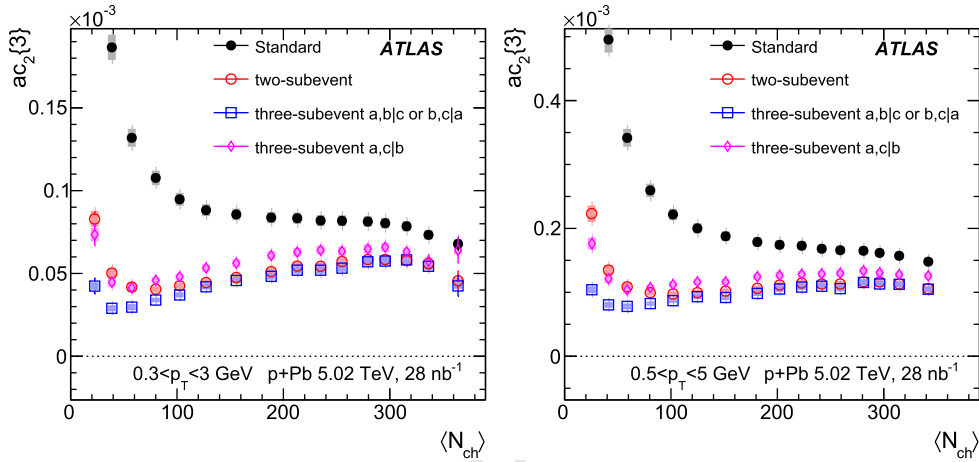


Fig. 9. The $ac_2\{3\}$ in $0.3 < p_T < 3$ GeV (left panel) and $0.5 < p_T < 5$ GeV (right panel) in p+Pb collisions. In each panel, they are compared between standard method (solid circles), two-subevent method (open circles), three-subevent where V_4 is determined in subevent a or c (open boxes), and three-subevent where V_4 is determined in subevent b (diamonds) according to Eq. (8). The error bars and shaded boxes represent the statistical and systematic uncertainties, respectively.

of a large residual non-flow bias. In contrast, the differences of v_3 between the direct Fourier transform and the template fit are much smaller in the p+Pb and the Pb+Pb collisions, except in the very low $\langle N_{ch} \rangle$ region. Therefore, the v_3 values in p+Pb and Pb+Pb systems extracted from the template fit procedure are expected to be less affected by the dijets.

Appendix B. Effects of flow decorrelations in the subevent cumulant methods

As discussed in Section 8, the differences between the standard method and subevent methods for $ac_2\{3\}$ can be partially attributed to longitudinal flow decorrelations [38,41]. Since subevent methods correlate flow vectors obtained from different η regions, the influence of decorrelations can be studied by comparing different variants of the three-subevent method. This comparison is carried out using asymmetric cumulant $ac_2 = \langle V_2^2 V_4^* \rangle$, however, the statistical precision of $sc_{n,m}\{4\}$ is not sufficient for such comparison.

The three-subevent method uses flow vectors from three subevents a , b and c , covering $-2.5 < \eta_a < -2.5/3$, $|\eta_b| \leq 2.5/3$ and $2.5/3 < \eta_c < 2.5$, and have three independent definitions for asymmetric cumulant: $ac_2^{a,b|c}\{3\}$, $ac_2^{b,c|a}\{3\}$ and $ac_2^{a,c|b}\{3\}$. Because

of symmetry between subevents a and c , $ac_2^{a,b|c}\{3\}$ and $ac_2^{b,c|a}\{3\}$ measure the same physics, and are therefore averaged into a single result, denoted as $ac_2^{a,b|c \text{ or } b,c|a}\{3\}$. Fig. 8 compares the two three-subevent results with results for the standard and two-subevent methods. The results based on various subevent methods show a small decrease with $\langle N_{ch} \rangle$ in the $\langle N_{ch} \rangle < 50$ region, reflecting a modest contribution from non-flow. On the other hand, all the subevent-based results increase gradually with $\langle N_{ch} \rangle$ for $\langle N_{ch} \rangle > 50$, reflecting a dominant contribution from flow.

Fig. 8 shows that the values of $ac_2^{a,c|b}\{3\} = \langle V_{2,a} V_{4,b}^* V_{2,c} \rangle$ are larger than $ac_2^{a,b|c \text{ or } b,c|a}\{3\}$ at larger $\langle N_{ch} \rangle$ region. This is because the subevent for V_4 is in between the two subevents used to calculate V_2 . This configuration has much smaller decorrelation effects [41]. For $ac_2^{a,b|c \text{ or } b,c|a}\{3\}$, the two subevents for V_2 are on the same side of the subevent for V_4 , leading to larger decorrelation effects. Interestingly, such configuration gives results that are very similar to those from the two-subevent method. Figs. 9 and 10 show the results for the p+Pb and pp collisions, respectively. Similar observations as in Pb+Pb collisions can be made, although in pp collisions the results from the two-subevent method are larger than those obtained with the three-subevent method, due to significant non-flow contribution even in the large $\langle N_{ch} \rangle$ region.

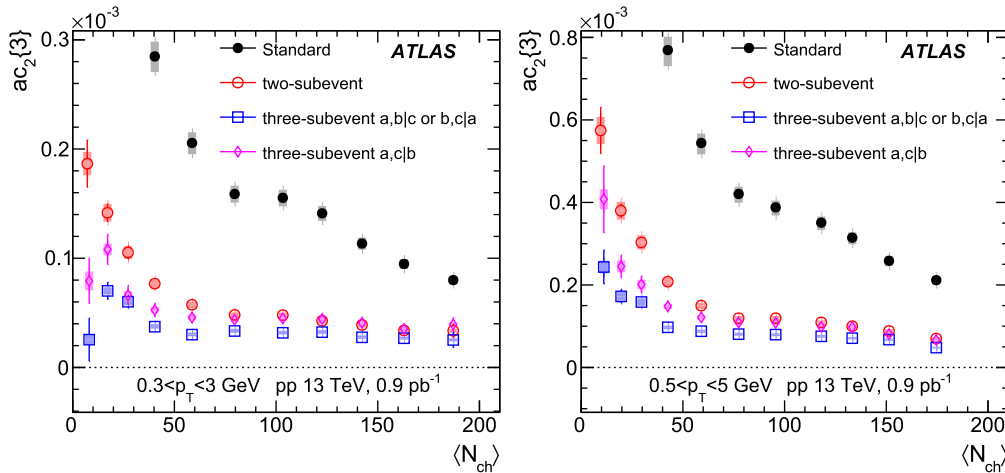


Fig. 10. The $ac_2\{3\}$ in $0.3 < p_T < 3$ GeV (left panel) and $0.5 < p_T < 5$ GeV (right panel) in pp collisions. In each panel, they are compared between standard method (solid circles), two-subevent method (open circles), three-subevent where V_4 is determined in subevent a or c (open boxes), and three-subevent where V_4 is determined in subevent b (diamonds) according to Eq. (8). The error bars and shaded boxes represent the statistical and systematic uncertainties, respectively.

References

- [1] E. Shuryak, Strongly coupled quark-gluon plasma in heavy ion collisions, *Rev. Mod. Phys.* **89** (2017) 035001, arXiv:1412.8393 [hep-ph].
- [2] CMS Collaboration, Observation of long-range near-side angular correlations in proton-lead collisions at the LHC, *Phys. Lett. B* **718** (2013) 795, arXiv:1210.5482 [nucl-ex].
- [3] ALICE Collaboration, Long-range angular correlations on the near and away side in p -Pb collisions at $\sqrt{s_{NN}} = 5.02$ TeV, *Phys. Lett. B* **719** (2013) 29, arXiv:1212.2001 [nucl-ex].
- [4] ATLAS Collaboration, Observation of associated near-side and away-side long-range correlations in $\sqrt{s_{NN}} = 5.02$ TeV proton-lead collisions with the ATLAS detector, *Phys. Rev. Lett.* **110** (2013) 182302, arXiv:1212.5198 [hep-ex].
- [5] ATLAS Collaboration, Measurement of long-range pseudorapidity correlations and azimuthal harmonics in $\sqrt{s_{NN}} = 5.02$ TeV proton-lead collisions with the ATLAS detector, *Phys. Rev. C* **90** (2014) 044906, arXiv:1409.1792 [hep-ex].
- [6] CMS Collaboration, Evidence for collective multiparticle correlations in p -Pb collisions, *Phys. Rev. Lett.* **115** (2015) 012301, arXiv:1502.05382 [nucl-ex].
- [7] ATLAS Collaboration, Measurements of long-range azimuthal anisotropies and associated Fourier coefficients for pp collisions at $\sqrt{s} = 5.02$ and 13 TeV and p +Pb collisions at $\sqrt{s_{NN}} = 5.02$ TeV with the ATLAS detector, *Phys. Rev. C* **96** (2017) 024908, arXiv:1609.06213 [nucl-ex].
- [8] K. Dusling, R. Venugopalan, Comparison of the color glass condensate to di-hadron correlations in proton-proton and proton-nucleus collisions, *Phys. Rev. D* **87** (2013) 094034, arXiv:1302.7018 [hep-ph].
- [9] P. Bozek, W. Broniowski, Collective dynamics in high-energy proton-nucleus collisions, *Phys. Rev. C* **88** (2013) 014903, arXiv:1304.3044 [nucl-th].
- [10] N. Borghini, P.M. Dinh, J.-Y. Ollitrault, New method for measuring azimuthal distributions in nucleus-nucleus collisions, *Phys. Rev. C* **63** (2001) 054906, arXiv:nucl-th/0007063 [nucl-th].
- [11] A. Bilandzic, R. Snellings, S. Voloshin, Flow analysis with cumulants: direct calculations, *Phys. Rev. C* **83** (2011) 044913, arXiv:1010.0233 [nucl-ex].
- [12] A. Bilandzic, C.H. Christensen, K. Gulbrandsen, A. Hansen, Y. Zhou, Generic framework for anisotropic flow analyses with multiparticle azimuthal correlations, *Phys. Rev. C* **89** (2014) 064904, arXiv:1312.3572 [nucl-ex].
- [13] J. Jia, M. Zhou, A. Trzupek, Revealing long-range multiparticle collectivity in small collision systems via subevent cumulants, *Phys. Rev. C* **96** (2017) 034906, arXiv:1701.03830 [nucl-th].
- [14] ATLAS Collaboration, Observation of long-range elliptic azimuthal anisotropies in $\sqrt{s} = 13$ and 2.76 TeV pp collisions with the ATLAS detector, *Phys. Rev. Lett.* **116** (2016) 172301, arXiv:1509.04776 [hep-ex].
- [15] CMS Collaboration, Evidence for collectivity in pp collisions at the LHC, *Phys. Lett. B* **765** (2017) 193–220, arXiv:1606.06198 [nucl-ex].
- [16] P. Huo, K. Gajdošová, J. Jia, Y. Zhou, Importance of non-flow in mixed-harmonic multi-particle correlations in small collision systems, *Phys. Lett. B* **777** (2018) 201, arXiv:1710.07567 [nucl-ex].
- [17] ATLAS Collaboration, Measurement of multi-particle azimuthal correlations in pp , p +Pb and low-multiplicity Pb+Pb collisions with the ATLAS detector, *Eur. Phys. J. C* **77** (2017) 428, arXiv:1705.04176 [hep-ex].
- [18] ATLAS Collaboration, Measurement of multi-particle azimuthal correlations with the subevent cumulant method in pp and p +Pb collisions with the ATLAS detector at the LHC, *Phys. Rev. C* **97** (2018) 024904, arXiv:1708.03559 [hep-ex].
- [19] CMS Collaboration, Observation of correlated azimuthal anisotropy Fourier harmonics in pp and p Pb collisions at the LHC, *Phys. Rev. Lett.* **120** (2018) 092301, arXiv:1709.09189 [nucl-ex].
- [20] ATLAS Collaboration, The ATLAS experiment at the CERN Large Hadron Collider, *J. Instrum.* **3** (2008) S08003.
- [21] ATLAS Collaboration, The ATLAS inner detector commissioning and calibration, *Eur. Phys. J. C* **70** (2010) 787, arXiv:1004.5293 [physics.ins-det].
- [22] ATLAS Collaboration, ATLAS Insertable B-Layer Technical Design Report, ATLAS-TDR-19, <https://cds.cern.ch/record/1291633>, 2010; ATLAS Insertable B-Layer Technical Design Report Addendum, ATLAS-TDR-19-ADD-1, <https://cds.cern.ch/record/1451888>, 2012.
- [23] ATLAS Collaboration, Performance of the ATLAS trigger system in 2010, *Eur. Phys. J. C* **72** (2012) 1849, arXiv:1110.1530 [hep-ex].
- [24] ATLAS Collaboration, Performance of the ATLAS trigger system in 2015, *Eur. Phys. J. C* **77** (2017) 317, arXiv:1611.09661 [hep-ex].
- [25] ATLAS Collaboration, Charged-particle distributions in $\sqrt{s} = 13$ TeV pp interactions measured with the ATLAS detector at the LHC, *Phys. Lett. B* **758** (2016) 67, arXiv:1602.01633 [hep-ex].
- [26] ATLAS Collaboration, Performance of the ATLAS minimum bias and forward detector triggers in p Pb collisions, ATLAS-CONF-2013-104, <https://cds.cern.ch/record/1624013>.
- [27] T. Sjöstrand, S. Mrenna, P.Z. Skands, A brief introduction to PYTHIA 8.1, *Comput. Phys. Commun.* **178** (2008) 852, arXiv:0710.3820 [hep-ph].
- [28] ATLAS Collaboration, ATLAS tunes of PYTHIA 6 and Pythia 8 for MC11, ATLAS-PHYS-PUB-2011-009, <https://cds.cern.ch/record/1363300>.
- [29] M. Gyulassy, X.-N. Wang, HIJING 1.0: a Monte Carlo program for parton and particle production in high-energy hadronic and nuclear collisions, *Comput. Phys. Commun.* **83** (1994) 307, arXiv:nucl-th/9502021.
- [30] GEANT4 Collaboration, S. Agostinelli, et al., GEANT4: a simulation toolkit, *Nucl. Instrum. Methods A* **506** (2003) 250.
- [31] ATLAS Collaboration, The ATLAS simulation infrastructure, *Eur. Phys. J. C* **70** (2010) 823, arXiv:1005.4568 [physics.ins-det].
- [32] ATLAS Collaboration, Measurement of forward-backward multiplicity correlations in lead-lead, proton-lead and proton-proton collisions with the ATLAS detector, *Phys. Rev. C* **95** (2017) 064914, arXiv:1606.08170 [hep-ex].
- [33] P. Di Francesco, M. Guibaud, M. Luzum, J.-Y. Ollitrault, Systematic procedure for analyzing cumulants at any order, *Phys. Rev. C* **95** (2017) 044911, arXiv:1612.05634 [nucl-th].
- [34] G. Giacalone, L. Yan, J. Noronha-Hostler, J.-Y. Ollitrault, Symmetric cumulants and event-plane correlations in Pb + Pb collisions, *Phys. Rev. C* **94** (2016) 014906, arXiv:1605.08303 [nucl-th].
- [35] S.J. Das, G. Giacalone, P.-A. Monard, J.-Y. Ollitrault, Relating centrality to impact parameter in nucleus-nucleus collisions, *Phys. Rev. C* **97** (2018) 014905, arXiv:1708.00081 [nucl-th].
- [36] R.S. Bhalerao, J.-Y. Ollitrault, S. Pal, Event-plane correlators, *Phys. Rev. C* **88** (2013) 024909, arXiv:1307.0980 [nucl-th].
- [37] ATLAS Collaboration, Measurement of the azimuthal anisotropy for charged particle production in $\sqrt{s_{NN}} = 2.76$ TeV lead-lead collisions with the ATLAS detector, *Phys. Rev. C* **86** (2012) 014907, arXiv:1203.3087 [hep-ex].
- [38] P. Bozek, W. Broniowski, J. Moreira, Torqued fireballs in relativistic heavy-ion collisions, *Phys. Rev. C* **83** (2011) 034911, arXiv:1011.3354 [nucl-th].
- [39] L.-G. Pang, G.-Y. Qin, V. Roy, X.-N. Wang, G.-L. Ma, Longitudinal decorrelation of anisotropic flows in heavy-ion collisions at the CERN Large Hadron Collider, *Phys. Rev. C* **91** (2015) 044904, arXiv:1410.8690 [nucl-th].

- [40] CMS Collaboration, Evidence for transverse momentum and pseudorapidity dependent event plane fluctuations in PbPb and pPb collisions, *Phys. Rev. C* 92 (2015) 034911, arXiv:1503.01692 [nucl-ex].
- [41] ATLAS Collaboration, Measurement of longitudinal flow de-correlations in Pb+Pb collisions at $\sqrt{s_{NN}} = 2.76$ and 5.02 TeV with the ATLAS detector, *Eur. Phys. J. C* 78 (2018) 142, arXiv:1709.02301 [nucl-ex].
- [42] ATLAS Collaboration, Measurement of event-plane correlations in $\sqrt{s_{NN}} = 2.76$ TeV lead–lead collisions with the ATLAS detector, *Phys. Rev. C* 90 (2014) 024905, arXiv:1403.0489 [hep-ex].
- [43] ATLAS Collaboration, Measurement of the correlation between flow harmonics of different order in lead–lead collisions at $\sqrt{s_{NN}} = 2.76$ TeV with the ATLAS detector, *Phys. Rev. C* 92 (2015) 034903, arXiv:1504.01289 [hep-ex].
- [44] ALICE Collaboration, J. Adam, et al., Correlated event-by-event fluctuations of flow harmonics in Pb+Pb collisions at $\sqrt{s_{NN}} = 2.76$ TeV, *Phys. Rev. Lett.* 117 (2016) 182301, arXiv:1604.07663 [nucl-ex].
- [45] ATLAS Collaboration, ATLAS computing acknowledgements, ATL-GEN-PUB-2016-002, <https://cds.cern.ch/record/2202407>.

The ATLAS Collaboration

M. Aaboud^{34d}, G. Aad⁹⁹, B. Abbott¹²⁵, O. Abidinov^{13,*}, B. Abeloos¹²⁹, D.K. Abhayasinghe⁹¹, S.H. Abidi¹⁶⁴, O.S. AbouZeid³⁹, N.L. Abraham¹⁵³, H. Abramowicz¹⁵⁸, H. Abreu¹⁵⁷, Y. Abulaiti⁶, B.S. Acharya^{64a,64b,p}, S. Adachi¹⁶⁰, L. Adamczyk^{81a}, J. Adelman¹¹⁹, M. Adersberger¹¹², A. Adiguzel^{12c,qj}, T. Adye¹⁴¹, A.A. Affolder¹⁴³, Y. Afik¹⁵⁷, C. Agheorghiesei^{27c}, J.A. Aguilar-Saavedra^{137f,137a,ai}, F. Ahmadov^{77,ag}, G. Aielli^{71a,71b}, S. Akatsuka⁸³, T.P.A. Åkesson⁹⁴, E. Akilli⁵², A.V. Akimov¹⁰⁸, G.L. Alberghi^{23b,23a}, J. Albert¹⁷³, P. Albicocco⁴⁹, M.J. Alconada Verzini⁸⁶, S. Alderweireldt¹¹⁷, M. Aleksa³⁵, I.N. Aleksandrov⁷⁷, C. Alexa^{27b}, T. Alexopoulos¹⁰, M. Alhroob¹²⁵, B. Ali¹³⁹, G. Alimonti^{66a}, J. Alison³⁶, S.P. Alkire¹⁴⁵, C. Allaire¹²⁹, B.M.M. Allbrooke¹⁵³, B.W. Allen¹²⁸, P.P. Allport²¹, A. Aloisio^{67a,67b}, A. Alonso³⁹, F. Alonso⁸⁶, C. Alpigiani¹⁴⁵, A.A. Alshehri⁵⁵, M.I. Alstaty⁹⁹, B. Alvarez Gonzalez³⁵, D. Álvarez Piqueras¹⁷¹, M.G. Alviggi^{67a,67b}, B.T. Amadio¹⁸, Y. Amaral Coutinho^{78b}, L. Ambroz¹³², C. Amelung²⁶, D. Amidei¹⁰³, S.P. Amor Dos Santos^{137a,137c}, S. Amoroso⁴⁴, C.S. Amrouche⁵², C. Anastopoulos¹⁴⁶, L.S. Ancu⁵², N. Andari¹⁴², T. Andeen¹¹, C.F. Anders^{59b}, J.K. Anders²⁰, K.J. Anderson³⁶, A. Andreazza^{66a,66b}, V. Andrei^{59a}, C.R. Anelli¹⁷³, S. Angelidakis³⁷, I. Angelozzi¹¹⁸, A. Angerami³⁸, A.V. Anisenkov^{120b,120a}, A. Annovi^{69a}, C. Antel^{59a}, M.T. Anthony¹⁴⁶, M. Antonelli⁴⁹, D.J.A. Antrim¹⁶⁸, F. Anulli^{70a}, M. Aoki⁷⁹, J.A. Aparisi Pozo¹⁷¹, L. Aperio Bella³⁵, G. Arabidze¹⁰⁴, J.P. Araque^{137a}, V. Araujo Ferraz^{78b}, R. Araujo Pereira^{78b}, A.T.H. Arce⁴⁷, R.E. Ardell⁹¹, F.A. Arduh⁸⁶, J-F. Arguin¹⁰⁷, S. Argyropoulos⁷⁵, A.J. Armbruster³⁵, L.J. Armitage⁹⁰, A. Armstrong¹⁶⁸, O. Arnaez¹⁶⁴, H. Arnold¹¹⁸, M. Arratia³¹, O. Arslan²⁴, A. Artamonov^{109,*}, G. Artoni¹³², S. Artz⁹⁷, S. Asai¹⁶⁰, N. Asbah⁵⁷, A. Ashkenazi¹⁵⁸, E.M. Asimakopoulou¹⁶⁹, L. Asquith¹⁵³, K. Assamagan²⁹, R. Astalos^{28a}, R.J. Atkin^{32a}, M. Atkinson¹⁷⁰, N.B. Atlay¹⁴⁸, K. Augsten¹³⁹, G. Avolio³⁵, R. Avramidou^{58a}, M.K. Ayoub^{15a}, G. Azuelos^{107,av}, A.E. Baas^{59a}, M.J. Baca²¹, H. Bachacou¹⁴², K. Bachas^{65a,65b}, M. Backes¹³², P. Bagnaia^{70a,70b}, M. Bahmani⁸², H. Bahrsemani¹⁴⁹, A.J. Bailey¹⁷¹, J.T. Baines¹⁴¹, M. Bajic³⁹, C. Bakalis¹⁰, O.K. Baker¹⁸⁰, P.J. Bakker¹¹⁸, D. Bakshi Gupta⁹³, E.M. Baldin^{120b,120a}, P. Balek¹⁷⁷, F. Balli¹⁴², W.K. Balunas¹³⁴, J. Balz⁹⁷, E. Banas⁸², A. Bandyopadhyay²⁴, S. Banerjee^{178,l}, A.A.E. Bannoura¹⁷⁹, L. Barak¹⁵⁸, W.M. Barbe³⁷, E.L. Barberio¹⁰², D. Barberis^{53b,53a}, M. Barbero⁹⁹, T. Barillari¹¹³, M-S. Barisits³⁵, J. Barkeloo¹²⁸, T. Barklow¹⁵⁰, N. Barlow³¹, R. Barnea¹⁵⁷, S.L. Barnes^{58c}, B.M. Barnett¹⁴¹, R.M. Barnett¹⁸, Z. Barnovska-Blenessy^{58a}, A. Baroncelli^{72a}, G. Barone²⁶, A.J. Barr¹³², L. Barranco Navarro¹⁷¹, F. Barreiro⁹⁶, J. Barreiro Guimarães da Costa^{15a}, R. Bartoldus¹⁵⁰, A.E. Barton⁸⁷, P. Bartos^{28a}, A. Basalae¹³⁵, A. Bassalat¹²⁹, R.L. Bates⁵⁵, S.J. Batista¹⁶⁴, S. Batlamous^{34e}, J.R. Batley³¹, M. Battaglia¹⁴³, M. Bause^{70a,70b}, F. Bauer¹⁴², K.T. Bauer¹⁶⁸, H.S. Bawa^{150,n}, J.B. Beacham¹²³, T. Beau¹³³, P.H. Beauchemin¹⁶⁷, P. Bechtel²⁴, H.C. Beck⁵¹, H.P. Beck^{20,s}, K. Becker⁵⁰, M. Becker⁹⁷, C. Becot⁴⁴, A. Beddall^{12d}, A.J. Beddall^{12a}, V.A. Bednyakov⁷⁷, M. Bedognetti¹¹⁸, C.P. Bee¹⁵², T.A. Beermann³⁵, M. Begalli^{78b}, M. Begel²⁹, A. Behera¹⁵², J.K. Behr⁴⁴, A.S. Bell⁹², G. Bella¹⁵⁸, L. Bellagamba^{23b}, A. Bellerive³³, M. Bellomo¹⁵⁷, P. Bellos⁹, K. Belotskiy¹¹⁰, N.L. Belyaev¹¹⁰, O. Benary^{158,*}, D. Bencheikroun^{34a}, M. Bender¹¹², N. Benekos¹⁰, Y. Benhammou¹⁵⁸, E. Benhar Noccioli¹⁸⁰, J. Benitez⁷⁵, D.P. Benjamin⁴⁷, M. Benoit⁵², J.R. Bensinger²⁶, S. Bentvelsen¹¹⁸, L. Beresford¹³², M. Beretta⁴⁹, D. Berge⁴⁴, E. Bergeaas Kuutmann¹⁶⁹, N. Berger⁵, L.J. Bergsten²⁶, J. Beringer¹⁸, S. Berlendis⁷, N.R. Bernard¹⁰⁰, G. Bernardi¹³³, C. Bernius¹⁵⁰, F.U. Bernlochner²⁴, T. Berry⁹¹, P. Berta⁹⁷, C. Bertella^{15a}, G. Bertoli^{43a,43b}, I.A. Bertram⁸⁷, G.J. Besjes³⁹, O. Bessidskaia Bylund¹⁷⁹, M. Bessner⁴⁴, N. Besson¹⁴², A. Bethani⁹⁸, S. Bethke¹¹³, A. Betti²⁴, A.J. Bevan⁹⁰, J. Beyer¹¹³, R.M. Bianchi¹³⁶, O. Biebel¹¹², D. Biedermann¹⁹, R. Bielski³⁵, K. Bierwagen⁹⁷, N.V. Biesuz^{69a,69b}, M. Biglietti^{72a}, T.R.V. Billoud¹⁰⁷, M. Bindi⁵¹, A. Bingul^{12d}, C. Bini^{70a,70b}, S. Biondi^{23b,23a}, M. Birman¹⁷⁷, T. Bisanz⁵¹, J.P. Biswal¹⁵⁸, C. Bittrich⁴⁶, D.M. Bjergaard⁴⁷, J.E. Black¹⁵⁰, K.M. Black²⁵, T. Blazek^{28a}, I. Bloch⁴⁴, C. Blocker²⁶, A. Blue⁵⁵, U. Blumenschein⁹⁰, Dr. Blunier^{144a}, G.J. Bobbink¹¹⁸, V.S. Bobrovnikov^{120b,120a},

S.S. Bocchetta⁹⁴, A. Bocci⁴⁷, D. Boerner¹⁷⁹, D. Bogavac¹¹², A.G. Bogdanchikov^{120b,120a}, C. Bohm^{43a}, V. Boisvert⁹¹, P. Bokač¹⁶⁹, T. Bold^{81a}, A.S. Boldyrev¹¹¹, A.E. Bolz^{59b}, M. Bomben¹³³, M. Bona⁹⁰, J.S. Bonilla¹²⁸, M. Boonekamp¹⁴², A. Borisov¹²¹, G. Borissov⁸⁷, J. Bortfeldt³⁵, D. Bortoletto¹³², V. Bortolotto^{71a,71b}, D. Boscherini^{23b}, M. Bosman¹⁴, J.D. Bossio Sola³⁰, K. Bouaouda^{34a}, J. Boudreau¹³⁶, E.V. Bouhova-Thacker⁸⁷, D. Boumediene³⁷, C. Bourdarios¹²⁹, S.K. Boutle⁵⁵, A. Boveia¹²³, J. Boyd³⁵, D. Boye^{32b}, I.R. Boyko⁷⁷, A.J. Bozson⁹¹, J. Bracinik²¹, N. Brahimi⁹⁹, A. Brandt⁸, G. Brandt¹⁷⁹, O. Brandt^{59a}, F. Braren⁴⁴, U. Bratzler¹⁶¹, B. Brau¹⁰⁰, J.E. Brau¹²⁸, W.D. Breaden Madden⁵⁵, K. Brendlinger⁴⁴, L. Brenner⁴⁴, R. Brenner¹⁶⁹, S. Bressler¹⁷⁷, B. Brickwedde⁹⁷, D.L. Briglin²¹, D. Britton⁵⁵, D. Britzger^{59b}, I. Brock²⁴, R. Brock¹⁰⁴, G. Brooijmans³⁸, T. Brooks⁹¹, W.K. Brooks^{144b}, E. Brost¹¹⁹, J.H. Broughton²¹, P.A. Bruckman de Renstrom⁸², D. Bruncko^{28b}, A. Bruni^{23b}, G. Bruni^{23b}, L.S. Bruni¹¹⁸, S. Bruno^{71a,71b}, B.H. Brunt³¹, M. Bruschi^{23b}, N. Bruscino¹³⁶, P. Bryant³⁶, L. Bryngemark⁴⁴, T. Buanes¹⁷, Q. Buat³⁵, P. Buchholz¹⁴⁸, A.G. Buckley⁵⁵, I.A. Budagov⁷⁷, M.K. Bugge¹³¹, F. Bühner⁵⁰, O. Bulekov¹¹⁰, D. Bullock⁸, T.J. Burch¹¹⁹, S. Burdın⁸⁸, C.D. Burgard¹¹⁸, A.M. Burger⁵, B. Burghgrave¹¹⁹, K. Burka⁸², S. Burke¹⁴¹, I. Burmeister⁴⁵, J.T.P. Burr¹³², D. Büscher⁵⁰, V. Büscher⁹⁷, E. Buschmann⁵¹, P. Bussey⁵⁵, J.M. Butler²⁵, C.M. Buttar⁵⁵, J.M. Butterworth⁹², P. Butti³⁵, W. Buttinger³⁵, A. Buzatu¹⁵⁵, A.R. Buzykaev^{120b,120a}, G. Cabras^{23b,23a}, S. Cabrera Urbán¹⁷¹, D. Caforio¹³⁹, H. Cai¹⁷⁰, V.M.M. Cairo², O. Cakir^{4a}, N. Calace⁵², P. Calafiura¹⁸, A. Calandri⁹⁹, G. Calderini¹³³, P. Calfayan⁶³, G. Callea^{40b,40a}, L.P. Caloba^{78b}, S. Calvente Lopez⁹⁶, D. Calvet³⁷, S. Calvet³⁷, T.P. Calvet¹⁵², M. Calvetti^{69a,69b}, R. Camacho Toro¹³³, S. Camarda³⁵, P. Camarri^{71a,71b}, D. Cameron¹³¹, R. Caminal Armadans¹⁰⁰, C. Camincher³⁵, S. Campana³⁵, M. Campanelli⁹², A. Camplani³⁹, A. Campoverde¹⁴⁸, V. Canale^{67a,67b}, M. Cano Bret^{58c}, J. Cantero¹²⁶, T. Cao¹⁵⁸, Y. Cao¹⁷⁰, M.D.M. Capeans Garrido³⁵, I. Caprini^{27b}, M. Caprini^{27b}, M. Capua^{40b,40a}, R.M. Carbone³⁸, R. Cardarelli^{71a}, F.C. Cardillo¹⁴⁶, I. Carli¹⁴⁰, T. Carli³⁵, G. Carlino^{67a}, B.T. Carlson¹³⁶, L. Carminati^{66a,66b}, R.M.D. Carney^{43a,43b}, S. Caron¹¹⁷, E. Carquin^{144b}, S. Carrá^{66a,66b}, G.D. Carrillo-Montoya³⁵, D. Casadei^{32b}, M.P. Casado^{14g}, A.F. Casha¹⁶⁴, D.W. Casper¹⁶⁸, R. Castelijns¹¹⁸, F.L. Castillo¹⁷¹, V. Castillo Gimenez¹⁷¹, N.F. Castro^{137a,137e}, A. Catinaccio³⁵, J.R. Catmore¹³¹, A. Cattai³⁵, J. Caudron²⁴, V. Cavaliere²⁹, E. Cavallaro¹⁴, D. Cavalli^{66a}, M. Cavalli-Sforza¹⁴, V. Cavasinni^{69a,69b}, E. Celebi^{12b}, F. Ceradini^{72a,72b}, L. Cerda Alberich¹⁷¹, A.S. Cerqueira^{78a}, A. Cerri¹⁵³, L. Cerrito^{71a,71b}, F. Cerutti¹⁸, A. Cervelli^{23b,23a}, S.A. Cetin^{12b}, A. Chafaq^{34a}, D. Chakraborty¹¹⁹, S.K. Chan⁵⁷, W.S. Chan¹¹⁸, Y.L. Chan^{61a}, J.D. Chapman³¹, B. Chargeishvili^{156b}, D.G. Charlton²¹, C.C. Chau³³, C.A. Chavez Barajas¹⁵³, S. Che¹²³, A. Chegwidan¹⁰⁴, S. Chekanov⁶, S.V. Chekulaev^{165a}, G.A. Chelkov^{77,au}, M.A. Chelstowska³⁵, C. Chen^{58a}, C.H. Chen⁷⁶, H. Chen²⁹, J. Chen^{58a}, J. Chen³⁸, S. Chen¹³⁴, S.J. Chen^{15c}, X. Chen^{15b,at}, Y. Chen⁸⁰, Y.-H. Chen⁴⁴, H.C. Cheng¹⁰³, H.J. Cheng^{15d}, A. Cheplakov⁷⁷, E. Cheremushkina¹²¹, R. Cherkaoui El Moursli^{34e}, E. Cheu⁷, K. Cheung⁶², L. Chevalier¹⁴², V. Chiarella⁴⁹, G. Chiarelli^{69a}, G. Chiodini^{65a}, A.S. Chisholm³⁵, A. Chitan^{27b}, I. Chiu¹⁶⁰, Y.H. Chiu¹⁷³, M.V. Chizhov⁷⁷, K. Choi⁶³, A.R. Chomont¹²⁹, S. Chouridou¹⁵⁹, Y.S. Chow¹¹⁸, V. Christodoulou⁹², M.C. Chu^{61a}, J. Chudoba¹³⁸, A.J. Chuinard¹⁰¹, J.J. Chwastowski⁸², L. Chytka¹²⁷, D. Cinca⁴⁵, V. Cindro⁸⁹, I.A. Cioară²⁴, A. Ciochio¹⁸, F. Ciotto^{67a,67b}, Z.H. Citron¹⁷⁷, M. Citterio^{66a}, A. Clark⁵², M.R. Clark³⁸, P.J. Clark⁴⁸, C. Clement^{43a,43b}, Y. Coadou⁹⁹, M. Cobal^{64a,64c}, A. Coccaro^{53b,53a}, J. Cochran⁷⁶, H. Cohen¹⁵⁸, A.E.C. Coimbra¹⁷⁷, L. Colasurdo¹¹⁷, B. Cole³⁸, A.P. Colijn¹¹⁸, J. Collot⁵⁶, P. Conde Muñio^{137a,i}, E. Coniavitis⁵⁰, S.H. Connell^{32b}, I.A. Connelly⁹⁸, S. Constantinescu^{27b}, F. Conventi^{67a,aw}, A.M. Cooper-Sarkar¹³², F. Cormier¹⁷², K.J.R. Cormier¹⁶⁴, M. Corradi^{70a,70b}, E.E. Corrigan⁹⁴, F. Corriveau^{101,ae}, A. Cortes-Gonzalez³⁵, M.J. Costa¹⁷¹, D. Costanzo¹⁴⁶, G. Cottin³¹, G. Cowan⁹¹, B.E. Cox⁹⁸, J. Crane⁹⁸, K. Cranmer¹²², S.J. Crawley⁵⁵, R.A. Creager¹³⁴, G. Cree³³, S. Crépé-Renaudin⁵⁶, F. Crescioli¹³³, M. Cristinziani²⁴, V. Croft¹²², G. Crosetti^{40b,40a}, A. Cueto⁹⁶, T. Cuhadar Donszelmann¹⁴⁶, A.R. Cukierman¹⁵⁰, J. Cúth⁹⁷, S. Czekierda⁸², P. Czodrowski³⁵, M.J. Da Cunha Sargedas De Sousa^{58b}, C. Da Via⁹⁸, W. Dabrowski^{81a}, T. Dado^{28a,z}, S. Dahbi^{34e}, T. Dai¹⁰³, F. Dallaire¹⁰⁷, C. Dallapiccola¹⁰⁰, M. Dam³⁹, G. D'amen^{23b,23a}, J. Damp⁹⁷, J.R. Dandoy¹³⁴, M.F. Daneri³⁰, N.P. Dang^{178,i}, N.D. Dann⁹⁸, M. Danninger¹⁷², V. Dao³⁵, G. Darbo^{53b}, S. Darmora⁸, O. Dartsı⁵, A. Dattagupta¹²⁸, T. Daubney⁴⁴, S. D'Auria⁵⁵, W. Davey²⁴, C. David⁴⁴, T. Davidek¹⁴⁰, D.R. Davis⁴⁷, E. Dawe¹⁰², I. Dawson¹⁴⁶, K. De⁸, R. De Asmundis^{67a}, A. De Benedetti¹²⁵, M. De Beurs¹¹⁸, S. De Castro^{23b,23a}, S. De Cecco^{70a,70b}, N. De Groot¹¹⁷, P. de Jong¹¹⁸, H. De la Torre¹⁰⁴, F. De Lorenzi⁷⁶, A. De Maria^{51,u}, D. De Pedis^{70a}, A. De Salvo^{70a}, U. De Sanctis^{71a,71b},

M. De Santis^{71a,71b}, A. De Santo¹⁵³, K. De Vasconcelos Corga⁹⁹, J.B. De Vivie De Regie¹²⁹,
 C. Debenedetti¹⁴³, D.V. Dedovich⁷⁷, N. Dehghanian³, M. Del Gaudio^{40b,40a}, J. Del Peso⁹⁶,
 Y. Delabat Diaz⁴⁴, D. Delgove¹²⁹, F. Deliot¹⁴², C.M. Delitzsch⁷, M. Della Pietra^{67a,67b}, D. Della Volpe⁵²,
 A. Dell'Acqua³⁵, L. Dell'Asta²⁵, M. Delmastro⁵, C. Delporte¹²⁹, P.A. Delsart⁵⁶, D.A. DeMarco¹⁶⁴,
 S. Demers¹⁸⁰, M. Demichev⁷⁷, S.P. Denisov¹²¹, D. Denysiuk¹¹⁸, L. D'Eramo¹³³, D. Derendarz⁸²,
 J.E. Derkaoui^{34d}, F. Derue¹³³, P. Dervan⁸⁸, K. Desch²⁴, C. Deterre⁴⁴, K. Dette¹⁶⁴, M.R. Devesa³⁰,
 P.O. Deviveiros³⁵, A. Dewhurst¹⁴¹, S. Dhaliwal²⁶, F.A. Di Bello⁵², A. Di Ciaccio^{71a,71b}, L. Di Ciaccio⁵,
 W.K. Di Clemente¹³⁴, C. Di Donato^{67a,67b}, A. Di Girolamo³⁵, B. Di Micco^{72a,72b}, R. Di Nardo¹⁰⁰,
 K.F. Di Petrillo⁵⁷, R. Di Sipio¹⁶⁴, D. Di Valentino³³, C. Diaconu⁹⁹, M. Diamond¹⁶⁴, F.A. Dias³⁹,
 T. Dias Do Vale^{137a}, M.A. Diaz^{144a}, J. Dickinson¹⁸, E.B. Diehl¹⁰³, J. Dietrich¹⁹, S. Díez Cornell⁴⁴,
 A. Dimitrievska¹⁸, J. Dingfelder²⁴, F. Dittus³⁵, F. Djama⁹⁹, T. Djobava^{156b}, J.L. Djuvsland^{59a},
 M.A.B. Do Vale^{78c}, M. Dobre^{27b}, D. Dodsworth²⁶, C. Doglioni⁹⁴, J. Dolejsi¹⁴⁰, Z. Dolezal¹⁴⁰,
 M. Donadelli^{78d}, J. Donini³⁷, A. D'onofrio⁹⁰, M. D'Onofrio⁸⁸, J. Dopke¹⁴¹, A. Doria^{67a}, M.T. Dova⁸⁶,
 A.T. Doyle⁵⁵, E. Drechsler⁵¹, E. Dreyer¹⁴⁹, T. Dreyer⁵¹, Y. Du^{58b}, J. Duarte-Campderros¹⁵⁸, F. Dubinin¹⁰⁸,
 M. Dubovsky^{28a}, A. Dubreuil⁵², E. Duchovni¹⁷⁷, G. Duckeck¹¹², A. Ducourthial¹³³, O.A. Ducu^{107,y},
 D. Duda¹¹³, A. Dudarev³⁵, A.C. Dudder⁹⁷, E.M. Duffield¹⁸, L. Duflot¹²⁹, M. Dührssen³⁵, C. Dülse¹⁷⁹,
 M. Dumancic¹⁷⁷, A.E. Dumitriu^{27b,e}, A.K. Duncan⁵⁵, M. Dunford^{59a}, A. Duperrin⁹⁹, H. Duran Yildiz^{4a},
 M. Düren⁵⁴, A. Durglishvili^{156b}, D. Duschinger⁴⁶, B. Dutta⁴⁴, D. Duvnjak¹, M. Dyndal⁴⁴, S. Dysch⁹⁸,
 B.S. Dziedzic⁸², C. Eckardt⁴⁴, K.M. Ecker¹¹³, R.C. Edgar¹⁰³, T. Eifert³⁵, G. Eigen¹⁷, K. Einsweiler¹⁸,
 T. Ekelof¹⁶⁹, M. El Kacimi^{34c}, R. El Kosseifi⁹⁹, V. Ellajosyula⁹⁹, M. Ellert¹⁶⁹, F. Ellinghaus¹⁷⁹,
 A.A. Elliot⁹⁰, N. Ellis³⁵, J. Elmsheuser²⁹, M. Elsing³⁵, D. Emelianov¹⁴¹, Y. Enari¹⁶⁰, J.S. Ennis¹⁷⁵,
 M.B. Epland⁴⁷, J. Erdmann⁴⁵, A. Ereditato²⁰, S. Errede¹⁷⁰, M. Escalier¹²⁹, C. Escobar¹⁷¹,
 O. Estrada Pastor¹⁷¹, A.I. Etievre¹⁴², E. Etzion¹⁵⁸, H. Evans⁶³, A. Ezhilov¹³⁵, M. Ezzi^{34e}, F. Fabbri⁵⁵,
 L. Fabbri^{23b,23a}, V. Fabiani¹¹⁷, G. Facini⁹², R.M. Faisca Rodrigues Pereira^{137a}, R.M. Fakhrutdinov¹²¹,
 S. Falciano^{70a}, P.J. Falke⁵, S. Falke⁵, J. Faltova¹⁴⁰, Y. Fang^{15a}, M. Fanti^{66a,66b}, A. Farbin⁸, A. Farilla^{72a},
 E.M. Farina^{68a,68b}, T. Farooque¹⁰⁴, S. Farrell¹⁸, S.M. Farrington¹⁷⁵, P. Farthouat³⁵, F. Fassi^{34e},
 P. Fassnacht³⁵, D. Fassouliotis⁹, M. Fauci Giannelli⁴⁸, A. Favareto^{53b,53a}, W.J. Fawcett³¹, L. Fayard¹²⁹,
 O.L. Fedin^{135,q}, W. Fedorko¹⁷², M. Feickert⁴¹, S. Feigl¹³¹, L. Feligioni⁹⁹, C. Feng^{58b}, E.J. Feng³⁵,
 M. Feng⁴⁷, M.J. Fenton⁵⁵, A.B. Fenyuk¹²¹, L. Feremenga⁸, J. Ferrando⁴⁴, A. Ferrari¹⁶⁹, P. Ferrari¹¹⁸,
 R. Ferrari^{68a}, D.E. Ferreira de Lima^{59b}, A. Ferrer¹⁷¹, D. Ferrere⁵², C. Ferretti¹⁰³, F. Fiedler⁹⁷, A. Filipčič⁸⁹,
 F. Filthaut¹¹⁷, K.D. Finelli²⁵, M.C.N. Fiolhais^{137a,137c,a}, L. Fiorini¹⁷¹, C. Fischer¹⁴, W.C. Fisher¹⁰⁴,
 N. Flaschel⁴⁴, I. Fleck¹⁴⁸, P. Fleischmann¹⁰³, R.R.M. Fletcher¹³⁴, T. Flick¹⁷⁹, B.M. Flierl¹¹², L.M. Flores¹³⁴,
 L.R. Flores Castillo^{61a}, F.M. Follega^{73a,73b}, N. Fomin¹⁷, G.T. Forcolin⁹⁸, A. Formica¹⁴², F.A. Förster¹⁴,
 A.C. Forti⁹⁸, A.G. Foster²¹, D. Fournier¹²⁹, H. Fox⁸⁷, S. Fracchia¹⁴⁶, P. Francavilla^{69a,69b},
 M. Franchini^{23b,23a}, S. Franchino^{59a}, D. Francis³⁵, L. Franconi¹³¹, M. Franklin⁵⁷, M. Frate¹⁶⁸,
 M. Fraternali^{68a,68b}, A.N. Fray⁹⁰, D. Freeborn⁹², S.M. Fressard-Batraneanu³⁵, B. Freund¹⁰⁷,
 W.S. Freund^{78b}, D.C. Frizzell¹²⁵, D. Froidevaux³⁵, J.A. Frost¹³², C. Fukunaga¹⁶¹, E. Fullana Torregrosa¹⁷¹,
 T. Fusayasu¹¹⁴, J. Fuster¹⁷¹, O. Gabizon¹⁵⁷, A. Gabrielli^{23b,23a}, A. Gabrielli¹⁸, G.P. Gach^{81a},
 S. Gadatsch⁵², P. Gadow¹¹³, G. Gagliardi^{53b,53a}, L.G. Gagnon¹⁰⁷, C. Galea^{27b}, B. Galhardo^{137a,137c},
 E.J. Gallas¹³², B.J. Gallop¹⁴¹, P. Gallus¹³⁹, G. Galster³⁹, R. Gamboa Goni⁹⁰, K.K. Gan¹²³, S. Ganguly¹⁷⁷,
 J. Gao^{58a}, Y. Gao⁸⁸, Y.S. Gao^{150,n}, C. García¹⁷¹, J.E. García Navarro¹⁷¹, J.A. García Pascual^{15a},
 M. Garcia-Sciveres¹⁸, R.W. Gardner³⁶, N. Garelli¹⁵⁰, V. Garonne¹³¹, K. Gasnikova⁴⁴, A. Gaudiello^{53b,53a},
 G. Gaudio^{68a}, I.L. Gavrilenko¹⁰⁸, A. Gavrilyuk¹⁰⁹, C. Gay¹⁷², G. Gaycken²⁴, E.N. Gazis¹⁰, C.N.P. Gee¹⁴¹,
 J. Geisen⁵¹, M. Geisen⁹⁷, M.P. Geisler^{59a}, K. Gellerstedt^{43a,43b}, C. Gemme^{53b}, M.H. Genest⁵⁶, C. Geng¹⁰³,
 S. Gentile^{70a,70b}, S. George⁹¹, D. Gerbaudo¹⁴, G. Gessner⁴⁵, S. Ghasemi¹⁴⁸, M. Ghasemi Bostanabad¹⁷³,
 M. Ghneimat²⁴, B. Giacobbe^{23b}, S. Giagu^{70a,70b}, N. Giangiacomi^{23b,23a}, P. Giannetti^{69a},
 A. Giannini^{67a,67b}, S.M. Gibson⁹¹, M. Gignac¹⁴³, D. Gillberg³³, G. Gilles¹⁷⁹, D.M. Gingrich^{3,av},
 M.P. Giordani^{64a,64c}, F.M. Giorgi^{23b}, P.F. Giraud¹⁴², P. Giromini⁵⁷, G. Giugliarelli^{64a,64c}, D. Giugni^{66a},
 F. Giuli¹³², M. Giulini^{59b}, S. Gkaitatzis¹⁵⁹, I. Gkialas^{9,k}, E.L. Gkougkousis¹⁴, P. Gkoutoumis¹⁰,
 L.K. Gladilin¹¹¹, C. Glasman⁹⁶, J. Glatzer¹⁴, P.C.F. Glaysher⁴⁴, A. Glazov⁴⁴, M. Goblirsch-Kolb²⁶,
 J. Godlewski⁸², S. Goldfarb¹⁰², T. Golling⁵², D. Golubkov¹²¹, A. Gomes^{137a,137b}, R. Goncalves Gama^{78a},
 R. Gonçalves^{137a}, G. Gonella⁵⁰, L. Gonella²¹, A. Gongadze⁷⁷, F. Gonnella²¹, J.L. Gonski⁵⁷,

S. González de la Hoz¹⁷¹, S. Gonzalez-Sevilla⁵², L. Goossens³⁵, P.A. Gorbounov¹⁰⁹, H.A. Gordon²⁹,
 B. Gorini³⁵, E. Gorini^{65a,65b}, A. Gorišek⁸⁹, A.T. Goshaw⁴⁷, C. Gössling⁴⁵, M.I. Gostkin⁷⁷, C.A. Gottardo²⁴,
 C.R. Goudet¹²⁹, D. Goujdami^{34c}, A.G. Goussiou¹⁴⁵, N. Govender^{32b,c}, C. Goy⁵, E. Gozani¹⁵⁷,
 I. Grabowska-Bold^{81a}, P.O.J. Gradin¹⁶⁹, E.C. Graham⁸⁸, J. Gramling¹⁶⁸, E. Gramstad¹³¹, S. Grancagnolo¹⁹,
 V. Gratchev¹³⁵, P.M. Gravila^{27f}, F.G. Gravili^{65a,65b}, C. Gray⁵⁵, H.M. Gray¹⁸, Z.D. Greenwood^{93,al},
 C. Greife²⁴, K. Gregersen⁹⁴, I.M. Gregor⁴⁴, P. Grenier¹⁵⁰, K. Grevtsov⁴⁴, N.A. Grieser¹²⁵, J. Griffiths⁸,
 A.A. Grillo¹⁴³, K. Grimm^{150,b}, S. Grinstein^{14,aa}, Ph. Gris³⁷, J.-F. Grivaz¹²⁹, S. Groh⁹⁷, E. Gross¹⁷⁷,
 J. Grosse-Knetter⁵¹, G.C. Grossi⁹³, Z.J. Grout⁹², C. Grud¹⁰³, A. Grummer¹¹⁶, L. Guan¹⁰³, W. Guan¹⁷⁸,
 J. Guenther³⁵, A. Guerguichon¹²⁹, F. Guescini^{165a}, D. Guest¹⁶⁸, R. Gugel⁵⁰, B. Gui¹²³, T. Guillemain⁵,
 S. Guindon³⁵, U. Gul⁵⁵, C. Gumpert³⁵, J. Guo^{58c}, W. Guo¹⁰³, Y. Guo^{58a,t}, Z. Guo⁹⁹, R. Gupta⁴¹,
 S. Gurbuz^{12c}, G. Gustavino¹²⁵, B.J. Gutelman¹⁵⁷, P. Gutierrez¹²⁵, C. Gutsche⁹², C. Guyot¹⁴²,
 M.P. Guzik^{81a}, C. Gwenlan¹³², C.B. Gwilliam⁸⁸, A. Haas¹²², C. Haber¹⁸, H.K. Hadavand⁸, N. Haddad^{34e},
 A. Hadeef^{58a}, S. Hageböck²⁴, M. Hagihara¹⁶⁶, H. Hakobyan^{181,*}, M. Haleem¹⁷⁴, J. Haley¹²⁶,
 G. Halladjian¹⁰⁴, G.D. Hallowell⁹⁹, K. Hamacher¹⁷⁹, P. Hamal¹²⁷, K. Hamano¹⁷³, A. Hamilton^{32a},
 G.N. Hamity¹⁴⁶, K. Han^{58a,ak}, L. Han^{58a}, S. Han^{15d}, K. Hanagaki^{79,w}, M. Hance¹⁴³, D.M. Handl¹¹²,
 B. Haney¹³⁴, R. Hankache¹³³, P. Hanke^{59a}, E. Hansen⁹⁴, J.B. Hansen³⁹, J.D. Hansen³⁹, M.C. Hansen²⁴,
 P.H. Hansen³⁹, K. Hara¹⁶⁶, A.S. Hard¹⁷⁸, T. Harenberg¹⁷⁹, S. Harkusha¹⁰⁵, P.F. Harrison¹⁷⁵,
 N.M. Hartmann¹¹², Y. Hasegawa¹⁴⁷, A. Hasib⁴⁸, S. Hassani¹⁴², S. Haug²⁰, R. Hauser¹⁰⁴, L. Hauswald⁴⁶,
 L.B. Havener³⁸, M. Havranek¹³⁹, C.M. Hawkes²¹, R.J. Hawking³⁵, D. Hayden¹⁰⁴, C. Hayes¹⁵²,
 C.P. Hays¹³², J.M. Hays⁹⁰, H.S. Hayward⁸⁸, S.J. Haywood¹⁴¹, M.P. Heath⁴⁸, V. Hedberg⁹⁴, L. Heelan⁸,
 S. Heer²⁴, K.K. Heidegger⁵⁰, J. Heilman³³, S. Heim⁴⁴, T. Heim¹⁸, B. Heinemann^{44,aq}, J.J. Heinrich¹¹²,
 L. Heinrich¹²², C. Heinz⁵⁴, J. Hejbal¹³⁸, L. Helary³⁵, A. Held¹⁷², S. Hellesund¹³¹, S. Hellman^{43a,43b},
 C. Helsens³⁵, R.C.W. Henderson⁸⁷, Y. Heng¹⁷⁸, S. Henkelmann¹⁷², A.M. Henriques Correia³⁵,
 G.H. Herbert¹⁹, H. Herde²⁶, V. Herget¹⁷⁴, Y. Hernández Jiménez^{32c}, H. Herr⁹⁷, M.G. Herrmann¹¹²,
 G. Herten⁵⁰, R. Hertenberger¹¹², L. Hervas³⁵, T.C. Herwig¹³⁴, G.G. Hesketh⁹², N.P. Hessey^{165a},
 J.W. Hetherly⁴¹, S. Higashino⁷⁹, E. Higón-Rodríguez¹⁷¹, K. Hildebrand³⁶, E. Hill¹⁷³, J.C. Hill³¹,
 K.K. Hill²⁹, K.H. Hiller⁴⁴, S.J. Hillier²¹, M. Hils⁴⁶, I. Hinchliffe¹⁸, M. Hirose¹³⁰, D. Hirschbuehl¹⁷⁹,
 B. Hiti⁸⁹, O. Hladik¹³⁸, D.R. Hlaluku^{32c}, X. Hoad⁴⁸, J. Hobbs¹⁵², N. Hod^{165a}, M.C. Hodgkinson¹⁴⁶,
 A. Hoecker³⁵, M.R. Hoferkamp¹¹⁶, F. Hoenig¹¹², D. Hohn²⁴, D. Hohov¹²⁹, T.R. Holmes³⁶,
 M. Holzbock¹¹², M. Homann⁴⁵, S. Honda¹⁶⁶, T. Honda⁷⁹, T.M. Hong¹³⁶, A. Hönle¹¹³,
 B.H. Hooberman¹⁷⁰, W.H. Hopkins¹²⁸, Y. Horii¹¹⁵, P. Horn⁴⁶, A.J. Horton¹⁴⁹, L.A. Horyn³⁶,
 J.-Y. Hostachy⁵⁶, A. Hostiuc¹⁴⁵, S. Hou¹⁵⁵, A. Hoummada^{34a}, J. Howarth⁹⁸, J. Hoya⁸⁶, M. Hrabovsky¹²⁷,
 J. Hrdinka³⁵, I. Hristova¹⁹, J. Hrivnac¹²⁹, A. Hrynevich¹⁰⁶, T. Hryn'ova⁵, P.J. Hsu⁶², S.-C. Hsu¹⁴⁵,
 Q. Hu²⁹, S. Hu^{58c}, Y. Huang^{15a}, Z. Hubacek¹³⁹, F. Hubaut⁹⁹, M. Huebner²⁴, F. Huegging²⁴,
 T.B. Huffman¹³², E.W. Hughes³⁸, M. Huhtinen³⁵, R.F.H. Hunter³³, P. Huo¹⁵², A.M. Hupe³³,
 N. Huseynov^{77,ag}, J. Huston¹⁰⁴, J. Huth⁵⁷, R. Hyneman¹⁰³, G. Iacobucci⁵², G. Iakovidis²⁹,
 I. Ibragimov¹⁴⁸, L. Iconomidou-Fayard¹²⁹, Z. Idrissi^{34e}, P. Iengo³⁵, R. Ignazzi³⁹, O. Igonkina^{118,ac},
 R. Iguchi¹⁶⁰, T. Iizawa⁵², Y. Ikegami⁷⁹, M. Ikeno⁷⁹, D. Iliadis¹⁵⁹, N. Ilic¹¹⁷, F. Iltzsche⁴⁶,
 G. Introzzi^{68a,68b}, M. Iodice^{72a}, K. Iordanidou³⁸, V. Ippolito^{70a,70b}, M.F. Isacson¹⁶⁹, N. Ishijima¹³⁰,
 M. Ishino¹⁶⁰, M. Ishitsuka¹⁶², W. Islam¹²⁶, C. Issever¹³², S. Istin¹⁵⁷, F. Ito¹⁶⁶, J.M. Iturbe Ponce^{61a},
 R. Iuppa^{73a,73b}, A. Ivina¹⁷⁷, H. Iwasaki⁷⁹, J.M. Izen⁴², V. Izzo^{67a}, P. Jacka¹³⁸, P. Jackson¹, R.M. Jacobs²⁴,
 V. Jain², G. Jäkel¹⁷⁹, K.B. Jakobi⁹⁷, K. Jakobs⁵⁰, S. Jakobsen⁷⁴, T. Jakoubek¹³⁸, D.O. Jamin¹²⁶, D.K. Jana⁹³,
 R. Jansky⁵², J. Janssen²⁴, M. Janus⁵¹, P.A. Janus^{81a}, G. Jarlskog⁹⁴, N. Javadov^{77,ag}, T. Javůrek³⁵,
 M. Javurkova⁵⁰, F. Jeanneau¹⁴², L. Jeanty¹⁸, J. Jejelava^{156a,ah}, A. Jelinskas¹⁷⁵, P. Jenni^{50,d}, J. Jeong⁴⁴,
 S. Jézéquel⁵, H. Ji¹⁷⁸, J. Jia¹⁵², H. Jiang⁷⁶, Y. Jiang^{58a}, Z. Jiang^{150,r}, S. Jiggins⁵⁰, F.A. Jimenez Morales³⁷,
 J. Jimenez Pena¹⁷¹, S. Jin^{15c}, A. Jinaru^{27b}, O. Jinnouchi¹⁶², H. Jivan^{32c}, P. Johansson¹⁴⁶, K.A. Johns⁷,
 C.A. Johnson⁶³, W.J. Johnson¹⁴⁵, K. Jon-And^{43a,43b}, R.W.L. Jones⁸⁷, S.D. Jones¹⁵³, S. Jones⁷, T.J. Jones⁸⁸,
 J. Jongmanns^{59a}, P.M. Jorge^{137a,137b}, J. Jovicevic^{165a}, X. Ju¹⁸, J.J. Junggeburth¹¹³, A. Juste Rozas^{14,aa},
 A. Kaczmarska⁸², M. Kado¹²⁹, H. Kagan¹²³, M. Kagan¹⁵⁰, T. Kaji¹⁷⁶, E. Kajomovitz¹⁵⁷, C.W. Kalderon⁹⁴,
 A. Kaluza⁹⁷, S. Kama⁴¹, A. Kamenshchikov¹²¹, L. Kanjir⁸⁹, Y. Kano¹⁶⁰, V.A. Kantserov¹¹⁰, J. Kanzaki⁷⁹,
 B. Kaplan¹²², L.S. Kaplan¹⁷⁸, D. Kar^{32c}, M.J. Kareem^{165b}, E. Karentzos¹⁰, S.N. Karpov⁷⁷, Z.M. Karpova⁷⁷,
 V. Kartvelishvili⁸⁷, A.N. Karyukhin¹²¹, L. Kashif¹⁷⁸, R.D. Kass¹²³, A. Kastanas¹⁵¹, Y. Kataoka¹⁶⁰,

C. Kato^{58d,58c}, J. Katzy⁴⁴, K. Kawade⁸⁰, K. Kawagoe⁸⁵, T. Kawamoto¹⁶⁰, G. Kawamura⁵¹, E.F. Kay⁸⁸, V.F. Kazanin^{120b,120a}, R. Keeler¹⁷³, R. Kehoe⁴¹, J.S. Keller³³, E. Kellermann⁹⁴, J.J. Kempster²¹, J. Kendrick²¹, O. Kepka¹³⁸, S. Kersten¹⁷⁹, B.P. Kerševan⁸⁹, R.A. Keyes¹⁰¹, M. Khader¹⁷⁰, F. Khalil-Zada¹³, A. Khanov¹²⁶, A.G. Kharlamov^{120b,120a}, T. Kharlamova^{120b,120a}, E.E. Khoda¹⁷², A. Khodinov¹⁶³, T.J. Khoo⁵², E. Khramov⁷⁷, J. Khubua^{156b}, S. Kido⁸⁰, M. Kiehn⁵², C.R. Kilby⁹¹, Y.K. Kim³⁶, N. Kimura^{64a,64c}, O.M. Kind¹⁹, B.T. King⁸⁸, D. Kirchmeier⁴⁶, J. Kirk¹⁴¹, A.E. Kiryunin¹¹³, T. Kishimoto¹⁶⁰, D. Kisielewska^{81a}, V. Kitali⁴⁴, O. Kivernyk⁵, E. Kladiva^{28b,*}, T. Klapdor-Kleingrothaus⁵⁰, M.H. Klein¹⁰³, M. Klein⁸⁸, U. Klein⁸⁸, K. Kleinknecht⁹⁷, P. Klimek¹¹⁹, A. Klimentov²⁹, R. Klingenberg^{45,*}, T. Klingl²⁴, T. Klioutchnikova³⁵, F.F. Klitzner¹¹², P. Kluit¹¹⁸, S. Kluth¹¹³, E. Kneringer⁷⁴, E.B.F.G. Knoops⁹⁹, A. Knue⁵⁰, A. Kobayashi¹⁶⁰, D. Kobayashi⁸⁵, T. Kobayashi¹⁶⁰, M. Kobel⁴⁶, M. Kocian¹⁵⁰, P. Kodys¹⁴⁰, P.T. Koenig²⁴, T. Koffas³³, E. Koffeman¹¹⁸, N.M. Köhler¹¹³, T. Koi¹⁵⁰, M. Kolb^{59b}, I. Koletsou⁵, T. Kondo⁷⁹, N. Kondrashova^{58c}, K. Köneke⁵⁰, A.C. König¹¹⁷, T. Kono⁷⁹, R. Konoplich^{122,an}, V. Konstantinides⁹², N. Konstantinidis⁹², B. Konya⁹⁴, R. Kopeliansky⁶³, S. Koperny^{81a}, K. Korcyl⁸², K. Kordas¹⁵⁹, G. Koren¹⁵⁸, A. Korn⁹², I. Korolkov¹⁴, E.V. Korolkova¹⁴⁶, N. Korotkova¹¹¹, O. Kortner¹¹³, S. Kortner¹¹³, T. Kosek¹⁴⁰, V.V. Kostyukhin²⁴, A. Kotwal⁴⁷, A. Koulouris¹⁰, A. Kourkouveli-Charalampidi^{68a,68b}, C. Kourkouvelis⁹, E. Kourlitis¹⁴⁶, V. Kouskoura²⁹, A.B. Kowalewska⁸², R. Kowalewski¹⁷³, T.Z. Kowalski^{81a}, C. Kozakai¹⁶⁰, W. Kozanecki¹⁴², A.S. Kozhin¹²¹, V.A. Kramarenko¹¹¹, G. Kramberger⁸⁹, D. Krasnopevtsev^{58a}, M.W. Krasny¹³³, A. Krasznahorkay³⁵, D. Krauss¹¹³, J.A. Kremer^{81a}, J. Kretzschmar⁸⁸, P. Krieger¹⁶⁴, K. Krizka¹⁸, K. Kroeninger⁴⁵, H. Kroha¹¹³, J. Kroll¹³⁸, J. Kroll¹³⁴, J. Krstic¹⁶, U. Kruchonak⁷⁷, H. Krüger²⁴, N. Krumnack⁷⁶, M.C. Kruse⁴⁷, T. Kubota¹⁰², S. Kuday^{4b}, J.T. Kuechler¹⁷⁹, S. Kuehn³⁵, A. Kugel^{59a}, F. Kuger¹⁷⁴, T. Kuhl⁴⁴, V. Kukhtin⁷⁷, R. Kukla⁹⁹, Y. Kulchitsky¹⁰⁵, S. Kuleshov^{144b}, Y.P. Kulinich¹⁷⁰, M. Kuna⁵⁶, T. Kunigo⁸³, A. Kupco¹³⁸, T. Kupfer⁴⁵, O. Kuprash¹⁵⁸, H. Kurashige⁸⁰, L.L. Kurchaninov^{165a}, Y.A. Kurochkin¹⁰⁵, M.G. Kurth^{15d}, E.S. Kuwertz³⁵, M. Kuze¹⁶², J. Kvita¹²⁷, T. Kwan¹⁰¹, A. La Rosa¹¹³, J.L. La Rosa Navarro^{78d}, L. La Rotonda^{40b,40a}, F. La Ruffa^{40b,40a}, C. Lacasta¹⁷¹, F. Lacava^{70a,70b}, J. Lacey⁴⁴, D.P.J. Lack⁹⁸, H. Lacker¹⁹, D. Lacour¹³³, E. Ladygin⁷⁷, R. Lafaye⁵, B. Laforge¹³³, T. Lagouri^{32c}, S. Lai⁵¹, S. Lammers⁶³, W. Lampl⁷, E. Lançon²⁹, U. Landgraf⁵⁰, M.P.J. Landon⁹⁰, M.C. Lanfermann⁵², V.S. Lang⁴⁴, J.C. Lange¹⁴, R.J. Langenberg³⁵, A.J. Lankford¹⁶⁸, F. Lanni²⁹, K. Lantzsch²⁴, A. Lanza^{68a}, A. Lapertosa^{53b,53a}, S. Laplace¹³³, J.F. Laporte¹⁴², T. Lari^{66a}, F. Lasagni Manghi^{23b,23a}, M. Lassnig³⁵, T.S. Lau^{61a}, A. Laudrain¹²⁹, M. Lavorgna^{67a,67b}, A.T. Law¹⁴³, P. Laycock⁸⁸, M. Lazzaroni^{66a,66b}, B. Le¹⁰², O. Le Dortz¹³³, E. Le Guirriec⁹⁹, E.P. Le Quilleuc¹⁴², M. LeBlanc⁷, T. LeCompte⁶, F. Ledroit-Guillon⁵⁶, C.A. Lee²⁹, G.R. Lee^{144a}, L. Lee⁵⁷, S.C. Lee¹⁵⁵, B. Lefebvre¹⁰¹, M. Lefebvre¹⁷³, F. Legger¹¹², C. Leggett¹⁸, K. Lehmann¹⁴⁹, N. Lehmann¹⁷⁹, G. Lehmann Miotto³⁵, W.A. Leight⁴⁴, A. Leisos^{159,x}, M.A.L. Leite^{78d}, R. Leitner¹⁴⁰, D. Lellouch¹⁷⁷, B. Lemmer⁵¹, K.J.C. Leney⁹², T. Lenz²⁴, B. Lenzi³⁵, R. Leone⁷, S. Leone^{69a}, C. Leonidopoulos⁴⁸, G. Lerner¹⁵³, C. Leroy¹⁰⁷, R. Les¹⁶⁴, A.A.J. Lesage¹⁴², C.G. Lester³¹, M. Levchenko¹³⁵, J. Levêque⁵, D. Levin¹⁰³, L.J. Levinson¹⁷⁷, D. Lewis⁹⁰, B. Li¹⁰³, C-Q. Li^{58a,am}, H. Li^{58b}, L. Li^{58c}, Q. Li^{15d}, Q.Y. Li^{58a}, S. Li^{58d,58c}, X. Li^{58c}, Y. Li¹⁴⁸, Z. Liang^{15a}, B. Liberti^{71a}, A. Liblong¹⁶⁴, K. Lie^{61c}, S. Liem¹¹⁸, A. Limosani¹⁵⁴, C.Y. Lin³¹, K. Lin¹⁰⁴, T.H. Lin⁹⁷, R.A. Linck⁶³, J.H. Lindon²¹, B.E. Lindquist¹⁵², A.L. Lioni⁵², E. Lipeles¹³⁴, A. Lipniacka¹⁷, M. Lisovsky^{59b}, T.M. Liss^{170,as}, A. Lister¹⁷², A.M. Litke¹⁴³, J.D. Little⁸, B. Liu⁷⁶, B.L. Liu⁶, H.B. Liu²⁹, H. Liu¹⁰³, J.B. Liu^{58a}, J.K.K. Liu¹³², K. Liu¹³³, M. Liu^{58a}, P. Liu¹⁸, Y. Liu^{15a}, Y.L. Liu^{58a}, Y.W. Liu^{58a}, M. Livan^{68a,68b}, A. Lleres⁵⁶, J. Llorente Merino^{15a}, S.L. Lloyd⁹⁰, C.Y. Lo^{61b}, F. Lo Sterzo⁴¹, E.M. Lobodzinska⁴⁴, P. Loch⁷, T. Lohse¹⁹, K. Lohwasser¹⁴⁶, M. Lokajicek¹³⁸, B.A. Long²⁵, J.D. Long¹⁷⁰, R.E. Long⁸⁷, L. Longo^{65a,65b}, K.A. Looper¹²³, J.A. Lopez^{144b}, I. Lopez Paz¹⁴, A. Lopez Solis¹⁴⁶, J. Lorenz¹¹², N. Lorenzo Martinez⁵, M. Losada²², P.J. Lösel¹¹², A. Lösle⁵⁰, X. Lou⁴⁴, X. Lou^{15a}, A. Lounis¹²⁹, J. Love⁶, P.A. Love⁸⁷, J.J. Lozano Bahilo¹⁷¹, H. Lu^{61a}, M. Lu^{58a}, N. Lu¹⁰³, Y.J. Lu⁶², H.J. Lubatti¹⁴⁵, C. Luci^{70a,70b}, A. Lucotte⁵⁶, C. Luedtke⁵⁰, F. Luehring⁶³, I. Luise¹³³, L. Luminari^{70a}, B. Lund-Jensen¹⁵¹, M.S. Lutz¹⁰⁰, P.M. Luzi¹³³, D. Lynn²⁹, R. Lysak¹³⁸, E. Lytken⁹⁴, F. Lyu^{15a}, V. Lyubushkin⁷⁷, H. Ma²⁹, L.L. Ma^{58b}, Y. Ma^{58b}, G. Maccarrone⁴⁹, A. Macchiolo¹¹³, C.M. Macdonald¹⁴⁶, J. Machado Miguens^{134,137b}, D. Madaffari¹⁷¹, R. Madar³⁷, W.F. Mader⁴⁶, A. Madsen⁴⁴, N. Madysa⁴⁶, J. Maeda⁸⁰, K. Maekawa¹⁶⁰, S. Maeland¹⁷, T. Maeno²⁹, A.S. Maevskiy¹¹¹, V. Magerl⁵⁰, C. Maidantchik^{78b}, T. Maier¹¹², A. Maio^{137a,137b,137d}, O. Majersky^{28a}, S. Majewski¹²⁸, Y. Makida⁷⁹, N. Makovec¹²⁹, B. Malaescu¹³³, Pa. Malecki⁸², V.P. Maleev¹³⁵, F. Malek⁵⁶

U. Mallik⁷⁵, D. Malon⁶, C. Malone³¹, S. Maltezos¹⁰, S. Malyukov³⁵, J. Mamuzic¹⁷¹, G. Mancini⁴⁹,
 I. Mandić⁸⁹, J. Maneira^{137a}, L. Manhaes de Andrade Filho^{78a}, J. Manjarres Ramos⁴⁶, K.H. Mankinen⁹⁴,
 A. Mann¹¹², A. Manousos⁷⁴, B. Mansoulie¹⁴², J.D. Mansour^{15a}, M. Mantoani⁵¹, S. Manzoni^{66a,66b},
 G. Marceca³⁰, L. March⁵², L. Marchese¹³², G. Marchiori¹³³, M. Marcisovsky¹³⁸, C.A. Marin Tobon³⁵,
 M. Marjanovic³⁷, D.E. Marley¹⁰³, F. Marroquim^{78b}, Z. Marshall¹⁸, M.U.F. Martensson¹⁶⁹,
 S. Marti-Garcia¹⁷¹, C.B. Martin¹²³, T.A. Martin¹⁷⁵, V.J. Martin⁴⁸, B. Martin dit Latour¹⁷,
 M. Martinez^{14,aa}, V.I. Martinez Outschoorn¹⁰⁰, S. Martin-Haugh¹⁴¹, V.S. Martoiu^{27b}, A.C. Martyniuk⁹²,
 A. Marzin³⁵, L. Masetti⁹⁷, T. Mashimo¹⁶⁰, R. Mashinistov¹⁰⁸, J. Masik⁹⁸, A.L. Maslennikov^{120b,120a},
 L.H. Mason¹⁰², L. Massa^{71a,71b}, P. Massarotti^{67a,67b}, P. Mastrandrea⁵, A. Mastroberardino^{40b,40a},
 T. Masubuchi¹⁶⁰, P. Mättig¹⁷⁹, J. Maurer^{27b}, B. Maček⁸⁹, S.J. Maxfield⁸⁸, D.A. Maximov^{120b,120a},
 R. Mazini¹⁵⁵, I. Maznas¹⁵⁹, S.M. Mazza¹⁴³, N.C. Mc Fadden¹¹⁶, G. Mc Goldrick¹⁶⁴, S.P. Mc Kee¹⁰³,
 A. McCarn¹⁰³, T.G. McCarthy¹¹³, L.I. McClymont⁹², E.F. McDonald¹⁰², J.A. Mcfayden³⁵, G. Mchedlidze⁵¹,
 M.A. McKay⁴¹, K.D. McLean¹⁷³, S.J. McMahon¹⁴¹, P.C. McNamara¹⁰², C.J. McNicol¹⁷⁵,
 R.A. McPherson^{173,ae}, J.E. Mdhluli^{32c}, Z.A. Meadows¹⁰⁰, S. Meehan¹⁴⁵, T.M. Megy⁵⁰, S. Mehlhase¹¹²,
 A. Mehta⁸⁸, T. Meideck⁵⁶, B. Meirose⁴², D. Melini^{171,h}, B.R. Mellado Garcia^{32c}, J.D. Mellenthin⁵¹,
 M. Melo^{28a}, F. Meloni⁴⁴, A. Melzer²⁴, S.B. Menary⁹⁸, E.D. Mendes Gouveia^{137a}, L. Meng⁸⁸,
 X.T. Meng¹⁰³, A. Mengarelli^{23b,23a}, S. Menke¹¹³, E. Meoni^{40b,40a}, S. Mergelmeyer¹⁹, C. Merlassino²⁰,
 P. Mermod⁵², L. Merola^{67a,67b}, C. Meroni^{66a}, F.S. Merritt³⁶, A. Messina^{70a,70b}, J. Metcalfe⁶, A.S. Mete¹⁶⁸,
 C. Meyer¹³⁴, J. Meyer¹⁵⁷, J.-P. Meyer¹⁴², H. Meyer Zu Theenhausen^{59a}, F. Miano¹⁵³, R.P. Middleton¹⁴¹,
 L. Mijović⁴⁸, G. Mikenberg¹⁷⁷, M. Mikestikova¹³⁸, M. Mikuž⁸⁹, M. Milesi¹⁰², A. Milic¹⁶⁴, D.A. Millar⁹⁰,
 D.W. Miller³⁶, A. Milov¹⁷⁷, D.A. Milstead^{43a,43b}, A.A. Minaenko¹²¹, M. Miñano Moya¹⁷¹,
 I.A. Minashvili^{156b}, A.I. Mincer¹²², B. Mindur^{81a}, M. Mineev⁷⁷, Y. Minegishi¹⁶⁰, Y. Ming¹⁷⁸, L.M. Mir¹⁴,
 A. Mirto^{65a,65b}, K.P. Mistry¹³⁴, T. Mitani¹⁷⁶, J. Mitrevski¹¹², V.A. Mitsou¹⁷¹, A. Miucci²⁰,
 P.S. Miyagawa¹⁴⁶, A. Mizukami⁷⁹, J.U. Mjörnmark⁹⁴, T. Mkrtchyan¹⁸¹, M. Mlynarikova¹⁴⁰, T. Moa^{43a,43b},
 K. Mochizuki¹⁰⁷, P. Mogg⁵⁰, S. Mohapatra³⁸, S. Molander^{43a,43b}, R. Moles-Valls²⁴, M.C. Mondragon¹⁰⁴,
 K. Mönig⁴⁴, J. Monk³⁹, E. Monnier⁹⁹, A. Montalbano¹⁴⁹, J. Montejo Berlingen³⁵, F. Monticelli⁸⁶,
 S. Monzani^{66a}, N. Morange¹²⁹, D. Moreno²², M. Moreno Llácer³⁵, P. Morettini^{53b}, M. Morgenstern¹¹⁸,
 S. Morgenstern⁴⁶, D. Mori¹⁴⁹, M. Morii⁵⁷, M. Morinaga¹⁷⁶, V. Morisbak¹³¹, A.K. Morley³⁵,
 G. Mornacchi³⁵, A.P. Morris⁹², J.D. Morris⁹⁰, L. Morvaj¹⁵², P. Moschovakos¹⁰, M. Mosidze^{156b},
 H.J. Moss¹⁴⁶, J. Moss^{150,o}, K. Motohashi¹⁶², R. Mount¹⁵⁰, E. Mountricha³⁵, E.J.W. Moyse¹⁰⁰,
 S. Muanza⁹⁹, F. Mueller¹¹³, J. Mueller¹³⁶, R.S.P. Mueller¹¹², D. Muenstermann⁸⁷, G.A. Mullier²⁰,
 F.J. Munoz Sanchez⁹⁸, P. Murin^{28b}, W.J. Murray^{175,141}, A. Murrone^{66a,66b}, M. Muškinja⁸⁹, C. Mwewa^{32a},
 A.G. Myagkov^{121,ao}, J. Myers¹²⁸, M. Myska¹³⁹, B.P. Nachman¹⁸, O. Nackenhorst⁴⁵, K. Nagai¹³²,
 K. Nagano⁷⁹, Y. Nagasaka⁶⁰, M. Nagel⁵⁰, E. Nagy⁹⁹, A.M. Nairz³⁵, Y. Nakahama¹¹⁵, K. Nakamura⁷⁹,
 T. Nakamura¹⁶⁰, I. Nakano¹²⁴, H. Nanjo¹³⁰, F. Napolitano^{59a}, R.F. Naranjo Garcia⁴⁴, R. Narayan¹¹,
 D.I. Narrias Villar^{59a}, I. Naryshkin¹³⁵, T. Naumann⁴⁴, G. Navarro²², R. Nayyar⁷, H.A. Neal^{103,*},
 P.Y. Nechaeva¹⁰⁸, T.J. Neep¹⁴², A. Negri^{68a,68b}, M. Negrini^{23b}, S. Nektarijevic¹¹⁷, C. Nellist⁵¹,
 M.E. Nelson¹³², S. Nemecek¹³⁸, P. Nemethy¹²², M. Nessi^{35,f}, M.S. Neubauer¹⁷⁰, M. Neumann¹⁷⁹,
 P.R. Newman²¹, T.Y. Ng^{61c}, Y.S. Ng¹⁹, H.D.N. Nguyen⁹⁹, T. Nguyen Manh¹⁰⁷, E. Nibigira³⁷,
 R.B. Nickerson¹³², R. Nicolaidou¹⁴², J. Nielsen¹⁴³, N. Nikiforou¹¹, V. Nikolaenko^{121,ao},
 I. Nikolic-Audit¹³³, K. Nikolopoulos²¹, P. Nilsson²⁹, Y. Ninomiya⁷⁹, A. Nisati^{70a}, N. Nishu^{58c},
 R. Nisius¹¹³, I. Nitsche⁴⁵, T. Nitta¹⁷⁶, T. Nobe¹⁶⁰, Y. Noguchi⁸³, M. Nomachi¹³⁰, I. Nomidis¹³³,
 M.A. Nomura²⁹, T. Nooney⁹⁰, M. Nordberg³⁵, N. Norjoharuddeen¹³², T. Novak⁸⁹, O. Novgorodova⁴⁶,
 R. Novotny¹³⁹, L. Nozka¹²⁷, K. Ntekas¹⁶⁸, E. Nurse⁹², F. Nuti¹⁰², F.G. Oakham^{33,av}, H. Oberlack¹¹³,
 T. Obermann²⁴, J. Ocariz¹³³, A. Ochi⁸⁰, I. Ochoa³⁸, J.P. Ochoa-Ricoux^{144a}, K. O'Connor²⁶, S. Oda⁸⁵,
 S. Odaka⁷⁹, S. Oerdek⁵¹, A. Oh⁹⁸, S.H. Oh⁴⁷, C.C. Ohm¹⁵¹, H. Oide^{53b,53a}, M.L. Ojeda¹⁶⁴, H. Okawa¹⁶⁶,
 Y. Okazaki⁸³, Y. Okumura¹⁶⁰, T. Okuyama⁷⁹, A. Olariu^{27b}, L.F. Oleiro Seabra^{137a}, S.A. Olivares Pino^{144a},
 D. Oliveira Damazio²⁹, J.L. Oliver¹, M.J.R. Olsson³⁶, A. Olszewski⁸², J. Olszowska⁸², D.C. O'Neil¹⁴⁹,
 A. Onofre^{137a,137e}, K. Onogi¹¹⁵, P.U.E. Onyisi¹¹, H. Oppen¹³¹, M.J. Oreglia³⁶, Y. Oren¹⁵⁸,
 D. Orestano^{72a,72b}, E.C. Orgill⁹⁸, N. Orlando^{61b}, A.A. O'Rourke⁴⁴, R.S. Orr¹⁶⁴, B. Osculati^{53b,53a,*},
 V. O'Shea⁵⁵, R. Ospanov^{58a}, G. Otero y Garzon³⁰, H. Otono⁸⁵, M. Ouchrif^{34d}, F. Ould-Saada¹³¹,
 A. Ouraou¹⁴², Q. Ouyang^{15a}, M. Owen⁵⁵, R.E. Owen²¹, V.E. Ozcan^{12c}, N. Ozturk⁸, J. Pacalt¹²⁷,

H.A. Pacey³¹, K. Pachal¹⁴⁹, A. Pacheco Pages¹⁴, L. Pacheco Rodriguez¹⁴², C. Padilla Aranda¹⁴,
S. Pagan Griso¹⁸, M. Paganini¹⁸⁰, G. Palacino⁶³, S. Palazzo^{40b,40a}, S. Palestini³⁵, M. Palka^{81b}, D. Pallin³⁷,
I. Panagoulas¹⁰, C.E. Pandini³⁵, J.G. Panduro Vazquez⁹¹, P. Pani³⁵, G. Panizzo^{64a,64c}, L. Paolozzi⁵²,
T.D. Papadopoulou¹⁰, K. Papageorgiou^{9,k}, A. Paramonov⁶, D. Paredes Hernandez^{61b},
S.R. Paredes Saenz¹³², B. Parida^{58c}, A.J. Parker⁸⁷, K.A. Parker⁴⁴, M.A. Parker³¹, F. Parodi^{53b,53a},
J.A. Parsons³⁸, U. Parzefall⁵⁰, V.R. Pascuzzi¹⁶⁴, J.M.P. Pasner¹⁴³, E. Pasqualucci^{70a}, S. Passaggio^{53b},
F. Pastore⁹¹, P. Pasuwan^{43a,43b}, S. Pataria⁹⁷, J.R. Pater⁹⁸, A. Pathak^{178,l}, T. Pauly³⁵, B. Pearson¹¹³,
M. Pedersen¹³¹, L. Pedraza Diaz¹¹⁷, R. Pedro^{137a,137b}, S.V. Peleganchuk^{120b,120a}, O. Penc¹³⁸, C. Peng^{15d},
H. Peng^{58a}, B.S. Peralva^{78a}, M.M. Perego¹⁴², A.P. Pereira Peixoto^{137a}, D.V. Perepelitsa²⁹, F. Peri¹⁹,
L. Perini^{66a,66b}, H. Pernegger³⁵, S. Perrella^{67a,67b}, V.D. Peshekhonov^{77,*}, K. Peters⁴⁴, R.F.Y. Peters⁹⁸,
B.A. Petersen³⁵, T.C. Petersen³⁹, E. Petit⁵⁶, A. Petridis¹, C. Petridou¹⁵⁹, P. Petroff¹²⁹, M. Petrov¹³²,
F. Petrucci^{72a,72b}, M. Pettee¹⁸⁰, N.E. Pettersson¹⁰⁰, A. Peyaud¹⁴², R. Pezoa^{144b}, T. Pham¹⁰²,
F.H. Phillips¹⁰⁴, P.W. Phillips¹⁴¹, G. Piacquadio¹⁵², E. Pianori¹⁸, A. Picazio¹⁰⁰, M.A. Pickering¹³²,
R.H. Pickles⁹⁸, R. Piegai³⁰, J.E. Pilcher³⁶, A.D. Pilkington⁹⁸, M. Pinamonti^{71a,71b}, J.L. Pinfold³,
M. Pitt¹⁷⁷, M.-A. Pleier²⁹, V. Pleskot¹⁴⁰, E. Plotnikova⁷⁷, D. Pluth⁷⁶, P. Podberezko^{120b,120a},
R. Poettgen⁹⁴, R. Poggi⁵², L. Poggioli¹²⁹, I. Pogrebnyak¹⁰⁴, D. Pohl²⁴, I. Pokharel⁵¹, G. Polesello^{68a},
A. Poley¹⁸, A. Policicchio^{70a,70b}, R. Polifka³⁵, A. Polini^{23b}, C.S. Pollard⁴⁴, V. Polychronakos²⁹,
D. Ponomarenko¹¹⁰, L. Pontecorvo³⁵, G.A. Popeneciu^{27d}, D.M. Portillo Quintero¹³³, S. Pospisil¹³⁹,
K. Potamianos⁴⁴, I.N. Potrap⁷⁷, C.J. Potter³¹, H. Potti¹¹, T. Poulsen⁹⁴, J. Poveda³⁵, T.D. Powell¹⁴⁶,
M.E. Pozo Astigarraga³⁵, P. Pralavorio⁹⁹, S. Prell⁷⁶, D. Price⁹⁸, M. Primavera^{65a}, S. Prince¹⁰¹,
N. Proklova¹¹⁰, K. Prokofiev^{61c}, F. Prokoshin^{144b}, S. Protopopescu²⁹, J. Proudfoot⁶, M. Przybycien^{81a},
A. Puri¹⁷⁰, P. Puzo¹²⁹, J. Qian¹⁰³, Y. Qin⁹⁸, A. Quadt⁵¹, M. Queitsch-Maitland⁴⁴, A. Qureshi¹,
P. Rados¹⁰², F. Ragusa^{66a,66b}, G. Rahal⁹⁵, J.A. Raine⁵², S. Rajagopalan²⁹, A. Ramirez Morales⁹⁰,
T. Rashid¹²⁹, S. Raspopov⁵, M.G. Ratti^{66a,66b}, D.M. Rauch⁴⁴, F. Rauscher¹¹², S. Rave⁹⁷, B. Ravina¹⁴⁶,
I. Ravinovich¹⁷⁷, J.H. Rawling⁹⁸, M. Raymond³⁵, A.L. Read¹³¹, N.P. Readoff⁵⁶, M. Reale^{65a,65b},
D.M. Rebuzzi^{68a,68b}, A. Redelbach¹⁷⁴, G. Redlinger²⁹, R. Reece¹⁴³, R.G. Reed^{32c}, K. Reeves⁴²,
L. Rehnisch¹⁹, J. Reichert¹³⁴, A. Reiss⁹⁷, C. Rembser³⁵, H. Ren^{15d}, M. Rescigno^{70a}, S. Resconi^{66a},
E.D. Resseguie¹³⁴, S. Rettie¹⁷², E. Reynolds²¹, O.L. Rezanova^{120b,120a}, P. Reznicek¹⁴⁰, E. Ricci^{73a,73b},
R. Richter¹¹³, S. Richter⁹², E. Richter-Was^{81b}, O. Ricken²⁴, M. Ridel¹³³, P. Rieck¹¹³, C.J. Riegel¹⁷⁹,
O. Rifki⁴⁴, M. Rijssenbeek¹⁵², A. Rimoldi^{68a,68b}, M. Rimoldi²⁰, L. Rinaldi^{23b}, G. Ripellino¹⁵¹, B. Ristić⁸⁷,
E. Ritsch³⁵, I. Riu¹⁴, J.C. Rivera Vergara^{144a}, F. Rizatdinova¹²⁶, E. Rizvi⁹⁰, C. Rizzi¹⁴, R.T. Roberts⁹⁸,
S.H. Robertson^{101,ae}, D. Robinson³¹, J.E.M. Robinson⁴⁴, A. Robson⁵⁵, E. Rocco⁹⁷, C. Roda^{69a,69b},
Y. Rodina⁹⁹, S. Rodriguez Bosca¹⁷¹, A. Rodriguez Perez¹⁴, D. Rodriguez Rodriguez¹⁷¹,
A.M. Rodríguez Vera^{165b}, S. Roe³⁵, C.S. Rogan⁵⁷, O. Röhne¹³¹, R. Röhrig¹¹³, C.P.A. Roland⁶³, J. Roloff⁵⁷,
A. Romaniouk¹¹⁰, M. Romano^{23b,23a}, N. Rompotis⁸⁸, M. Ronzani¹²², L. Roos¹³³, S. Rosati^{70a},
K. Rosbach⁵⁰, P. Rose¹⁴³, N.-A. Rosien⁵¹, E. Rossi⁴⁴, E. Rossi^{67a,67b}, L.P. Rossi^{53b}, L. Rossini^{66a,66b},
J.H.N. Rosten³¹, R. Rosten¹⁴, M. Rotaru^{27b}, J. Rothberg¹⁴⁵, D. Rousseau¹²⁹, D. Roy^{32c}, A. Rozanov⁹⁹,
Y. Rozen¹⁵⁷, X. Ruan^{32c}, F. Rubbo¹⁵⁰, F. Rühr⁵⁰, A. Ruiz-Martinez¹⁷¹, Z. Rurikova⁵⁰, N.A. Rusakovich⁷⁷,
H.L. Russell¹⁰¹, J.P. Rutherford⁷, E.M. Rüttinger^{44,m}, Y.F. Ryabov¹³⁵, M. Rybar¹⁷⁰, G. Rybkin¹²⁹, S. Ryu⁶,
A. Ryzhov¹²¹, G.F. Rzehorz⁵¹, P. Sabatini⁵¹, G. Sabato¹¹⁸, S. Sacerdoti¹²⁹, H.F.-W. Sadrozinski¹⁴³,
R. Sadykov⁷⁷, F. Safai Tehrani^{70a}, P. Saha¹¹⁹, M. Sahinsoy^{59a}, A. Sahu¹⁷⁹, M. Saimpert⁴⁴, M. Saito¹⁶⁰,
T. Saito¹⁶⁰, H. Sakamoto¹⁶⁰, A. Sakharov^{122,an}, D. Salamani⁵², G. Salamanna^{72a,72b},
J.E. Salazar Loyola^{144b}, D. Salek¹¹⁸, P.H. Sales De Bruin¹⁶⁹, D. Salihagic¹¹³, A. Salnikov¹⁵⁰, J. Salt¹⁷¹,
D. Salvatore^{40b,40a}, F. Salvatore¹⁵³, A. Salvucci^{61a,61b,61c}, A. Salzburger³⁵, J. Samarati³⁵, D. Sammel⁵⁰,
D. Sampsonidis¹⁵⁹, D. Sampsonidou¹⁵⁹, J. Sánchez¹⁷¹, A. Sanchez Pineda^{64a,64c}, H. Sandaker¹³¹,
C.O. Sander⁴⁴, M. Sandhoff¹⁷⁹, C. Sandoval²², D.P.C. Sankey¹⁴¹, M. Sannino^{53b,53a}, Y. Sano¹¹⁵,
A. Sansoni⁴⁹, C. Santoni³⁷, H. Santos^{137a}, I. Santoyo Castillo¹⁵³, A. Santra¹⁷¹, A. Saponov⁷⁷,
J.G. Saraiva^{137a,137d}, O. Sasaki⁷⁹, K. Sato¹⁶⁶, E. Sauvan⁵, P. Savard^{164,av}, N. Savic¹¹³, R. Sawada¹⁶⁰,
C. Sawyer¹⁴¹, L. Sawyer^{93,al}, C. Sbarra^{23b}, A. Sbrizzi^{23a}, T. Scanlon⁹², J. Schaarschmidt¹⁴⁵, P. Schacht¹¹³,
B.M. Schachtner¹¹², D. Schaefer³⁶, L. Schaefer¹³⁴, J. Schaeffer⁹⁷, S. Schaepe³⁵, U. Schäfer⁹⁷,
A.C. Schaffer¹²⁹, D. Schaile¹¹², R.D. Schamberger¹⁵², N. Scharmberg⁹⁸, V.A. Schegelsky¹³⁵,
D. Scheirich¹⁴⁰, F. Schenck¹⁹, M. Schernau¹⁶⁸, C. Schiavi^{53b,53a}, S. Schier¹⁴³, L.K. Schildgen²⁴,

Z.M. Schillaci²⁶, E.J. Schioppa³⁵, M. Schioppa^{40b,40a}, K.E. Schleicher⁵⁰, S. Schlenker³⁵,
K.R. Schmidt-Sommerfeld¹¹³, K. Schmieden³⁵, C. Schmitt⁹⁷, S. Schmitt⁴⁴, S. Schmitz⁹⁷,
J.C. Schmoeckel⁴⁴, U. Schnoor⁵⁰, L. Schoeffel¹⁴², A. Schoening^{59b}, E. Schopf²⁴, M. Schott⁹⁷,
J.F.P. Schouwenberg¹¹⁷, J. Schovancova³⁵, S. Schramm⁵², A. Schulte⁹⁷, H.-C. Schultz-Coulon^{59a},
M. Schumacher⁵⁰, B.A. Schumm¹⁴³, Ph. Schune¹⁴², A. Schwartzman¹⁵⁰, T.A. Schwarz¹⁰³,
H. Schweiger⁹⁸, Ph. Schwemling¹⁴², R. Schwienhorst¹⁰⁴, A. Sciandra²⁴, G. Sciolla²⁶,
M. Scornajenghi^{40b,40a}, F. Scuri^{69a}, F. Scutti¹⁰², L.M. Scyboz¹¹³, J. Searcy¹⁰³, C.D. Sebastiani^{70a,70b},
P. Seema²⁴, S.C. Seidel¹¹⁶, A. Seiden¹⁴³, T. Seiss³⁶, J.M. Seixas^{78b}, G. Sekhniadze^{67a}, K. Sekhon¹⁰³,
S.J. Sekula⁴¹, N. Semprini-Cesari^{23b,23a}, S. Sen⁴⁷, S. Senkin³⁷, C. Serfon¹³¹, L. Serin¹²⁹, L. Serkin^{64a,64b},
M. Sessa^{72a,72b}, H. Severini¹²⁵, F. Sforza¹⁶⁷, A. Sfyrila⁵², E. Shabalina⁵¹, J.D. Shahinian¹⁴³,
N.W. Shaikh^{43a,43b}, L.Y. Shan^{15a}, R. Shang¹⁷⁰, J.T. Shank²⁵, M. Shapiro¹⁸, A.S. Sharma¹, A. Sharma¹³²,
P.B. Shatalov¹⁰⁹, K. Shaw¹⁵³, S.M. Shaw⁹⁸, A. Shcherbakova¹³⁵, Y. Shen¹²⁵, N. Sherafati³³,
A.D. Sherman²⁵, P. Sherwood⁹², L. Shi^{155,ar}, S. Shimizu⁷⁹, C.O. Shimmin¹⁸⁰, M. Shimojima¹¹⁴,
I.P.J. Shipsey¹³², S. Shirabe⁸⁵, M. Shiyakova⁷⁷, J. Shlomi¹⁷⁷, A. Shmeleva¹⁰⁸, D. Shoaleh Saadi¹⁰⁷,
M.J. Shochet³⁶, S. Shojaii¹⁰², D.R. Shope¹²⁵, S. Shrestha¹²³, E. Shulga¹¹⁰, P. Sicho¹³⁸, A.M. Sickles¹⁷⁰,
P.E. Sidebo¹⁵¹, E. Sideras Haddad^{32c}, O. Sidiropoulou³⁵, A. Sidoti^{23b,23a}, F. Siegert⁴⁶, Dj. Sijacki¹⁶,
J. Silva^{137a}, M. Silva Jr.¹⁷⁸, M.V. Silva Oliveira^{78a}, S.B. Silverstein^{43a}, L. Simic⁷⁷, S. Simion¹²⁹,
E. Simioni⁹⁷, M. Simon⁹⁷, R. Simoniello⁹⁷, P. Sinervo¹⁶⁴, N.B. Sinev¹²⁸, M. Sioli^{23b,23a}, G. Siragusa¹⁷⁴,
I. Siral¹⁰³, S.Yu. Sivoklokov¹¹¹, J. Sjölin^{43a,43b}, P. Skubic¹²⁵, M. Slater²¹, T. Slavicek¹³⁹, M. Slawinska⁸²,
K. Sliwa¹⁶⁷, R. Slovak¹⁴⁰, V. Smakhtin¹⁷⁷, B.H. Smart⁵, J. Smiesko^{28a}, N. Smirnov¹¹⁰, S.Yu. Smirnov¹¹⁰,
Y. Smirnov¹¹⁰, L.N. Smirnova¹¹¹, O. Smirnova⁹⁴, J.W. Smith⁵¹, M.N.K. Smith³⁸, M. Smizanska⁸⁷,
K. Smolek¹³⁹, A. Smykiewicz⁸², A.A. Snesarev¹⁰⁸, I.M. Snyder¹²⁸, S. Snyder²⁹, R. Sobie^{173,ae},
A.M. Soffa¹⁶⁸, A. Soffer¹⁵⁸, A. Søgaard⁴⁸, D.A. Soh¹⁵⁵, G. Sokhrannyi⁸⁹, C.A. Solans Sanchez³⁵,
M. Solar¹³⁹, E.Yu. Soldatov¹¹⁰, U. Soldevila¹⁷¹, A.A. Solodkov¹²¹, A. Soloshenko⁷⁷, O.V. Solovyanov¹²¹,
V. Solovyev¹³⁵, P. Sommer¹⁴⁶, H. Son¹⁶⁷, W. Song¹⁴¹, W.Y. Song^{165b}, A. Sopczak¹³⁹, F. Sopkova^{28b},
D. Sosa^{59b}, C.L. Sotiropoulou^{69a,69b}, S. Sottocornola^{68a,68b}, R. Soualah^{64a,64c,j}, A.M. Soukharev^{120b,120a},
D. South⁴⁴, B.C. Sowden⁹¹, S. Spagnolo^{65a,65b}, M. Spalla¹¹³, M. Spangenberg¹⁷⁵, F. Spanò⁹¹,
D. Sperlich¹⁹, F. Spettel¹¹³, T.M. Spieker^{59a}, R. Spighi^{23b}, G. Spigo³⁵, L.A. Spiller¹⁰², D.P. Spiteri⁵⁵,
M. Spousta¹⁴⁰, A. Stabile^{66a,66b}, R. Stamen^{59a}, S. Stamm¹⁹, E. Stanecka⁸², R.W. Staneke⁶, C. Stanescu^{72a},
B. Stanislaus¹³², M.M. Stanitzki⁴⁴, B. Stapf¹¹⁸, S. Stapnes¹³¹, E.A. Starchenko¹²¹, G.H. Stark³⁶, J. Stark⁵⁶,
S.H. Stark³⁹, P. Staroba¹³⁸, P. Starovoitov^{59a}, S. Stärz³⁵, R. Staszewski⁸², M. Stegler⁴⁴, P. Steinberg²⁹,
B. Stelzer¹⁴⁹, H.J. Stelzer³⁵, O. Stelzer-Chilton^{165a}, H. Stenzel⁵⁴, T.J. Stevenson⁹⁰, G.A. Stewart³⁵,
M.C. Stockton¹²⁸, G. Stoica^{27b}, P. Stolte⁵¹, S. Stonjek¹¹³, A. Straessner⁴⁶, J. Strandberg¹⁵¹,
S. Strandberg^{43a,43b}, M. Strauss¹²⁵, P. Strizenec^{28b}, R. Ströhmer¹⁷⁴, D.M. Strom¹²⁸, R. Stroynowski⁴¹,
A. Strubig⁴⁸, S.A. Stucci²⁹, B. Stugu¹⁷, J. Stupak¹²⁵, N.A. Styles⁴⁴, D. Su¹⁵⁰, J. Su¹³⁶, S. Suchek^{59a},
Y. Sugaya¹³⁰, M. Suk¹³⁹, V.V. Sulin¹⁰⁸, D.M.S. Sultan⁵², S. Sultansoy^{4c}, T. Sumida⁸³, S. Sun¹⁰³, X. Sun³,
K. Suruliz¹⁵³, C.J.E. Suster¹⁵⁴, M.R. Sutton¹⁵³, S. Suzuki⁷⁹, M. Svatos¹³⁸, M. Swiatlowski³⁶, S.P. Swift²,
A. Sydorenko⁹⁷, I. Sykora^{28a}, T. Sykora¹⁴⁰, D. Ta⁹⁷, K. Tackmann^{44,ab}, J. Taenzer¹⁵⁸, A. Taffard¹⁶⁸,
R. Tahirout^{165a}, E. Tahirovic⁹⁰, N. Taiblum¹⁵⁸, H. Takai²⁹, R. Takashima⁸⁴, E.H. Takasugi¹¹³, K. Takeda⁸⁰,
T. Takeshita¹⁴⁷, Y. Takubo⁷⁹, M. Talby⁹⁹, A.A. Talyshev^{120b,120a}, J. Tanaka¹⁶⁰, M. Tanaka¹⁶²,
R. Tanaka¹²⁹, B.B. Tannenwald¹²³, S. Tapia Araya^{144b}, S. Tapprogge⁹⁷, A. Tarek Abouelfadl Mohamed¹³³,
S. Tarem¹⁵⁷, G. Tarna^{27b,e}, G.F. Tartarelli^{66a}, P. Tas¹⁴⁰, M. Tasevsky¹³⁸, T. Tashiro⁸³, E. Tassi^{40b,40a},
A. Tavares Delgado^{137a,137b}, Y. Tayalati^{34e}, A.C. Taylor¹¹⁶, A.J. Taylor⁴⁸, G.N. Taylor¹⁰², P.T.E. Taylor¹⁰²,
W. Taylor^{165b}, A.S. Tee⁸⁷, P. Teixeira-Dias⁹¹, H. Ten Kate³⁵, P.K. Teng¹⁵⁵, J.J. Teoh¹¹⁸, F. Tepel¹⁷⁹,
S. Terada⁷⁹, K. Terashi¹⁶⁰, J. Terron⁹⁶, S. Terzo¹⁴, M. Testa⁴⁹, R.J. Teuscher^{164,ae}, S.J. Thais¹⁸⁰,
T. Theveniaux-Pelzer⁴⁴, F. Thiele³⁹, D.W. Thomas⁹¹, J.P. Thomas²¹, A.S. Thompson⁵⁵, P.D. Thompson²¹,
L.A. Thomsen¹⁸⁰, E. Thomson¹³⁴, Y. Tian³⁸, R.E. Ticse Torres⁵¹, V.O. Tikhomirov^{108,ap},
Yu.A. Tikhonov^{120b,120a}, S. Timoshenko¹¹⁰, P. Tipton¹⁸⁰, S. Tisserant⁹⁹, K. Todome¹⁶²,
S. Todorova-Nova⁵, S. Todt⁴⁶, J. Tojo⁸⁵, S. Tokár^{28a}, K. Tokushuku⁷⁹, E. Tolley¹²³, K.G. Tomiwa^{32c},
M. Tomoto¹¹⁵, L. Tompkins^{150,r}, K. Toms¹¹⁶, B. Tong⁵⁷, P. Tornambe⁵⁰, E. Torrence¹²⁸, H. Torres⁴⁶,
E. Torrón Pastor¹⁴⁵, C. Tosirci¹³², J. Toth^{99,ad}, F. Touchard⁹⁹, D.R. Tovey¹⁴⁶, C.J. Treado¹²², T. Trefzger¹⁷⁴,
F. Tresoldi¹⁵³, A. Tricoli²⁹, I.M. Trigger^{165a}, S. Trincaz-Duviois¹³³, M.F. Tripania¹⁴, W. Trischuk¹⁶⁴,

B. Trocme⁵⁶, A. Trofymov¹²⁹, C. Troncon^{66a}, M. Trovatelli¹⁷³, F. Trovato¹⁵³, L. Truong^{32b},
M. Trzebinski⁸², A. Trzupek⁸², F. Tsai⁴⁴, J.C.-L. Tseng¹³², P.V. Tsireshka¹⁰⁵, A. Tsirigotis¹⁵⁹,
N. Tsirintanis⁹, V. Tsiskaridze¹⁵², E.G. Tskhadadze^{156a}, I.I. Tsukerman¹⁰⁹, V. Tsulaia¹⁸, S. Tsuno⁷⁹,
D. Tsybychev^{152,163}, Y. Tu^{61b}, A. Tudorache^{27b}, V. Tudorache^{27b}, T.T. Tulbure^{27a}, A.N. Tuna⁵⁷,
S. Turchikhin⁷⁷, D. Turgeman¹⁷⁷, I. Turk Cakir^{4b,v}, R. Turra^{66a}, P.M. Tuts³⁸, E. Tzovara⁹⁷,
G. Ucchielli^{23b,23a}, I. Ueda⁷⁹, M. Ughetto^{43a,43b}, F. Ukegawa¹⁶⁶, G. Unal³⁵, A. Undrus²⁹, G. Unel¹⁶⁸,
F.C. Ungaro¹⁰², Y. Unno⁷⁹, K. Uno¹⁶⁰, J. Urban^{28b}, P. Urquijo¹⁰², P. Urrejola⁹⁷, G. Usai⁸, J. Usui⁷⁹,
L. Vacavant⁹⁹, V. Vacek¹³⁹, B. Vachon¹⁰¹, K.O.H. Vadla¹³¹, A. Vaidya⁹², C. Valderanis¹¹²,
E. Valdes Santurio^{43a,43b}, M. Valente⁵², S. Valentini^{23b,23a}, A. Valero¹⁷¹, L. Valéry⁴⁴, R.A. Vallance²¹,
A. Vallier⁵, J.A. Valls Ferrer¹⁷¹, T.R. Van Daalen¹⁴, H. Van der Graaf¹¹⁸, P. Van Gemmeren⁶,
J. Van Nieuwkoop¹⁴⁹, I. Van Vulpen¹¹⁸, M. Vanadia^{71a,71b}, W. Vandelli³⁵, A. Vaniachine¹⁶³,
P. Vankov¹¹⁸, R. Vari^{70a}, E.W. Varnes⁷, C. Varni^{53b,53a}, T. Varol⁴¹, D. Varouchas¹²⁹, K.E. Varvell¹⁵⁴,
G.A. Vasquez^{144b}, J.G. Vasquez¹⁸⁰, F. Vazeille³⁷, D. Vazquez Furelos¹⁴, T. Vazquez Schroeder¹⁰¹,
J. Veatch⁵¹, V. Vecchio^{72a,72b}, L.M. Veloce¹⁶⁴, F. Veloso^{137a,137c}, S. Veneziano^{70a}, A. Ventura^{65a,65b},
M. Venturi¹⁷³, N. Venturi³⁵, V. Vercesi^{68a}, M. Verducci^{72a,72b}, C.M. Vergel Infante⁷⁶, C. Vergis²⁴,
W. Verkerke¹¹⁸, A.T. Vermeulen¹¹⁸, J.C. Vermeulen¹¹⁸, M.C. Vetterli^{149,av}, N. Viaux Maira^{144b},
M. Vicente Barreto Pinto⁵², I. Vichou^{170,*}, T. Vickey¹⁴⁶, O.E. Vickey Boeriu¹⁴⁶, G.H.A. Viehhauser¹³²,
S. Viel¹⁸, L. Vigani¹³², M. Villa^{23b,23a}, M. Villaplana Perez^{66a,66b}, E. Vilucchi⁴⁹, M.G. Vinciter³³,
V.B. Vinogradov⁷⁷, A. Vishwakarma⁴⁴, C. Vittori^{23b,23a}, I. Vivarelli¹⁵³, S. Vlachos¹⁰, M. Vogel¹⁷⁹,
P. Vokac¹³⁹, G. Volpi¹⁴, S.E. von Buddenbrock^{32c}, E. Von Toerne²⁴, V. Vorobel¹⁴⁰, K. Vorobev¹¹⁰,
M. Vos¹⁷¹, J.H. Vosseveld⁸⁸, N. Vranjes¹⁶, M. Vranjes Milosavljevic¹⁶, V. Vrba¹³⁹, M. Vreeswijk¹¹⁸,
T. Šfligoy⁸⁹, R. Vuillermet³⁵, I. Vukotic³⁶, T. Ženiš^{28a}, L. Živković¹⁶, P. Wagner²⁴, W. Wagner¹⁷⁹,
J. Wagner-Kuhr¹¹², H. Wahlberg⁸⁶, S. Wahrmond⁴⁶, K. Wakamiya⁸⁰, V.M. Walbrecht¹¹³, J. Walder⁸⁷,
R. Walker¹¹², S.D. Walker⁹¹, W. Walkowiak¹⁴⁸, V. Wallangen^{43a,43b}, A.M. Wang⁵⁷, C. Wang^{58b,e},
F. Wang¹⁷⁸, H. Wang¹⁸, H. Wang³, J. Wang¹⁵⁴, J. Wang^{59b}, P. Wang⁴¹, Q. Wang¹²⁵, R.-J. Wang¹³³,
R. Wang^{58a}, R. Wang⁶, S.M. Wang¹⁵⁵, W.T. Wang^{58a}, W. Wang^{15c,af}, W.X. Wang^{58a,af}, Y. Wang^{58a,am},
Z. Wang^{58c}, C. Wanotayaroj⁴⁴, A. Warburton¹⁰¹, C.P. Ward³¹, D.R. Wardrope⁹², A. Washbrook⁴⁸,
P.M. Watkins²¹, A.T. Watson²¹, M.F. Watson²¹, G. Watts¹⁴⁵, S. Watts⁹⁸, B.M. Waugh⁹², A.F. Webb¹¹,
S. Webb⁹⁷, C. Weber¹⁸⁰, M.S. Weber²⁰, S.A. Weber³³, S.M. Weber^{59a}, A.R. Weidberg¹³², B. Weinert⁶³,
J. Weingarten⁴⁵, M. Weirich⁹⁷, C. Weiser⁵⁰, P.S. Wells³⁵, T. Wenaus²⁹, T. Wengler³⁵, S. Wenig³⁵,
N. Wermes²⁴, M.D. Werner⁷⁶, P. Werner³⁵, M. Wessels^{59a}, T.D. Weston²⁰, K. Whalen¹²⁸,
N.L. Whallon¹⁴⁵, A.M. Wharton⁸⁷, A.S. White¹⁰³, A. White⁸, M.J. White¹, R. White^{144b}, D. Whiteson¹⁶⁸,
B.W. Whitmore⁸⁷, F.J. Wickens¹⁴¹, W. Wiedenmann¹⁷⁸, M. Wielers¹⁴¹, C. Wiglesworth³⁹,
L.A.M. Wiik-Fuchs⁵⁰, A. Wildauer¹¹³, F. Wilk⁹⁸, H.G. Wilkens³⁵, L.J. Wilkins⁹¹, H.H. Williams¹³⁴,
S. Williams³¹, C. Willis¹⁰⁴, S. Willocq¹⁰⁰, J.A. Wilson²¹, I. Wingerter-Seez⁵, E. Winkels¹⁵³,
F. Winklmeier¹²⁸, O.J. Winston¹⁵³, B.T. Winter²⁴, M. Wittgen¹⁵⁰, M. Wobisch⁹³, A. Wolf⁹⁷,
T.M.H. Wolf¹¹⁸, R. Wolff⁹⁹, M.W. Wolter⁸², H. Wolters^{137a,137c}, V.W.S. Wong¹⁷², N.L. Woods¹⁴³,
S.D. Worm²¹, B.K. Wosiek⁸², K.W. Woźniak⁸², K. Wraight⁵⁵, M. Wu³⁶, S.L. Wu¹⁷⁸, X. Wu⁵², Y. Wu^{58a},
T.R. Wyatt⁹⁸, B.M. Wynne⁴⁸, S. Xella³⁹, Z. Xi¹⁰³, L. Xia¹⁷⁵, D. Xu^{15a}, H. Xu^{58a,e}, L. Xu²⁹, T. Xu¹⁴²,
W. Xu¹⁰³, B. Yabsley¹⁵⁴, S. Yacoob^{32a}, K. Yajima¹³⁰, D.P. Yallup⁹², D. Yamaguchi¹⁶², Y. Yamaguchi¹⁶²,
A. Yamamoto⁷⁹, T. Yamanaka¹⁶⁰, F. Yamane⁸⁰, M. Yamatani¹⁶⁰, T. Yamazaki¹⁶⁰, Y. Yamazaki⁸⁰, Z. Yan²⁵,
H.J. Yang^{58c,58d}, H.T. Yang¹⁸, S. Yang⁷⁵, Y. Yang¹⁶⁰, Z. Yang¹⁷, W.-M. Yao¹⁸, Y.C. Yap⁴⁴, Y. Yasu⁷⁹,
E. Yatsenko^{58c,58d}, J. Ye⁴¹, S. Ye²⁹, I. Yeletskikh⁷⁷, E. Yigitbasi²⁵, E. Yildirim⁹⁷, K. Yorita¹⁷⁶,
K. Yoshihara¹³⁴, C.J.S. Young³⁵, C. Young¹⁵⁰, J. Yu⁸, J. Yu⁷⁶, X. Yue^{59a}, S.P.Y. Yuen²⁴, B. Zabinski⁸²,
G. Zacharis¹⁰, E. Zaffaroni⁵², R. Zaidan¹⁴, A.M. Zaitsev^{121,ao}, T. Zakareishvili^{156b}, N. Zakharchuk⁴⁴,
J. Zalieckas¹⁷, S. Zambito⁵⁷, D. Zanzi³⁵, D.R. Zaripovas⁵⁵, S.V. Zeiřner⁴⁵, C. Zeitnitz¹⁷⁹, G. Zemaityte¹³²,
J.C. Zeng¹⁷⁰, Q. Zeng¹⁵⁰, O. Zenin¹²¹, D. Zerwas¹²⁹, M. Zgubić¹³², D.F. Zhang^{58b}, D. Zhang¹⁰³,
F. Zhang¹⁷⁸, G. Zhang^{58a}, H. Zhang^{15c}, J. Zhang⁶, L. Zhang^{15c}, L. Zhang^{58a}, M. Zhang¹⁷⁰, P. Zhang^{15c},
R. Zhang^{58a}, R. Zhang²⁴, X. Zhang^{58b}, Y. Zhang^{15d}, Z. Zhang¹²⁹, P. Zhao⁴⁷, X. Zhao⁴¹, Y. Zhao^{58b,129,ak},
Z. Zhao^{58a}, A. Zhemchugov⁷⁷, B. Zhou¹⁰³, C. Zhou¹⁷⁸, L. Zhou⁴¹, M.S. Zhou^{15d}, M. Zhou¹⁵², N. Zhou^{58c},
Y. Zhou⁷, C.G. Zhu^{58b}, H.L. Zhu^{58a}, H. Zhu^{15a}, J. Zhu¹⁰³, Y. Zhu^{58a}, X. Zhuang^{15a}, K. Zhukov¹⁰⁸,
V. Zhulanov^{120b,120a}, A. Zibell¹⁷⁴, D. Zieminska⁶³, N.I. Zimine⁷⁷, S. Zimmermann⁵⁰, Z. Zinonos¹¹³,

M. Zinser⁹⁷, M. Ziolkowski¹⁴⁸, G. Zobernig¹⁷⁸, A. Zoccoli^{23b,23a}, K. Zoch⁵¹, T.G. Zorbas¹⁴⁶, R. Zou³⁶,
M. Zur Nedden¹⁹, L. Zwalinski³⁵

¹ Department of Physics, University of Adelaide, Adelaide, Australia

² Physics Department, SUNY Albany, Albany, NY, United States of America

³ Department of Physics, University of Alberta, Edmonton, AB, Canada

⁴ (a) Department of Physics, Ankara University, Ankara; (b) Istanbul Aydin University, Istanbul; (c) Division of Physics, TOBB University of Economics and Technology, Ankara, Turkey

⁵ LAPP, Université Grenoble Alpes, Université Savoie Mont Blanc, CNRS/IN2P3, Annecy, France

⁶ High Energy Physics Division, Argonne National Laboratory, Argonne, IL, United States of America

⁷ Department of Physics, University of Arizona, Tucson, AZ, United States of America

⁸ Department of Physics, University of Texas at Arlington, Arlington, TX, United States of America

⁹ Physics Department, National and Kapodistrian University of Athens, Athens, Greece

¹⁰ Physics Department, National Technical University of Athens, Zografou, Greece

¹¹ Department of Physics, University of Texas at Austin, Austin, TX, United States of America

¹² (a) Bahcesehir University, Faculty of Engineering and Natural Sciences, Istanbul; (b) Istanbul Bilgi University, Faculty of Engineering and Natural Sciences, Istanbul; (c) Department of Physics, Bogazici University, Istanbul; (d) Department of Physics Engineering, Gaziantep University, Gaziantep, Turkey

¹³ Institute of Physics, Azerbaijan Academy of Sciences, Baku, Azerbaijan

¹⁴ Institut de Física d'Altes Energies (IFAE), Barcelona Institute of Science and Technology, Barcelona, Spain

¹⁵ (a) Institute of High Energy Physics, Chinese Academy of Sciences, Beijing; (b) Physics Department, Tsinghua University, Beijing; (c) Department of Physics, Nanjing University, Nanjing;

(d) University of Chinese Academy of Science (UCAS), Beijing, China

¹⁶ Institute of Physics, University of Belgrade, Belgrade, Serbia

¹⁷ Department for Physics and Technology, University of Bergen, Bergen, Norway

¹⁸ Physics Division, Lawrence Berkeley National Laboratory and University of California, Berkeley, CA, United States of America

¹⁹ Institut für Physik, Humboldt Universität zu Berlin, Berlin, Germany

²⁰ Albert Einstein Center for Fundamental Physics and Laboratory for High Energy Physics, University of Bern, Bern, Switzerland

²¹ School of Physics and Astronomy, University of Birmingham, Birmingham, United Kingdom

²² Centro de Investigaciones, Universidad Antonio Nariño, Bogota, Colombia

²³ (a) Dipartimento di Fisica e Astronomia, Università di Bologna, Bologna; (b) INFN Sezione di Bologna, Italy

²⁴ Physikalisches Institut, Universität Bonn, Bonn, Germany

²⁵ Department of Physics, Boston University, Boston, MA, United States of America

²⁶ Department of Physics, Brandeis University, Waltham, MA, United States of America

²⁷ (a) Transilvania University of Brasov, Brasov; (b) Horia Hulubei National Institute of Physics and Nuclear Engineering, Bucharest; (c) Department of Physics, Alexandru Ioan Cuza

University of Iasi, Iasi; (d) National Institute for Research and Development of Isotopic and Molecular Technologies, Physics Department, Cluj-Napoca; (e) University Politehnica Bucharest, Bucharest; (f) West University in Timisoara, Timisoara, Romania

²⁸ (a) Faculty of Mathematics, Physics and Informatics, Comenius University, Bratislava; (b) Department of Subnuclear Physics, Institute of Experimental Physics of the Slovak Academy of Sciences, Kosice, Slovak Republic

²⁹ Physics Department, Brookhaven National Laboratory, Upton, NY, United States of America

³⁰ Departamento de Física, Universidad de Buenos Aires, Buenos Aires, Argentina

³¹ Cavendish Laboratory, University of Cambridge, Cambridge, United Kingdom

³² (a) Department of Physics, University of Cape Town, Cape Town; (b) Department of Mechanical Engineering Science, University of Johannesburg, Johannesburg; (c) School of Physics, University of the Witwatersrand, Johannesburg, South Africa

³³ Department of Physics, Carleton University, Ottawa, ON, Canada

³⁴ (a) Faculté des Sciences Ain Chock, Réseau Universitaire de Physique des Hautes Energies – Université Hassan II, Casablanca; (b) Centre National de l'Energie des Sciences Techniques Nucleaires (CNESTEN), Rabat; (c) Faculté des Sciences Semlalia, Université Cadi Ayyad, LPHEA, Marrakech; (d) Faculté des Sciences, Université Mohamed Premier and LPTPM, Oujda;

(e) Faculté des sciences, Université Mohammed V, Rabat, Morocco

³⁵ CERN, Geneva, Switzerland

³⁶ Enrico Fermi Institute, University of Chicago, Chicago, IL, United States of America

³⁷ LPC, Université Clermont Auvergne, CNRS/IN2P3, Clermont-Ferrand, France

³⁸ Nevis Laboratory, Columbia University, Irvington, NY, United States of America

³⁹ Niels Bohr Institute, University of Copenhagen, Copenhagen, Denmark

⁴⁰ (a) Dipartimento di Fisica, Università della Calabria, Rende; (b) INFN Gruppo Collegato di Cosenza, Laboratori Nazionali di Frascati, Italy

⁴¹ Physics Department, Southern Methodist University, Dallas, TX, United States of America

⁴² Physics Department, University of Texas at Dallas, Richardson, TX, United States of America

⁴³ (a) Department of Physics, Stockholm University; (b) Oskar Klein Centre, Stockholm, Sweden

⁴⁴ Deutsches Elektronen-Synchrotron DESY, Hamburg and Zeuthen, Germany

⁴⁵ Lehrstuhl für Experimentelle Physik IV, Technische Universität Dortmund, Dortmund, Germany

⁴⁶ Institut für Kern- und Teilchenphysik, Technische Universität Dresden, Dresden, Germany

⁴⁷ Department of Physics, Duke University, Durham, NC, United States of America

⁴⁸ SUPA – School of Physics and Astronomy, University of Edinburgh, Edinburgh, United Kingdom

⁴⁹ INFN e Laboratori Nazionali di Frascati, Frascati, Italy

⁵⁰ Physikalisches Institut, Albert-Ludwigs-Universität Freiburg, Freiburg, Germany

⁵¹ II. Physikalisches Institut, Georg-August-Universität Göttingen, Göttingen, Germany

⁵² Département de Physique Nucléaire et Corpusculaire, Université de Genève, Genève, Switzerland

⁵³ (a) Dipartimento di Fisica, Università di Genova, Genova; (b) INFN Sezione di Genova, Italy

⁵⁴ II. Physikalisches Institut, Justus-Liebig-Universität Giessen, Giessen, Germany

⁵⁵ SUPA – School of Physics and Astronomy, University of Glasgow, Glasgow, United Kingdom

⁵⁶ LPSC, Université Grenoble Alpes, CNRS/IN2P3, Grenoble INP, Grenoble, France

⁵⁷ Laboratory for Particle Physics and Cosmology, Harvard University, Cambridge, MA, United States of America

⁵⁸ (a) Department of Modern Physics and State Key Laboratory of Particle Detection and Electronics, University of Science and Technology of China, Hefei; (b) Institute of Frontier and Interdisciplinary Science and Key Laboratory of Particle Physics and Particle Irradiation (MOE), Shandong University, Qingdao; (c) School of Physics and Astronomy, Shanghai Jiao Tong University, KLPPAC-MoE, SKLPPC, Shanghai; (d) Tsung-Dao Lee Institute, Shanghai, China

⁵⁹ (a) Kirchhoff-Institut für Physik, Ruprecht-Karls-Universität Heidelberg, Heidelberg; (b) Physikalisches Institut, Ruprecht-Karls-Universität Heidelberg, Heidelberg, Germany

⁶⁰ Faculty of Applied Information Science, Hiroshima Institute of Technology, Hiroshima, Japan

⁶¹ (a) Department of Physics, Chinese University of Hong Kong, Shatin, N.T., Hong Kong; (b) Department of Physics, University of Hong Kong, Hong Kong; (c) Department of Physics and Institute for Advanced Study, Hong Kong University of Science and Technology, Clear Water Bay, Kowloon, Hong Kong, China

⁶² Department of Physics, National Tsing Hua University, Hsinchu, Taiwan

⁶³ Department of Physics, Indiana University, Bloomington, IN, United States of America

⁶⁴ (a) INFN Gruppo Collegato di Udine, Sezione di Trieste, Udine; (b) ICTP, Trieste; (c) Dipartimento di Chimica, Fisica e Ambiente, Università di Udine, Udine, Italy

- ⁶⁵ (a) INFN Sezione di Lecce; (b) Dipartimento di Matematica e Fisica, Università del Salento, Lecce, Italy
- ⁶⁶ (a) INFN Sezione di Milano; (b) Dipartimento di Fisica, Università di Milano, Milano, Italy
- ⁶⁷ (a) INFN Sezione di Napoli; (b) Dipartimento di Fisica, Università di Napoli, Napoli, Italy
- ⁶⁸ (a) INFN Sezione di Pavia; (b) Dipartimento di Fisica, Università di Pavia, Pavia, Italy
- ⁶⁹ (a) INFN Sezione di Pisa; (b) Dipartimento di Fisica E. Fermi, Università di Pisa, Pisa, Italy
- ⁷⁰ (a) INFN Sezione di Roma; (b) Dipartimento di Fisica, Sapienza Università di Roma, Roma, Italy
- ⁷¹ (a) INFN Sezione di Roma Tor Vergata; (b) Dipartimento di Fisica, Università di Roma Tor Vergata, Roma, Italy
- ⁷² (a) INFN Sezione di Roma Tre; (b) Dipartimento di Matematica e Fisica, Università Roma Tre, Roma, Italy
- ⁷³ (a) INFN-TIFPA; (b) Università degli Studi di Trento, Trento, Italy
- ⁷⁴ Institut für Astro- und Teilchenphysik, Leopold-Franzens-Universität, Innsbruck, Austria
- ⁷⁵ University of Iowa, Iowa City, IA, United States of America
- ⁷⁶ Department of Physics and Astronomy, Iowa State University, Ames, IA, United States of America
- ⁷⁷ Joint Institute for Nuclear Research, Dubna, Russia
- ⁷⁸ (a) Departamento de Engenharia Elétrica, Universidade Federal de Juiz de Fora (UFJF), Juiz de Fora; (b) Universidade Federal do Rio De Janeiro COPPE/EE/IF, Rio de Janeiro;
- ⁷⁹ (c) Universidade Federal de São João del Rei (UFSJ), São João del Rei; (d) Instituto de Física, Universidade de São Paulo, São Paulo, Brazil
- ⁸⁰ KEK, High Energy Accelerator Research Organization, Tsukuba, Japan
- ⁸¹ Graduate School of Science, Kobe University, Kobe, Japan
- ⁸² (a) AGH University of Science and Technology, Faculty of Physics and Applied Computer Science, Krakow; (b) Marian Smoluchowski Institute of Physics, Jagiellonian University, Krakow, Poland
- ⁸³ Institute of Nuclear Physics Polish Academy of Sciences, Krakow, Poland
- ⁸⁴ Faculty of Science, Kyoto University, Kyoto, Japan
- ⁸⁵ Kyoto University of Education, Kyoto, Japan
- ⁸⁶ Research Center for Advanced Particle Physics and Department of Physics, Kyushu University, Fukuoka, Japan
- ⁸⁷ Instituto de Física La Plata, Universidad Nacional de La Plata and CONICET, La Plata, Argentina
- ⁸⁸ Physics Department, Lancaster University, Lancaster, United Kingdom
- ⁸⁹ Oliver Lodge Laboratory, University of Liverpool, Liverpool, United Kingdom
- ⁹⁰ Department of Experimental Particle Physics, Jožef Stefan Institute and Department of Physics, University of Ljubljana, Ljubljana, Slovenia
- ⁹¹ School of Physics and Astronomy, Queen Mary University of London, London, United Kingdom
- ⁹² Department of Physics, Royal Holloway University of London, Egham, United Kingdom
- ⁹³ Department of Physics and Astronomy, University College London, London, United Kingdom
- ⁹⁴ Louisiana Tech University, Ruston, LA, United States of America
- ⁹⁵ Fysiska institutionen, Lunds universitet, Lund, Sweden
- ⁹⁶ Centre de Calcul de l'Institut National de Physique Nucléaire et de Physique des Particules (IN2P3), Villeurbanne, France
- ⁹⁷ Departamento de Física Teórica C-15 and CIAFF, Universidad Autónoma de Madrid, Madrid, Spain
- ⁹⁸ Institut für Physik, Universität Mainz, Mainz, Germany
- ⁹⁹ School of Physics and Astronomy, University of Manchester, Manchester, United Kingdom
- ¹⁰⁰ CPPM, Aix-Marseille Université, CNRS/IN2P3, Marseille, France
- ¹⁰¹ Department of Physics, University of Massachusetts, Amherst, MA, United States of America
- ¹⁰² Department of Physics, McGill University, Montreal, QC, Canada
- ¹⁰³ School of Physics, University of Melbourne, Victoria, Australia
- ¹⁰⁴ Department of Physics, University of Michigan, Ann Arbor, MI, United States of America
- ¹⁰⁵ Department of Physics and Astronomy, Michigan State University, East Lansing, MI, United States of America
- ¹⁰⁶ B.I. Stepanov Institute of Physics, National Academy of Sciences of Belarus, Minsk, Belarus
- ¹⁰⁷ Research Institute for Nuclear Problems of Byelorussian State University, Minsk, Belarus
- ¹⁰⁸ Group of Particle Physics, University of Montreal, Montreal, QC, Canada
- ¹⁰⁹ P.N. Lebedev Physical Institute of the Russian Academy of Sciences, Moscow, Russia
- ¹¹⁰ Institute for Theoretical and Experimental Physics (ITEP), Moscow, Russia
- ¹¹¹ National Research Nuclear University MEPhI, Moscow, Russia
- ¹¹² D.V. Skobeltsyn Institute of Nuclear Physics, M.V. Lomonosov Moscow State University, Moscow, Russia
- ¹¹³ Fakultät für Physik, Ludwig-Maximilians-Universität München, München, Germany
- ¹¹⁴ Max-Planck-Institut für Physik (Werner-Heisenberg-Institut), München, Germany
- ¹¹⁵ Nagasaki Institute of Applied Science, Nagasaki, Japan
- ¹¹⁶ Graduate School of Science and Kobayashi-Maskawa Institute, Nagoya University, Nagoya, Japan
- ¹¹⁷ Department of Physics and Astronomy, University of New Mexico, Albuquerque, NM, United States of America
- ¹¹⁸ Institute for Mathematics, Astrophysics and Particle Physics, Radboud University Nijmegen/Nikhef, Nijmegen, Netherlands
- ¹¹⁹ Nikhef National Institute for Subatomic Physics and University of Amsterdam, Amsterdam, Netherlands
- ¹²⁰ Department of Physics, Northern Illinois University, DeKalb, IL, United States of America
- ¹²¹ (a) Budker Institute of Nuclear Physics and NSU, SB RAS, Novosibirsk; (b) Novosibirsk State University, Novosibirsk, Russia
- ¹²² Institute for High Energy Physics of the National Research Centre Kurchatov Institute, Protvino, Russia
- ¹²³ Department of Physics, New York University, New York, NY, United States of America
- ¹²⁴ Ohio State University, Columbus, OH, United States of America
- ¹²⁵ Faculty of Science, Okayama University, Okayama, Japan
- ¹²⁶ Homer L. Dodge Department of Physics and Astronomy, University of Oklahoma, Norman, OK, United States of America
- ¹²⁷ Department of Physics, Oklahoma State University, Stillwater, OK, United States of America
- ¹²⁸ Palacký University, RCPTM, Joint Laboratory of Optics, Olomouc, Czech Republic
- ¹²⁹ Center for High Energy Physics, University of Oregon, Eugene, OR, United States of America
- ¹³⁰ LAL, Université Paris-Sud, CNRS/IN2P3, Université Paris-Saclay, Orsay, France
- ¹³¹ Graduate School of Science, Osaka University, Osaka, Japan
- ¹³² Department of Physics, University of Oslo, Oslo, Norway
- ¹³³ Department of Physics, Oxford University, Oxford, United Kingdom
- ¹³⁴ LPNHE, Sorbonne Université, Paris Diderot Sorbonne Paris Cité, CNRS/IN2P3, Paris, France
- ¹³⁵ Department of Physics, University of Pennsylvania, Philadelphia, PA, United States of America
- ¹³⁶ Konstantinov Nuclear Physics Institute of National Research Centre "Kurchatov Institute", PNPI, St. Petersburg, Russia
- ¹³⁷ Department of Physics and Astronomy, University of Pittsburgh, Pittsburgh, PA, United States of America
- ¹³⁸ (a) Laboratório de Instrumentação e Física Experimental de Partículas – LIP; (b) Departamento de Física, Faculdade de Ciências, Universidade de Lisboa, Lisboa; (c) Departamento de Física, Universidade de Coimbra, Coimbra; (d) Centro de Física Nuclear da Universidade de Lisboa, Lisboa; (e) Departamento de Física, Universidade do Minho, Braga; (f) Departamento de Física Teórica y del Cosmos, Universidad de Granada, Granada (Spain); (g) Dep Física and CEFITEC de Faculdade de Ciências e Tecnologia, Universidade Nova de Lisboa, Caparica, Portugal
- ¹³⁹ Institute of Physics, Academy of Sciences of the Czech Republic, Prague, Czech Republic
- ¹⁴⁰ Czech Technical University in Prague, Prague, Czech Republic

- ¹⁴⁰ Charles University, Faculty of Mathematics and Physics, Prague, Czech Republic
- ¹⁴¹ Particle Physics Department, Rutherford Appleton Laboratory, Didcot, United Kingdom
- ¹⁴² IRFU, CEA, Université Paris-Saclay, Gif-sur-Yvette, France
- ¹⁴³ Santa Cruz Institute for Particle Physics, University of California Santa Cruz, Santa Cruz, CA, United States of America
- ¹⁴⁴ ^(a) Departamento de Física, Pontificia Universidad Católica de Chile, Santiago; ^(b) Departamento de Física, Universidad Técnica Federico Santa María, Valparaíso, Chile
- ¹⁴⁵ Department of Physics, University of Washington, Seattle, WA, United States of America
- ¹⁴⁶ Department of Physics and Astronomy, University of Sheffield, Sheffield, United Kingdom
- ¹⁴⁷ Department of Physics, Shinshu University, Nagano, Japan
- ¹⁴⁸ Department Physik, Universität Siegen, Siegen, Germany
- ¹⁴⁹ Department of Physics, Simon Fraser University, Burnaby, BC, Canada
- ¹⁵⁰ SLAC National Accelerator Laboratory, Stanford, CA, United States of America
- ¹⁵¹ Physics Department, Royal Institute of Technology, Stockholm, Sweden
- ¹⁵² Departments of Physics and Astronomy, Stony Brook University, Stony Brook, NY, United States of America
- ¹⁵³ Department of Physics and Astronomy, University of Sussex, Brighton, United Kingdom
- ¹⁵⁴ School of Physics, University of Sydney, Sydney, Australia
- ¹⁵⁵ Institute of Physics, Academia Sinica, Taipei, Taiwan
- ¹⁵⁶ ^(a) E. Andronikashvili Institute of Physics, Iv. Javakishvili Tbilisi State University, Tbilisi; ^(b) High Energy Physics Institute, Tbilisi State University, Tbilisi, Georgia
- ¹⁵⁷ Department of Physics, Technion, Israel Institute of Technology, Haifa, Israel
- ¹⁵⁸ Raymond and Beverly Sackler School of Physics and Astronomy, Tel Aviv University, Tel Aviv, Israel
- ¹⁵⁹ Department of Physics, Aristotle University of Thessaloniki, Thessaloniki, Greece
- ¹⁶⁰ International Center for Elementary Particle Physics and Department of Physics, University of Tokyo, Tokyo, Japan
- ¹⁶¹ Graduate School of Science and Technology, Tokyo Metropolitan University, Tokyo, Japan
- ¹⁶² Department of Physics, Tokyo Institute of Technology, Tokyo, Japan
- ¹⁶³ Tomsk State University, Tomsk, Russia
- ¹⁶⁴ Department of Physics, University of Toronto, Toronto, ON, Canada
- ¹⁶⁵ ^(a) TRIUMF, Vancouver, BC; ^(b) Department of Physics and Astronomy, York University, Toronto, ON, Canada
- ¹⁶⁶ Division of Physics and Tomonaga Center for the History of the Universe, Faculty of Pure and Applied Sciences, University of Tsukuba, Tsukuba, Japan
- ¹⁶⁷ Department of Physics and Astronomy, Tufts University, Medford, MA, United States of America
- ¹⁶⁸ Department of Physics and Astronomy, University of California Irvine, Irvine, CA, United States of America
- ¹⁶⁹ Department of Physics and Astronomy, University of Uppsala, Uppsala, Sweden
- ¹⁷⁰ Department of Physics, University of Illinois, Urbana, IL, United States of America
- ¹⁷¹ Instituto de Física Corpuscular (IFIC), Centro Mixto Universidad de Valencia – CSIC, Valencia, Spain
- ¹⁷² Department of Physics, University of British Columbia, Vancouver, BC, Canada
- ¹⁷³ Department of Physics and Astronomy, University of Victoria, Victoria, BC, Canada
- ¹⁷⁴ Fakultät für Physik und Astronomie, Julius-Maximilians-Universität Würzburg, Würzburg, Germany
- ¹⁷⁵ Department of Physics, University of Warwick, Coventry, United Kingdom
- ¹⁷⁶ Waseda University, Tokyo, Japan
- ¹⁷⁷ Department of Particle Physics, Weizmann Institute of Science, Rehovot, Israel
- ¹⁷⁸ Department of Physics, University of Wisconsin, Madison, WI, United States of America
- ¹⁷⁹ Fakultät für Mathematik und Naturwissenschaften, Fachgruppe Physik, Bergische Universität Wuppertal, Wuppertal, Germany
- ¹⁸⁰ Department of Physics, Yale University, New Haven, CT, United States of America
- ¹⁸¹ Yerevan Physics Institute, Yerevan, Armenia

^a Also at Borough of Manhattan Community College, City University of New York, NY; United States of America.

^b Also at California State University, East Bay; United States of America.

^c Also at Centre for High Performance Computing, CSIR Campus, Rosebank, Cape Town; South Africa.

^d Also at CERN, Geneva; Switzerland.

^e Also at CPPM, Aix-Marseille Université, CNRS/IN2P3, Marseille; France.

^f Also at Département de Physique Nucléaire et Corpusculaire, Université de Genève, Genève; Switzerland.

^g Also at Departament de Física de la Universitat Autònoma de Barcelona, Barcelona; Spain.

^h Also at Departamento de Física Teórica y del Cosmos, Universidad de Granada, Granada (Spain); Spain.

ⁱ Also at Departamento de Física, Instituto Superior Técnico, Universidade de Lisboa, Lisboa; Portugal.

^j Also at Department of Applied Physics and Astronomy, University of Sharjah, Sharjah; United Arab Emirates.

^k Also at Department of Financial and Management Engineering, University of the Aegean, Chios; Greece.

^l Also at Department of Physics and Astronomy, University of Louisville, Louisville, KY; United States of America.

^m Also at Department of Physics and Astronomy, University of Sheffield, Sheffield; United Kingdom.

ⁿ Also at Department of Physics, California State University, Fresno CA; United States of America.

^o Also at Department of Physics, California State University, Sacramento CA; United States of America.

^p Also at Department of Physics, King's College London, London; United Kingdom.

^q Also at Department of Physics, St. Petersburg State Polytechnical University, St. Petersburg; Russia.

^r Also at Department of Physics, Stanford University; United States of America.

^s Also at Department of Physics, University of Fribourg, Fribourg; Switzerland.

^t Also at Department of Physics, University of Michigan, Ann Arbor MI; United States of America.

^u Also at Dipartimento di Fisica E. Fermi, Università di Pisa, Pisa; Italy.

^v Also at Giresun University, Faculty of Engineering, Giresun; Turkey.

^w Also at Graduate School of Science, Osaka University, Osaka; Japan.

^x Also at Hellenic Open University, Patras; Greece.

^y Also at Horia Hulubei National Institute of Physics and Nuclear Engineering, Bucharest; Romania.

^z Also at II. Physikalisches Institut, Georg-August-Universität Göttingen, Göttingen; Germany.

^{aa} Also at Institut Catalana de Recerca i Estudis Avancats, ICREA, Barcelona; Spain.

^{ab} Also at Institut für Experimentalphysik, Universität Hamburg, Hamburg; Germany.

^{ac} Also at Institute for Mathematics, Astrophysics and Particle Physics, Radboud University Nijmegen/Nikhef, Nijmegen; Netherlands.

^{ad} Also at Institute for Particle and Nuclear Physics, Wigner Research Centre for Physics, Budapest; Hungary.

^{ae} Also at Institute of Particle Physics (IPP); Canada.

^{af} Also at Institute of Physics, Academia Sinica, Taipei; Taiwan.

^{ag} Also at Institute of Physics, Azerbaijan Academy of Sciences, Baku; Azerbaijan.

^{ah} Also at Institute of Theoretical Physics, Ilia State University, Tbilisi; Georgia.

^{ai} Also at Instituto de Física Teórica de la Universidad Autónoma de Madrid; Spain.

^{aj} Also at Istanbul University, Dept. of Physics, Istanbul; Turkey.

^{ak} Also at LAL, Université Paris-Sud, CNRS/IN2P3, Université Paris-Saclay, Orsay; France.

^{al} Also at Louisiana Tech University, Ruston LA; United States of America.

^{am} Also at LPNHE, Sorbonne Université, Paris Diderot Sorbonne Paris Cité, CNRS/IN2P3, Paris; France.

^{an} Also at Manhattan College, New York NY; United States of America.

^{ao} Also at Moscow Institute of Physics and Technology State University, Dolgoprudny; Russia.

^{ap} Also at National Research Nuclear University MEPhI, Moscow; Russia.

^{aq} Also at Physikalisches Institut, Albert-Ludwigs-Universität Freiburg, Freiburg; Germany.

^{ar} Also at School of Physics, Sun Yat-sen University, Guangzhou; China.

^{as} Also at The City College of New York, New York NY; United States of America.

^{at} Also at The Collaborative Innovation Center of Quantum Matter (CICQM), Beijing; China.

^{au} Also at Tomsk State University, Tomsk, and Moscow Institute of Physics and Technology State University, Dolgoprudny; Russia.

^{av} Also at TRIUMF, Vancouver BC; Canada.

^{aw} Also at Università di Napoli Parthenope, Napoli; Italy.

* Deceased.